

THESIS

INVESTIGATION OF RESIN INFUSION CONSUMABLE EFFECT ON FUSION BOND
STRENGTH IN THE MANUFACTURE OF A THERMOPLASTIC VERTICAL AXIS WIND
TURBINE PROTOTYPE

Submitted by

Jamison Bair

Department of Mechanical Engineering

In partial fulfilment of the requirements

For the Degree of Master of Science

Colorado State University

Fort Collins, Colorado

Spring 2020

Master's Committee:

Advisor: Thomas H. Bradley

Donald W. Radford

Paul R. Heyliger

Copyright by Jamison T. Bair 2020

All Rights Reserved

ABSTRACT

INVESTIGATION OF RESIN INFUSION CONSUMABLE EFFECT ON FUSION BOND STRENGTH IN THE MANUFACTURE OF A THERMOPLASTIC VERTICAL AXIS WIND TURBINE PROTOTYPE

To further research the economic viability, manufacturability, and wider adoption of Vertical Axis Wind Turbines (VAWT), a project team led by Steelhead Composites (SHC), with assistance from Colorado State University (CSU), National Renewable Energy Laboratory (NREL), and Arkema Inc. designed and fabricated VAWT rotor assembly with thermoplastic composite blades using novel fabrication techniques. Thermoplastics present many advantages over traditional thermosets including recyclability as well as the ability to be thermally welded and reformed without machining. Thermal welding, or fusion bonding can eliminate the need for adhesive bonding, a requirement in the manufacture of thermoset and thermoplastic turbine blades, as currently being produced. Colorado State University was tasked with using Elium®, a novel liquid poly methyl-methacrylate (PMMA) thermoplastic manufactured by Arkema to conduct the manufacture of prototype vertical axis wind turbine blades. Elium® is a reactive, in-situ polymerizing thermoplastic that is processed using liquid processing techniques and it has mechanical properties comparable to counterpart thermosetting resins. The CSU research team developed a resin infusion molding process with closed two-part molds to create thin, hollow fiber reinforced airfoils. When high quality airfoils were successfully manufactured the team investigated the feasibility of fusion bonding end fittings into the hollow airfoils to reduce part count and mass. It was hypothesized that the consumables that produced a rough, matrix rich

texture at the bond interface would lead to higher strength bonded joints. The fusion bonding focus investigated three different infusion consumables: Compoflex® RF3 a combination release film and flow media, G-FLOW™, a structural glass fiber flow media, and Release Ply Super A, a heavy weight nylon release film. The products produced varying surface textures that were measured using a surface profilometer to compare and quantify the roughness and form of the surface, to examine how the induced surface textures impacted the quality of fusion bonded joints. This hypothesis was tested via manufacture of double lap shear strength coupons which were tested via ASTM 3528. Processing parameters of the bulk heating fusion bonding process were varied included temperature, consolidation pressure and time, and cooling method. Strength testing results in addition to failure mode analysis and digital microscopy imaging were used to determine which consumables provided a higher bond strength in both glass fiber and carbon fiber Elium® thermoplastic reinforced specimens. The results of the double lap shear tests showed that with the right combination of surface texture and processing variables, lap shear strengths of over 16 MPa (2300 psi) were achieved with glass fiber reinforcements. Results indicated that more consistent strength values were obtained from infusion consumables that had smaller surface asperities, and that larger asperities often led to the inclusion of air bubbles creating voids thus reducing the strength of the bonded joints. Subsequent testing using carbon fiber as the reinforcement provided satisfactory values for lap shear strength and the team proceeded develop a process to fusion join to end attachment plates used to attach blades to the turbine hub. After successfully fusion bonding the tower to blade attachment plates into 129” long hollow airfoil sections, post-mold reforming was used to thermoform the blades into the desired geometry to complete a three-blade vertical axis wind turbine blade prototype.

ACKNOWLEDGEMENTS

To all those who helped me finish this research, I would like to express my deepest gratitude, I could not have done it without you. First, I would like to thank my parents Chip and Peggy for the continued support through all of my trials and tribulations, I love you so much. To my advisors, Dr. Thomas Bradley and Dr. Donald Radford, thank you so much for all the guidance throughout my undergraduate and graduate studies. I have learned valuable lessons from you, not only in academic settings, but more importantly, life skills that I will possess and apply into the future. To the CSU research team including Sam Strassler, Mark Bourgeois, Alice Pinter and Patrick Rodriguez, the success of this research was due to your contributions, I am so grateful to have had the opportunity to work with you and I could not have completed this without you.

I would like to acknowledge the support of the Institute for Advanced Composites Manufacturing and Innovation (IACMI) for funding this research through US Department of Energy Award DE-EE006926. Additional companies and individuals that aided this project include Steelhead Composites specifically Jake Schrader for his guidance during manufacturing, Highland Industries and Dr. David Branscomb for donation of braided material for airfoil manufacturing, Frank Roundy from Ability Composites for manufacturing the master for final wind turbine blades, Craig Larson from Composites One for supplying much of the consumables, as well as Saertex, A&P, AirTech, VectorPly, Mafic and Torr for equipment and material support. Great thanks also to CSU faculty members Steve Johnson and Dr. Steven Shafer for their assistance manufacturing tooling for this project and for many years of supporting my efforts in other areas of research.

I would additionally like to thank all the people that have had an impact on the large changes I made in my personal life while completing this project. This includes Jason Russell, Dustin Straight, Bryan Brennan, David Baker, Gabe DiDominico, and numerous others. Thank you for helping me keep my priorities straight.

TABLE OF CONTENTS

ABSTRACT.....	ii
ACKNOWLEDGEMENTS.....	iv
LIST OF TABLES.....	vii
LIST OF FIGURES.....	viii
1. Introduction.....	1
1.1. Vertical Axis Wind Turbines.....	1
1.2. Manufacture of Wind Turbine Blades.....	2
1.3. Polymer Matrixes in Turbine Manufacture.....	5
1.4. Elium® Poly Methyl-Methacrylate.....	7
1.5. Joining Methods of Thermoplastic Composites.....	11
1.6. Factors Impacting Quality of Bonded Joints.....	15
1.7. Steelhead VAWT With Thermoplastic Composite Blades Study.....	21
1.8. Research Hypothesis.....	25
2. Experimental Manufacture of VAWT Blade Prototype.....	27
2.1. Blade Geometry and Selection.....	27
2.2. Early VARIM Manufacturing Process.....	27
2.3. Evolution of Manufacturing Process and Infusion Consumables.....	28
2.4. Transition to 64” Mold.....	31
2.5. Successful Infusion and Trials with 64” Mold.....	33
2.6. Carbon trials with 64” Mold.....	34
3. Fusion Bonding Experimentation and Methods.....	36
3.1. Demonstrate Fusion Bonding with Elium® Thermoplastic Composites.....	36
3.2. Heat Fusion Bond Testing Overview.....	36
3.3. Experimental Testing via ASTM 3528.....	38
3.4. Materials and Manufacture of Double Lap Shear Laminates.....	39
3.5. Double Lap Shear Coupon Adherend Manufacture.....	40
3.6. Double Lap Shear Coupon Surface Roughness.....	44
3.7. Compression Molding ASTM 3528 Sample Coupons.....	49
3.8. Compression Molding and Processing Variables in DLS Bonding Trials.....	52
3.9. Double Lap Shear Strength Testing Procedure.....	53
3.10. Glass Fiber Double Lap Shear Bonding Trials and Processing Parameters.....	54

3.11.	Carbon Fiber Double Lap Shear Bonding Trials and Processing Parameters	55
4.	Experimental Results and Discussion.....	57
4.1.	Glass Fiber Double Lap Shear Strength Testing Results	57
4.2.	Surface Texture Effect on Bond Strength	59
4.3.	Results of Processing Variable Effect on Glass Fiber Samples	64
4.4.	Glass Fiber Double Lap Shear Failure Mode Analysis.....	66
4.5.	Microscopy Analysis of Glass Fiber Bonded Samples	70
4.6.	Discussion of Glass Fiber Sample Bonding Results	78
4.7.	Carbon Fiber Double Lap Shear Bonding Results	81
5.	Full Scale VAWT Manufacturing.....	87
5.1.	Evaluation of Post Process Reforming of Thermoplastic Airfoil Blade Sections	87
5.2.	3.4m Tooling for Full Scale Blade Infusion.....	89
5.3.	Full Scale 3.4m Blade Infusion	91
5.4.	Blade to Root Hub Attachment Via Fusion Bonding.....	92
5.5.	Final Thermoforming of and Post Processing of Thermoplastic Composite Blades	95
5.6.	Final Assembly of VAWT Prototype.....	96
6.	Conclusions.....	98
6.1.	Fusion Bonding Assembly Methods	98
6.2.	Surface Topology Effect on Strength of Fusion Bonding Joints	99
6.3.	Recommendations for Future Work.....	100
	REFERENCES	101

LIST OF TABLES

Table 1: Material properties of neat Elixir® 150 resin from Technical Data Sheet (TDS)	8
Table 2: Surface roughness measurement averages.....	45
Table 3: Glass fiber fusion bonding processing variables and trials tested via ASTM 3528	55
Table 4: Carbon fiber fusion bonding processing variables and trials tested via ASTM 3528	56
Table 5: G-FLOW™ lap shear strength values and corresponding processing variables	60
Table 6: Mold surface shear strength values and corresponding processing variables	62
Table 7: Compoflex® lap shear strength values and corresponding processing variables.....	63
Table 8: Peel ply lap shear strength values and corresponding processing variables.....	64
Table 9: Highest performing trials of all surface textures	65
Table 10: Strength results from carbon fiber peel ply trials	83

LIST OF FIGURES

Figure 1: Comparison of three styles of Darrieus Style Vertical Axis Wind Turbines from [3]....	2
Figure 2: VARIM process and materials adapted from [5]	4
Figure 3: Polymer chain configurations from [7]	5
Figure 4: Welding Elium® Laminates; Induction (left) vs. Resistance Welding (right) from Murray [24].....	9
Figure 5: Lap Shear Strength of Adhesive, Resistance, and Induction Welded Elium® from Murray [24].....	10
Figure 6: Ultrasonic welding configuration from [25]	11
Figure 7: Joining Methods of Polymer Matrix Composites	12
Figure 8: Fusion bonding process of thermoplastic composites displaying the five sequential stages as described by Wool. Figure Adapted from [27] and [32]	14
Figure 9: Pictorial Display of Surface Texture adapted from [41]	17
Figure 10: Roughness Profile Curve Terminology [42]	18
Figure 11: ASTM Standard Practice for Classifying Failure Modes in Fiber-Reinforced-Plastic Joints	21
Figure 12: Potential locations for fusion bonding in initial VAWT Design.....	23
Figure 13: Upper and lower airfoil blade strut to hub attachment points	24
Figure 14: Baseline rotor assembly with metal mounting bracket detail.....	24
Figure 15: Initial manufacturing process to infuse a 32”-long hollow airfoil cross section.....	28
Figure 16: Schematic of material placement and infusion terminology	29
Figure 17: Evolution of infusion material placement and consumables.....	31
Figure 18: Cross section view of consumable materials for infusion.....	32
Figure 19: Manufacturing of 64” glass fiber airfoil blades, including consumables, positioning in mold, and after infusion	34
Figure 20: Manufacturing process of 64" carbon fiber airfoils, illustrating UD & braided fabric usage, and completed airfoil	35
Figure 21: Description of sample coupon terminology	37
Figure 22. ASTM 3528 Double lap shear sample configuration and definitions according to ASTM International [50]	38
Figure 23: Glass Fiber Airfoil Cross-Section	39
Figure 24: Glass Fiber/Elium® Plate manufactured to give three distinct surface textures.....	40
Figure 25: Surface textures created from a) Compoflex® b) Peel Ply c) G-FLOW™	41
Figure 26: Comparison of Compoflex® (Left) Peel Ply (center) and G-FLOW™ (right) surface textures.....	42
Figure 27: Molded surface laminate showing regions of Compoflex® and vacuum bagged sections.....	43
Figure 28: 5”x 4.25” cut lap shear adherends with various surface finishes	44
Figure 29: Roughness (Blue Line) and Waviness (Red Line) Measured Profile of Peel Ply Sample Coupon.....	46
Figure 30: G-FLOW™ upper surface roughness (blue line) and waviness (red line) measured profile.....	46

Figure 31: G-FLOW™ bottom molded surface roughness (blue line) and waviness (red line) measured profile.....	47
Figure 32: Compoflex® roughness (blue line) and waviness (red line) measured profile	47
Figure 33: Side of Molded Surface (VB Side) Coupon roughness (blue line) and waviness (red line) measured profile	48
Figure 34: Molded Surface (CF Side) Coupon roughness (blue line) with 50 µm vertical axis scale.....	48
Figure 35: Molded surface after sanding with 220 grit roughness measured profile with 50 µm vertical scale.....	49
Figure 36: Double Lap Shear Molding Jig	49
Figure 37: ASTM 3528 Coupon Placement in DLS Molding Jig	50
Figure 38: Glass samples positioned in DLS bonding jig.....	51
Figure 39: Honacomp 8x8 inch 20 Ton Compression Molder and preliminary bonding trial Bond Test 1 (BT1).....	53
Figure 40: ASTM 3528 tensile coupon and measurement locations	54
Figure 41: Average values for double lap shear strength by surface texture.....	58
Figure 42: Lap Shear Strength Produced with Varying Surface Textures.....	59
Figure 43: Difference between Compoflex areas and Vacuum Bagged areas in molded surface coupons	61
Figure 44: Compoflex® trials CF2 and CF3 all exhibiting cohesive fiber tear failure	63
Figure 45: Comparison of strength values obtained when cooling samples under pressure	66
Figure 46: Collection of glass samples for failure analysis	67
Figure 47: Failure mode percentage by surface texture.....	68
Figure 48: Cohesive failure exhibited in all 4 surface finishes.....	69
Figure 49: Compoflex®, Mold Surface, and Peel ply coupons illustrating fiber tear during failure	70
Figure 50: Five microscopy cups manufactured; top row identifies samples, lower row is of the imaging surface.....	71
Figure 51: Resin rich area under Compoflex® in molded surface manufacturing sample (6.4x)	72
Figure 52: Unbonded Compoflex adherend (10x) illustrating resin rich areas and voids within the surface asperities	73
Figure 53: Peel ply adherend (6.4x) and enlargement of surface texture and topology (25x)	73
Figure 54: Difference in waviness of G-FLOW™ (A) upper (B) and lower (C) molded surfaces	74
Figure 55: CF1 bonded sample showing large voids and defects in the bondline (6.4x).....	75
Figure 56: Peel ply 3 bonded sample microscopy images (6.4x) illustrating various thickness bondline in B) & C) (10x).....	76
Figure 57: GF2 bonded sample showing large voids and defects in the bondline (6.4x).....	76
Figure 58: (Main) G-FLOW™ 3 bonded sample highlighting voids entrapped during manufacturing of G-FLOW™ adherends (25x).....	77
Figure 59: Molded surface bondline comparison between upper surface (molded) vs tool side of adherend.....	78
Figure 60: Carbon fiber reinforcement used in lap shear adherend and airfoil manufacture	82
Figure 61: Peel ply left on laminate until molding (left) and removal of peel ply from adherends (right)	83
Figure 62: Carbon double lap shear failed adherends.....	85

Figure 63: Bonded Carbon Fiber Peel Ply Double lap shear samples and cross section of bonded joint	86
Figure 64: A) 90 Degree bend locations in VAWT, B) preliminary matched die set, C) reversed bend die set	88
Figure 65: Wiping die set for full scale VAWT bending.....	89
Figure 66: Mold manufacturing sequence	90
Figure 67: Manufacturing process of 138" airfoil blades	92
Figure 68: Blade to Tower Mounting Tabs illustrating 16 in ² bonded region and completed set of 3 blades with bonded inserts	93
Figure 69: End Fitting Compression Mold Dies.....	94
Figure 70: Fusion bonding process showing a) 129" infused airfoils b) compression molding mounting tabs c) completed fusion bond within tooling	95
Figure 71: Completion of post process bending in completed airfoil blade	96
Figure 72: Comparison between molded surface and final post process clear coat finish	96
Figure 73: As designed versus as manufactured VAWT prototype	97

1. INTRODUCTION

1.1. Vertical Axis Wind Turbines

As global energy requirements continue to escalate, concerns about climate change, reducing pollution, and wider adoption of renewable energy sources has also accelerated. One method of addressing these issues currently being researched is decentralized wind power generation. Wind power generation has long been at the forefront of renewable power generation and in recent years the industry has been dominated by horizontal axis wind turbines (HAWT) due to the large power output and scalability with electrical energy output surpassing 12 MW.

However, in recent years decentralized power generation has become an area of focus as local energy production decreases the losses associated with long distance power transmission and gives individuals or organizations the ability to generate their own power. There currently is a commercial need for competitively priced vertical axis wind turbines for residential and urban areas due to their ability to perform at a variety of wind speeds, simplicity of fabrication, and ease of maintainability. Vertical axis wind turbines (VAWT) are electric power generating machinery which convert energy from the wind to mechanical energy, which is then converted to electrical energy [1]. VAWT can be contrasted to horizontal axis wind turbines in that the axis of rotation for the VAWT is in the vertical direction. The VAWT configuration has benefits in that the electricity generating machinery, gearboxes and interconnection can be located at the bottom of the rotational axis of the turbine, thereby improving the structural efficiency and economics of the turbine [2]. VAWTs have three primary configurations that can be seen in Figure 1. The Darrieus type VAWT consists of a set of curved or bent blades that interface at the top and bottom of a vertical structure. Darrieus type VAWTs have a long history of successful implementation, have relatively low bending moments in the airfoil structures, and are robust to changes in wind direction [2]. H-type VAWTs can be more aerodynamically efficient than the curved blades of

Darrieus type machines, do not require guidewires, and can be deployed on larger towers removing them from terrain boundary layer effects. The structural considerations of the rotating airfoils and stationary structure of the VAWT are considerably complicated by the full 360 degree inversion of the airfoil (and its corresponding lift and drag loads) relative to the prevailing wind, by the wake or upstream effects of the vertical rotating axis, and by stress concentrations at the joints and hubs that are characteristic of H-type VAWTs (which are the focus of this study).

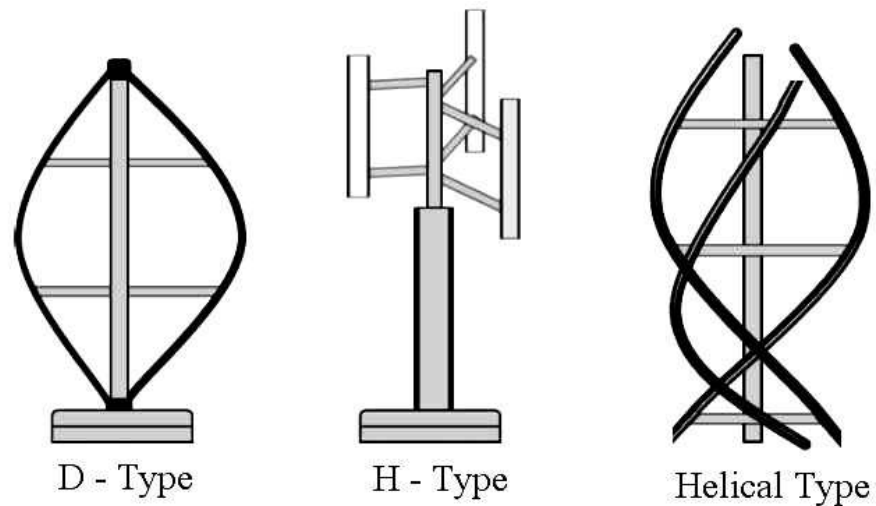


Figure 1: Comparison of three styles of Darrieus Style Vertical Axis Wind Turbines from [3]

1.2. Manufacture of Wind Turbine Blades

Material selection has always governed the manufacture and design of wind turbine blades. Early electricity producing wind turbine blades in the 1940's and 1950's were manufactured from steel, however they failed early in operation thus demonstrating the importance of material selection. Later in the late 1950's and 1960's the first demonstration of a composite turbine blade called the Gedser Wind Turbine was built with steel spars, aluminum shells, and wooden ribs and successfully ran for 11 years without maintenance [4]. In the 1970's the wind energy industry transitioned to using fiber reinforced polymer matrix composites for turbine blade manufacture.

1.2.1. *Fiber Reinforced Polymer Composite Usage in Wind Turbine Manufacture*

Composite materials are beneficial for their high strength-to-weight ratio which is a critical factor in the manufacture of wind turbine blades. In HAWT blades, as the size and weight of blades increases to generate larger amounts of power, gravitational loads become design drivers and stiffness-to-weight ratios also becomes increasingly important to prevent deflection and ensure tip-clearance from the tower [4]. Additionally, since turbine blades are being designed to operate in excess of 20+ years, the high cycle fatigue behavior of composites become increasingly important.

1.2.2. *Manufacturing of FRP Turbine Blades*

In the early history of fiber reinforced composite turbine blades the process traditionally used was a wet layup, where glass fibers were wet out with liquid thermosetting materials using paint brushes and rollers in an open mold. Once fully wet out and once the desired laminate thickness was reached, the blade skin was vacuum bagged and cured under vacuum. This process was used early on to create small and medium sized blades up to 55 meters. However, the one of the main drawbacks to this process was that it was extremely time consuming which resulted in high labor costs [4]. Additionally, the process exposed technicians to harmful volatile organic compounds (VOC's) that presented detrimental health effects. The major limitation of open molding turbine blades was that when blades design was getting larger and larger the blades required webs to be inserted in between either side of the blade shell and adhesively bonded in place. The adhesive bonding introduced large variability and defects that were areas of weakness in the blade that were often first to fail.

1.2.3. *Resin Infusion process*

The introduction of resin infusion technology was a major improvement to both the safety and quality of fiber reinforced blades, and it is currently the most common method of manufacturing turbine blades. Resin infusion (RI) is part of the liquid composite molding (LCM) process family. The term LCM describes the closed mold processes in which a liquid polymeric resin is impregnated through a fibrous reinforcement. Common LCM processes are resin transfer molding (RTM), injection/compression

molding (I/CM), RTM light and vacuum assisted resin infusion molding (VARIM) [5]. Figure 2 illustrates the terminology used in the resin infusion process. Dry fibers or the preform (1) are placed into sealed molds, either under vacuum or in a closed mold. Typically, a peel ply or other material used to separate the part from consumables is placed over the preform (2) In many infusion processes a distribution media (3) is placed on top of the peel ply to enhance resin flow if the preform has low in-plane permeability. After the resin inlet (5) and outlet tube (6) are positioned to allow resin flow through the part the entire layup is covered in a vacuum bag (4) and sealed with a sealant tape (7) to ensure vacuum and seal the system. Once air is evacuated from the system a low viscosity resin is either drawn into the mold under vacuum or injected in under pressure if using an RTM process. Once the preform is wet out, the resin inlet is clamped, and the resin can cure under vacuum.

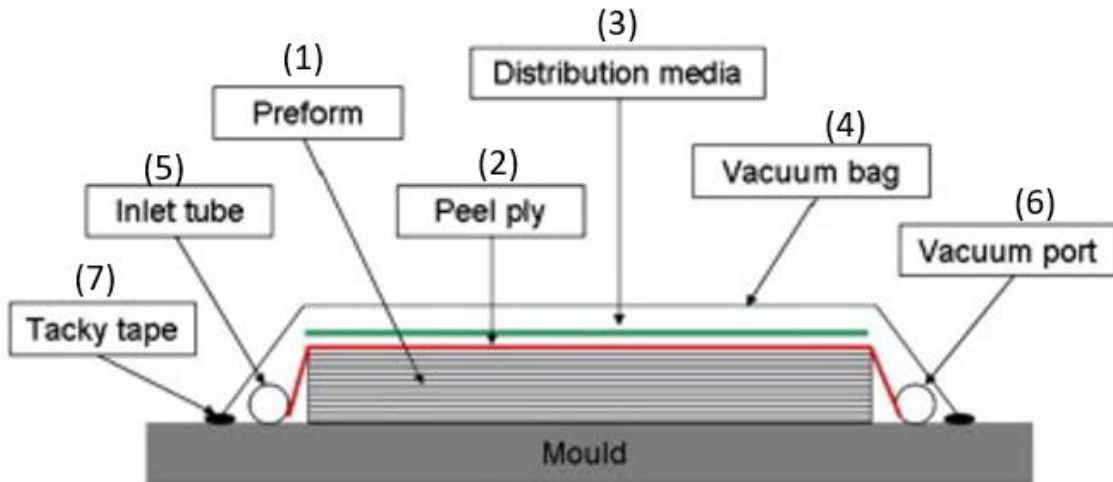


Figure 2: VARIM process and materials adapted from [5]

As compared to other traditional open molding techniques previously used to manufacture turbine blades, this liquid molding technique, specifically a resin infusion process, eliminated wetting out fabric by hand as well as kept all VOC's enclosed in the system. The final fiber volume fraction (V_F) achieved can be higher and more consistent than with more traditional open mold techniques leading to greater quality products and reduced labor costs.

1.3. Polymer Matrixes in Turbine Manufacture

The usage of polymer matrix composites in wind energy has drastically changed and advanced the industry. The wind energy industry is the largest consumer of glass fibers, carbon fibers, epoxy matrixes, as well as other consumables such as foam core, balsa wood core, adhesives and coatings [6]. The two types of polymer matrixes used in turbine manufacture are thermosets and thermoplastics. Both are relatively ductile and weak compared to the fibers in the blades with modulus values less than 4GPa so the purpose of the polymer matrix is to bind the fibers together so they can act synergistically and give a functional composite for the structural needs of turbine blades. This is accomplished by combining the stiff yet brittle properties of fibers with the higher toughness and failure strain of polymers. The matrix increases a composites toughness via energy absorbing mechanisms at the interface of the matrix and fiber [6]. Polymers are chainlike molecules with covalently bonded carbon atoms that form the backbone of the chain. The process of forming large strings of polymer molecules (polymers) from the individual building blocks monomers is called polymerization. There are two classes of polymerization, i) Condensation polymerization and ii) Addition polymerization. Condensation polymerization creates a bi-product where addition polymerization uses a catalyst and monomers join without creating any bi-products. Based on this behavior we have the two types of polymers, thermoset plastics produced via condensation polymerization and thermoplastics produced with addition polymerization [7]. Mechanical behavior of polymers is dependent first on the molecular chain configurations which can be seen below in Figure 3.

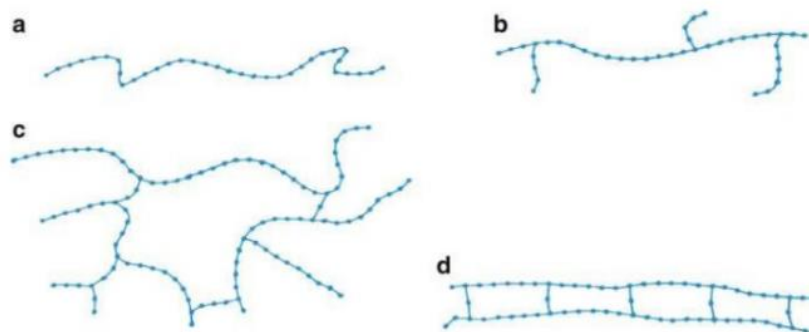


Figure 3: Polymer chain configurations from [7]

Rather than being cross-linked, thermoplastic composites consist of entangled chains. It is this architecture that allows thermoplastics to be thermally remolded or dissolved, techniques not available to thermosets. When an amorphous thermoplastic polymer is heated to a temperature referred to as the Glass Transition Temperature (T_G) the mechanical properties drop, and the polymer essentially becomes a viscous liquid. The T_G is analogous to the melting temperature in crystalline materials.

1.3.1. *Thermosetting (TS) Polymer Matrixes in Turbine Manufacture*

Thermosetting polymer matrix materials such as epoxy, polyester, and vinyl ester have been the major polymers chosen for turbine blade manufacture. They represent about 80% of the market usage for fiber reinforced polymers, especially in turbine blade manufacture [6]. They can be cured at room temperatures but for higher mechanical properties and to obtain processing speeds required in today's high paced manufacturing setting this often means that thermosets must be cured at high temperatures which often involves costly heated molds or large ovens. They have a low viscosity at room temperature which allowed for easy infusion [4]. TS polymers form dense three-dimensional, covalently bonded crosslinked networks upon polymerization and are not thermo-softening materials; as a result, they cannot be reshaped, joined and readily recycled like their TP counterparts. The cross-linked thermosetting nature of thermosets have stiffness values of between 3-4 GPa and a moderate strain to failure of 5-8% so they are usually stiffer than thermoplastics but more brittle [6]. Thermosets have additional drawbacks that include exothermic reactions as well as slow cure times if cured at room temperature, and lower fracture toughness than TS polymers.

1.3.2. *Thermoplastic (TP) Polymer Matrixes in Turbine Manufacture*

Thermoplastic (TP) matrix turbine blades are providing a possible alternative to the traditional thermosetting polymer composite blades due to their ability to be recycled, increased durability, impact toughness, ability to be reformed and increased mechanical properties obtained by novel thermoplastics being created. Prior drawbacks of thermoplastics were the difficulties manufacturing due to high melt viscosities and the increased energy usage when having to melt the polymer to wet out fibers. With newly

developed in-situ polymerizing thermoplastic resin systems for wind turbine blades that polymerize at room temperature, manufacture of thermoplastic turbines can be a low-cost and energy effective method. As the use of thermoplastic composites for structural applications expands, continued research on processing capabilities of novel materials such as Elium® is required. One of the greatest attributes of thermoplastic composites is the ability to be fusion bonded to eliminate the need for adhesives or mechanical fasteners. Eliminating adhesives can reduce manufacturing steps and cycle time, improve joint quality, and drastically decrease manufacturing costs.

1.4. Elium® Poly Methyl-Methacrylate

Arkema's Elium® resin is a liquid at room temperature with viscosity ranging between 100 and 500 cPs. It is a two-part reactive system in which the liquid MMA monomer is combined with a peroxide initiator, to form a branched poly methyl-methacrylate (PMMA) [8]. In this study Luperox LP40 which has 40% by weight water content was used to help control the exothermic reaction that occurs with higher Luperox content shown in prior studies [9].

These resins are low-viscosity liquids (100–200 cPs) at room temperature and are suited to processing by liquid composite molding techniques using room-temperature tooling, which were once exclusively used for TS-FRP production. This technology has already been demonstrated through the production of components such as wind turbine blades [10] and structural automotive components [11]. Furthermore, the recyclability and thermoformability of these materials have also been demonstrated [12].

The properties of this infusible acrylic and its composites have been studied by many authors. These works have effectively established the knowledge base on the material's mechanical characteristics, with extensive efforts in characterizing tensile, compressive, shear, impact, and fracture toughness [13, 14]. Much applied research has been conducted on understanding the material's fatigue [15]; moisture diffusivity and marine ageing [16]; interfacial adhesion [17]; damage evolution and fracture behavior [18, 19] and even the effects of processing on properties [20, 21]. Moreover, the thermomechanical properties

of this acrylic family and their composites have also been studied by a number of researchers [22, 23]. The material properties of the Elium® are similar to those of an epoxy counterpart resin. Key values for neat Elium® resin is found in other literature and is summarized in Table 1.

Table 1: Material properties of neat Elium® 150 resin from Technical Data Sheet (TDS)

Material Property of neat Elium® 150 Resin	Tensile strength (MPa)	Tensile modulus (GPa)	Elongation at break (%)	Flexural strength (MPa)	Flexural modulus (GPa)	Lap Shear Strength of UD Composite (MPa)	Glass transition temperature (°C)
	76	3.3	2.8	130	3.2	22	120

1.4.1. Manufacture of a 9m Thermoplastic Composite Wind Turbine Blade

NREL demonstrated the first application of using Elium® reactive thermoplastic in the manufacture of wind turbine blades using VARIM [10]. The project successfully manufactured a 9m wind turbine blade that exhibited rapid cure times below three hours and energy efficient manufacturing methods. All components were cured at room temperature without requiring heat for curing, leading to significant decreases associated with the large energy requirements of thermosetting resin materials. The project also illustrated the successful VARIM manufacturing process, as well as the resin characterization of Elium®, including both mechanical properties as well as the drawbacks associated with the exothermic reaction that occurs during the polymerization process. Specifically, the reaction between Elium® resin and the Luperox peroxide initiator caused the temperature of the resin to increase to above the boiling point of the polymer causing voids and imperfections in the laminate or causing damage to the molds. NREL was able to mitigate this issue, especially common in thick sections of the turbine blades using an exothermic control additive that did not affect mechanical properties. One of the issues encountered by the NREL team was bonding the high-pressure and low-pressure skins to the shear web. The team had to sand and clean bonding areas with 50 grit sandpaper followed by cleaning with acetone. An epoxy adhesive was used to bond the three blade components, however if the process was to be scaled it would require a great deal of effort to prepare the areas to be bonded. One of the suggestions for future work was to determine

methods for thermal welding blade skins and components to eliminate the need for adhesive bonds leading to stronger, longer lasting blades.

1.4.2. *Prior Research on Fusion Bonding Elium® Thermoplastic Composites*

Due to the interest and recent advent of the liquid thermoplastic Elium®, there is a great interest in the study of bonding methods using this novel thermoplastic. Two studies were performed to investigate the potential for fusion bonding Elium® TPCs, one using resistance and induction welding techniques for applications in wind turbines and the other focusing on ultrasonic welding. At this time there has not been any published literature on fusion bonding Elium® using bulk heating as used in this study.

The preliminary study on fusion bonding Elium® thermoplastic composites [24] was performed by researchers at the National Renewable Energy Laboratory investigated induction and resistance welding on Elium® composite lap shear coupons for application in manufacturing wind turbine blades. The research gives a baseline value for lap shear strength values obtained from fusion bonded fiber reinforced Elium® joints as compared to adhesively bonded joints. The adhesives used were three methacrylate-based adhesives commonly used in the wind industry; Acralock SA10-60, Plexus 590, and Plexus 310. The setup used in the research for welding lap shear samples can be seen Figure 4: Welding Elium® Laminates; Induction (left) vs. Resistance Welding. The resistance welded joints tested four types of heating elements including stainless steel mesh, unidirectional, plain-weave, and biaxial carbon fiber heating elements, and the induction weld used plain weave as the heating element.

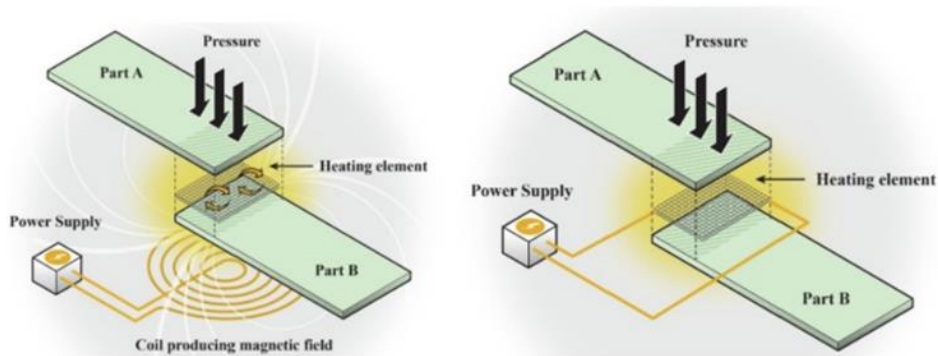


Figure 4: Welding Elium® Laminates; Induction (left) vs. Resistance Welding (right) from Murray [24]

This study first gave a comparison of static lap shear values obtained from ASTM D5868 between the adhesively bonded joints and the fusion bonded joints. The results from the static testing are shown below in Figure 5. The lap-shear strengths of fusion bonded joints were higher than the adhesive bonds by up to 100%. The highest average lap shear strength results of the adhesive joints were 17.4 MPa from the Plexus MA310 however the other two adhesives only achieved lap shear average below 10MPa. The fusion bonded joints performed much better on average, resistance values using the stainless-steel mesh in resistance welding achieved a value of 20.9 MPa. The fusion welded bonds using carbon fiber as the heating element depended on the type of carbon fiber used ranging from 19.7 MPa with FiberGlast UD and woven fabric while the bonds made with Vectorply biaxial carbon-fiber heating elements failed at an average of 22.5 MPa. The research then performed fatigue testing and recommended continued research on resistance welding and exploring failure mechanics with peel strength testing. At 10^7 cycles (defined stress for no failure), the fatigue limit for a fusion-welded sample was found to be 5 MPa as compared to 3 MPa in the case of the adhesively bonded sample displaying a much better fatigue response for fusion bonded sample than adhesively bonded samples [24].

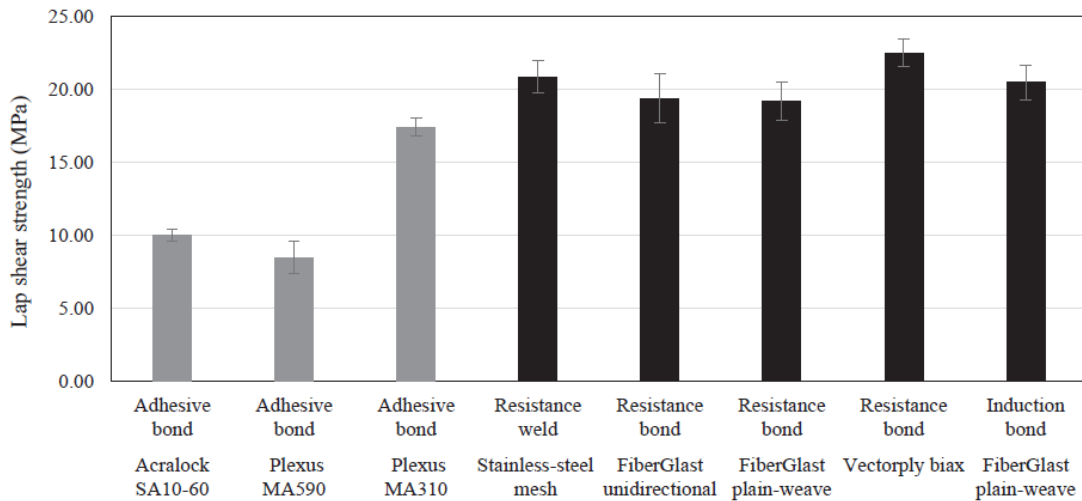


Figure 5: Lap Shear Strength of Adhesive, Resistance, and Induction Welded Elium® from Murray [24]

The second study [25] examining bonding properties of Elium® thermoplastic composites investigated the fatigue strength of ultrasonically welded composite joints using an integrated energy director

compared to a flat film of neat Elixir® resin. This research compared the static and fatigue response of US welded joints to a control of adhesively bonded joints and showed a 10-12% higher fatigue life at 10^5 and 10^6 fatigue cycles compared to the adhesively bonded joints. An important note to this research is that the research focused on the lap shear and fatigue values obtained from two different US welding configurations. As shown in Figure 6, the lap shear welding configuration either had an integrated triangular shaped energy director or a flat Elixir® film at the weld interface. The values at the right of the figure display the amount of additional neat resin available at the joint. After an optimization study with different welding parameters of weld time and weld pressure the integrated energy director produced a static Lap shear strength of $18.86 \text{ MPa} \pm 0.14$ whereas the configuration using film to increase the amount of resin at the bond interface obtained a LSS value of $14.04 \text{ MPa} \pm 0.01$. Again, the results of 14.2 MPa for adhesively bonded joints are similar to those obtained in other research. This study also illustrated that larger values that could be obtained by fusion welding with optimized parameters than with adhesive bonding.

	Configuration	Resin Volume (mm ³)
ELC_IED		150.7
ELC_FED (0.5mm ELF)		312.5

Figure 6: Ultrasonic welding configuration from [25]

1.5. Joining Methods of Thermoplastic Composites

Joining advanced composite components require careful consideration as they are a source of failure, increase manufacturing complications, and usually incur a weight penalty. However, it is often impossible to manufacture components without joints due to limitations on material size, assembly, or increased complications manufacturing joint free designs. Designers limit the number of joints when possible however quality joining methods can reduce manufacturing costs, ease assembly and obtain joint strengths equal to the materials being joined.

The most common methods for joining composite materials, as well as composite to metallic components are mechanical fastening and adhesive bonding. The use of thermoplastics composites allows the possibility of welding adherends, a process that is not possible with thermosetting polymer matrix composites. However, in all situations careful consideration must be taken based on the application and parent material composition [26]. Figure 7 shows the basic hierarchy of joining methods for polymeric materials. The process used in this study is highlighted in red.

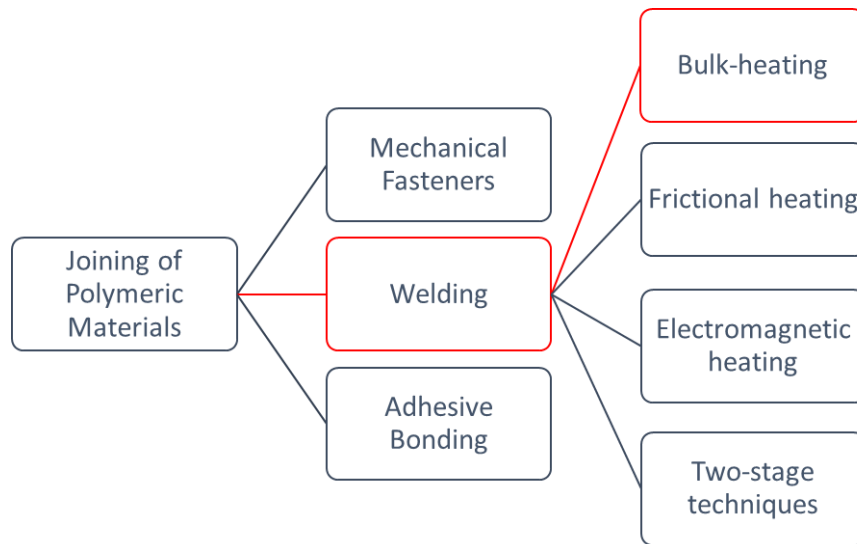


Figure 7: Joining Methods of Polymer Matrix Composites

Unfortunately, some issues appear when fusion bonding techniques are applied to continuous fiber reinforced thermoplastic composites. This is especially true in the case of high fiber volume fraction composites. Among the issues most mentioned in the literature are uneven heating, delamination, and distortion of the laminates [27], as well as a low amount of resin available to melt and reconsolidate into a fused bonded joint [28].

1.5.1. Mechanical Fasteners and Adhesive Bonding

Mechanical fasteners and adhesive bonding are the most common method of joining of polymeric composite materials, however issues with structural integrity due to localized stresses in the joint area requires additional considerations [28]. The goal in any joining operation is to have the joined area be as strong or stronger than the adherends or parent materials. When joining composite materials this becomes

a huge challenge because of stress concentration, the effects of drilling on the structural integrity, and localized delamination. Mechanical fasteners also allow water intrusion into the composite, are a source of galvanic corrosion, increase the weight of the system and require extensive time and labor for drilling hole locations. [27] In contrast, poor bonding properties between adhesives and polymers make adhesive bonding methods less desirable for most structural applications. Most wind turbine blades today are manufactured with two mold halves and then bonded together. This requires having to join areas such as the leading and trailing edges, web, and spar cap joints. This is not only a time-consuming process it inherently introduces stress concentrations and areas of weakness into the manufactured blade. With the complex curvature along the blade section, bonding this line becomes increasingly complicated and the stresses found in adhesively bonded joints is complex. The use of commercial additives requires special surface preparation, in turbine blades this includes sanding of the high pressure and low-pressure skins to achieve a uniform surface and increase contact area as well as additional surface pretreatments such as cleaning and degreasing to improve interfacial bonding. This is a major area of concern as there are many forms of contamination from release agents, bagging materials, and machining oils which makes surface preparation very difficult to control in an industrial environment. Coupled with the long curing times of traditional thermosetting adhesives, adhesive bonding becomes another time-consuming process. With the advent of thermoplastic turbine blades the joining process can be improved with methods of fusion bonding resulting in a higher quality and faster manufacturing process.

1.5.2. *Welding and other Methods of Fusion Bonding*

Fusion bonding is one of three distinct categories of joining methods for polymeric materials that also includes mechanical fastening and adhesive bonding. Fusion bonding itself can be divided into several subdivisions based on the method of heat generation mechanism at the bondline [1]. The four classes include bulk-heating, frictional heating, electromagnetic heating, and two-stage techniques [2]. Bulk-heating was the process used in this study and is an ideal joining method since no weight is added to the structure, the bond strength is potentially equal to the parent material and it requires little surface

preparation [2]. However, it does require that the entire thickness of the area being bonded must be brought to high temperature, whereas the other methods of heat generation only the interface is the only area brought above T_G . All methods of fusion bonding neat thermoplastics or thermoplastic composites (TPC) utilize the principal of heating a polymer (or polymer matrix in a TPC) above T_G at the interface to create a viscous state, then by applying pressure and bringing the bonded surfaces together polymer chains can entangle, and upon cooling form a bonded area of entwined polymer chains in a process called autohesion [29]. Thus, the main goal of fusion bonding is to produce a monolithic structure by the combination of intimate contact and molecular interdiffusion healing [30]. The consolidation process at the polymer interface which was first described by Wool et al. in five sequential stages of (1) surface rearrangement (2) surface approach (3) wetting (4) diffusion and (5) randomization [31].

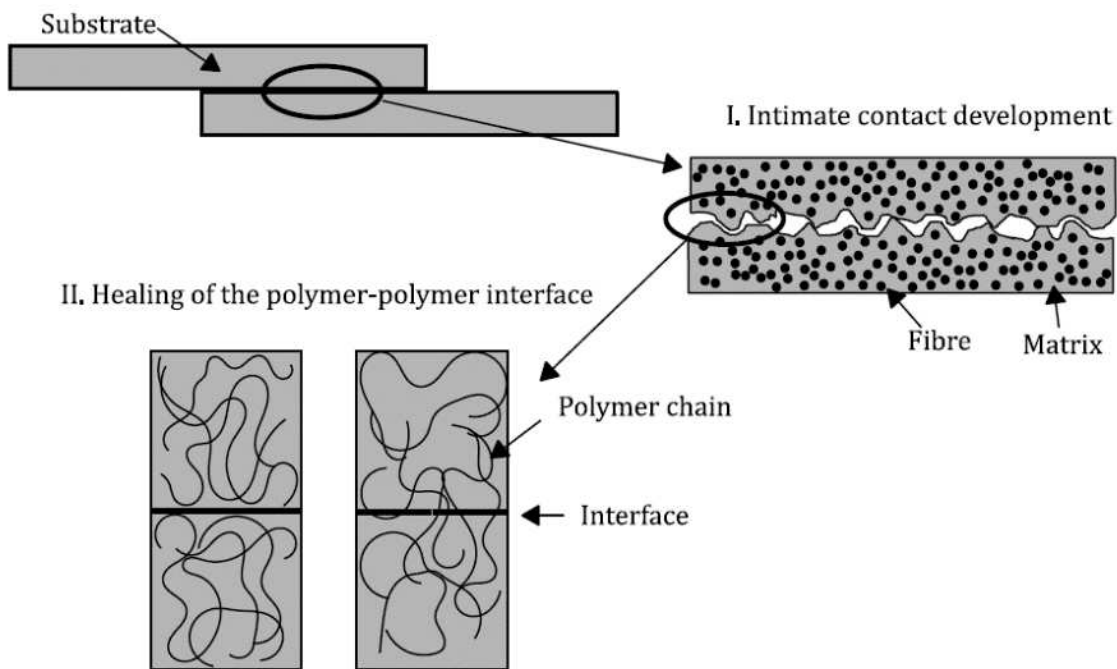


Figure 8: Fusion bonding process of thermoplastic composites displaying the five sequential stages as described by Wool. Figure Adapted from [27] and [32]

Stages 1-3 characterize the concept of intimate contact, where due to the heat and pressure surface asperities in the interface are allowed to spread resulting in a large contact area and combined with the high temperature of the polymer interdiffusion of polymer chains can occur in a process referred to as healing evident in stages 4 & 5 [33, 34]. This process is illustrated above in Figure 8.

1.6. Factors Impacting Quality of Bonded Joints

One needs to consider the microstructure of the fusion bonded interface. It does not only involve the degree of bonding, comprising intimate contact and healing, but also other structural features such as fiber-matrix distribution, contamination of the bondline, degree of crystallinity of the matrix, residual stresses, void fraction and degree of polymer degradation [35].

From a physical viewpoint, the fusion bonding process involves intimate contact development between the two surfaces (also known as wetting), followed by interdiffusion of polymer chains across the interface (also known as healing) [36]. Proper wetting may be a challenge for thermoplastic composites with a high fiber volume fraction due to the lack of matrix material at the interface; this may result in poor bond performance [28]. To solve this problem, some welding techniques may require such an additional resin layer at the in order to promote wetting, [37]. For example, a resin layer is added as an energy director in the case of ultrasonic welding [36]. This additional layer of pure polymer may lead to a matrix rich bondline which in turn may affect the joint performance. A proper understanding of the interrelation between the matrix rich bondline thickness and the joint performance is required to enable optimization of the joint design [38].

1.6.1. *Bondline Thickness*

The effect of a polymeric matrix-rich layer at the interface between the two substrates on the mechanical performance has been widely studied for adhesively bonded metallic and composites substrates [27, 28] as well as with composites using a thermoplastic or thermoset interleave where a layer of neat thermoplastic resin is inserted into the bondline prior to consolidation pressure being applied [39]. The prior research proposed the interlaminar fracture toughness has a tendency to increase with an increase in matrix-rich bondline thickness [35]. The effect of interleaving thickness on single lap shear strength, mode II fracture toughness, and mixed mode fracture toughness was also studied in the past suggesting more plastic energy dissipation before fracture occurs. In the aforementioned cases, the mechanical performance tends to improve with increasing interleaving thickness until reaching a plateau where the

mechanical performance is insensitive to any further increase of the thickness of the matrix-rich layer and tensile strength decreases as a result of the matrix rich layer [35].

Other research has suggested a matrix-rich bondline at the interface may be generated dependent on the nature of the manufacturing process used to manufacture the composite or the bonding parameters, such as a two stage process where additional matrix is interleaved in between adherends compared to a fusion bonding process where no additional materials are added to create the bonded region [40]. It has been observed that an increase in matrix interface thickness allows for a larger plastic yielding zone, resulting in a higher interlaminar fracture toughness. The relationship between the matrix-rich bondline thickness and the interlaminar fracture toughness was studied for unidirectional Carbon/PEEK fusion bonded laminates with different matrix-rich bondline thicknesses. A higher interlaminar fracture toughness was observed when the matrix-rich bondline thickness increased and the value was almost doubled with respect to that of the parent material when an approximately 200 μm -thick resin film was added to the bond interface [35].

1.6.2. *Surface Roughness and Waviness*

Two factors that were investigated in this study were the effects of roughness and waviness in the process of fusion bonding thermoplastic composites. Surface texture is the deviation from the nominal surface that forms the three-dimensional topography of the surface. Surface texture includes (1) roughness (2) waviness, (3) lay, and (4) flaws. Figure 9 is a pictorial display of surface texture with unidirectional lay. The red line in the figure illustrates roughness, which is formed by fluctuations in the surface of short wavelengths, characterized by hills (asperities) (local maxima) and valleys (local minima) of varying amplitudes and spacings. Asperities are referred to as peaks in a two-dimensional profile or summits in a three-dimensional surface map. Waviness as illustrated by the blue line is the surface irregularity of longer wavelengths. Waviness in manufacturing settings may result from such factors as machine or workpiece deflections, vibration, chatter, heat treatment, or warping strains. Waviness includes all

irregularities whose spacing is greater than the roughness sampling length and less than the waviness sampling length. Lay is the principal direction of the predominant surface pattern, determined by the production method, in the manufacture of composites in this study the lay would be classified as the direction of resin infusion. Flaws are unintentional, unwanted interruptions in the surface texture caused by air bubbles and voids created in the infusion [41]

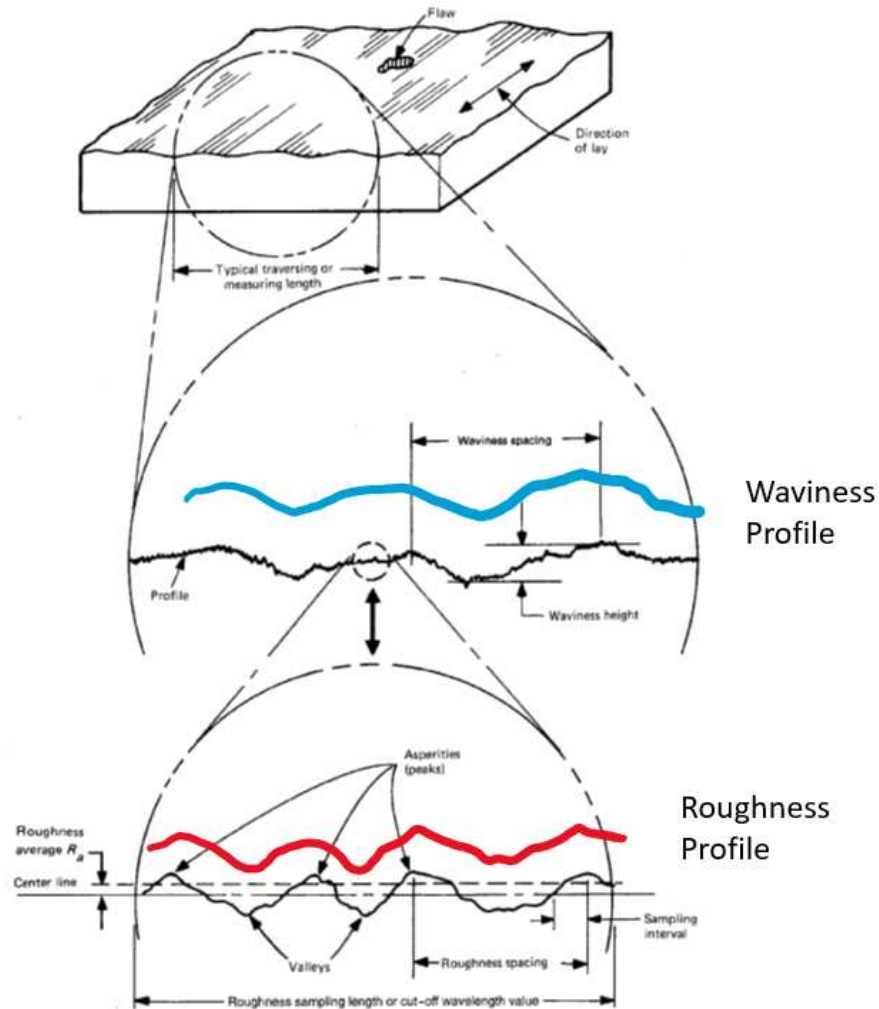


Figure 9: Pictorial Display of Surface Texture adapted from [41]

Surface roughness most commonly refers to the variations in the height of the surface relative to a reference plane typically defined as the center line. It is usually characterized by one of the two statistical height descriptors advocated by the American National Standards Institute (ANSI) and the International Standardization Organization (ISO). These are i) R_a and ii) the standard deviation or variance (σ). R_a is

the universally recognized, and most used, international parameter of roughness. It is the arithmetic mean of the absolute departures of the roughness profile from the mean line. The standard deviation (σ) is the square root of the arithmetic mean of the square of the vertical deviation from the mean line and is normally used for statistical analysis of surfaces where R_a is an official standard in most industrialized countries to give adopted roughness grade numbers. Additional measures of surface roughness are extreme-value height descriptors. Four other extreme-value height descriptors in limited use, are: R_p , the maximum peak height from mean, R_v , the maximum valley depth from the mean, R_z the average peak-to-valley height, and R_t is the maximum peak-to-valley height or simply P-V distance and it is the most common [41].

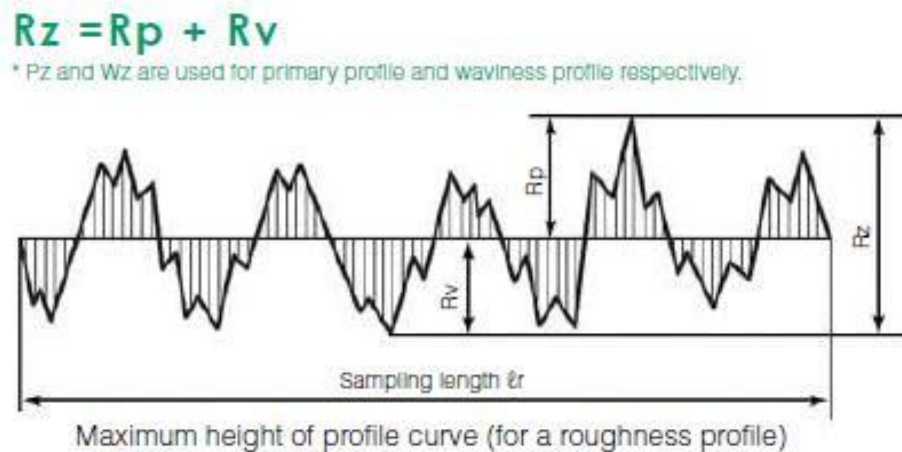


Figure 10: Roughness Profile Curve Terminology [42]

Various instruments are available for the roughness measurement. The measurement technique can be divided into two broad categories: (a) a contact type in which during measurement a component of the measurement instrument contacts the surface to be measured; and (2) a noncontact type. A contact type method uses an instrument that amplifies and records the vertical motions of a stylus displaced at a constant speed by the surface to be measured. The stylus is mechanically coupled most commonly to a linear variable differential transformer (LVDT), an optical or a capacitance sensor. The stylus arm is loaded against the sample and either the stylus is scanned across the stationary sample surface using a traverse unit at a constant speed or the sample is transported across an optical flat reference. As the stylus

or sample moves, the stylus rides over the sample surface detecting surface deviations by the transducer. It produces an analog signal corresponding the vertical stylus movement. This signal is then amplified, conditioned, and digitized. Optical measurements include but are not limited to confocal microscopy, focus variation microscopy, electron microscopy, and photogrammetry [43, 41].

The effect of surface roughness was modeled and studied by Lee and Springer [32] which modeled surface asperities as a series of rectangles. Using the laws of conservation of momentum to model the flattening of rectangles and assuming laminar flow they devised equations used to determine the extent of the flow occurring at the interface. Via modeling and empirical data found by measurements obtained with surface profilometry Yang and Pitchumani [33] found a correlation between the surface roughness and the time it takes to reach intimate contact. They stated that since tall narrow asperities spread quickly the governing factor was the widest ratio (h/w) asperities took the longest to flow and thus consolidation took longer to achieve. Surface roughness has been thoroughly studied for adhesive bonding and it has shown that increased surface roughness increases mechanical interlocking of adherent and adhesive [44] however there has been little research performed on the effect of surface preparation on fusion bonding using bulk heating as much of current research has investigated surface energy or contamination from consumables while performing vibration welding techniques . With the advent of liquid thermoplastics such as Elium®, a new opportunity arises to investigate the relationship between fusion bonding and surface textures created from infusion processes consumables with the goal of minimizing the need for additional surface preparation and processing to achieve high quality bonded joints.

1.6.3. Surface Contamination and Chemistry

One of the most studied areas of bonding research has been performed on various methods of surface preparation and methods of reducing contamination at the bondline that creates voids and prevents quality bonds from being achieved. Contrarily to adhesive bonding, which involves careful treatment of the surfaces to be bonded [45] fusion bonding is claimed not to require any special surface treatment other than degreasing since the thermoplastic matrix melts during the process [27]. However, the release media

used to treat the molds for forming and consolidation of thermoplastic composites can potentially leave contaminants on the surfaces, which will be trapped in the bondline during the fusion bonding process. Sachetti found the presence of release media contaminants on the surface of UD Carbon/PEEK substrates can have a significant detrimental effect on the toughness of the resulting joint; the interlaminar toughness was found to be reduced by more than 60 % in the worst case [46] Thus, contrary to popular belief as often mentioned in literature, surface contamination can greatly influence the mechanical performance of welded joints in thermoplastic composites.

1.6.4. *Adhesive and Cohesive Failure*

The aim of composite joint design is to design a joint to fail by bulk failure of the adherends. A margin of safety is generally incorporated in the design to account for factors, such as service environment, type of loading, degree of control in adhesive application, etc. It is important to ensure that the adhesive is not the weakest link. For composite adherends, failure is often observed to occur in the near surface plies of laminate materials. This is due to the low toughness associated with the thin resin layer present at the surface of these materials. Considerable care needs to be taken to ensure that the thin surface resin layer does not become the weakest link. The aim of designing adhesive joints is to maintain the adhesive in a state of shear or compression. Bonded joints are strongest under these loading conditions. Tension, cleavage or peel forces should be avoided, or their effect minimized. The presence of the stresses will compromise joint strength and fatigue performance. Structural adhesives have relatively poor resistance to through-thickness (peel) stresses, and therefore to obtain maximum efficiency, joints need to be designed to minimize tensile stresses. For composite laminates, resistance to peel stresses may be considerably lower, so even greater care must be taken with these materials to minimize these stresses. Adhesive failure is the rupture of the adhesive bond, such that separation occurs at the adherend/adhesive interface. Interfacial failure is one of the lowest shear strength failures, as it indicates that the adhesive was not bonded well to the adherends. This form of failure can result from either inadequate surface treatment or material mismatch such as voids or bubbles inside the adhesive layer during the

manufacturing. Information on interfacial strength, although qualitative, is normally obtained from adhesive joint tests (i.e. lap shear). The term “interface” is used for the layer of material bordering the adherend and adhesive, which encompasses the true interface, the interphase and the near surface area. Cohesive failure occurs when the load exceeds the adhesive strength. This tends to be a localized effect, occurring near stress concentrations (ends of joints). In laminate materials, this form of failure generally initiates from the matrix between layers as a result of out-of-plane tensile or interlaminar shear stresses [47]. Cohesive failure is characterized by the failure within the adhesive, typically through its thickness. This type of failure suggests that the bond between the adherends and the adhesive is stronger than the adhesive strength itself. Finally, adherent failure (coupon failure) is characterized by the failure of the adherent, which indicates that the adhesive is stronger than the adherents and therefore typically comes with high-strength bonds. The type of macroscopic failure mode is identified by observing the adherend fracture surfaces [24]. ASTM D5573 - Standard Practice for Classifying Failure Modes in Fiber-Reinforced-Plastic (FRP) Joints gives the definitions used for classifying failure modes and representative failure modes are show below in Figure 11.

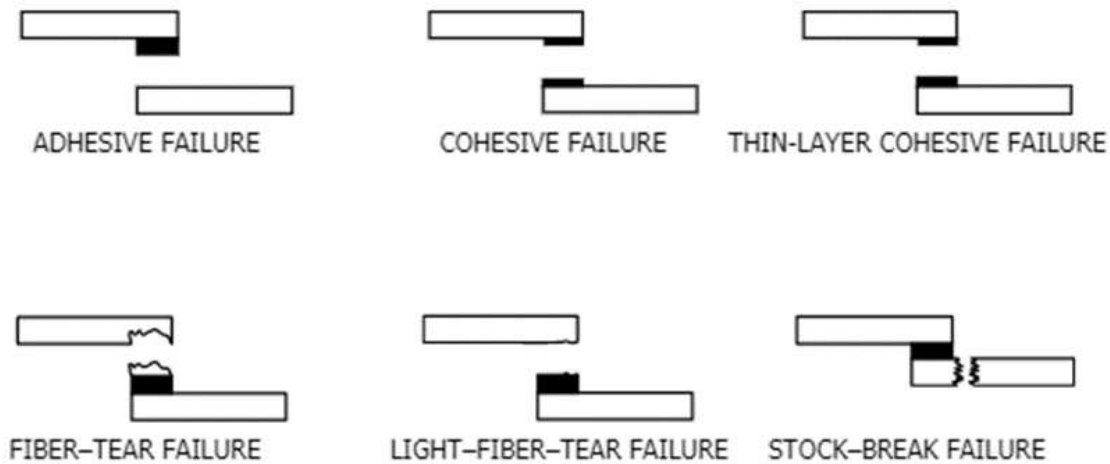


Figure 11: ASTM Standard Practice for Classifying Failure Modes in Fiber-Reinforced-Plastic Joints

1.7. Steelhead VAWT With Thermoplastic Composite Blades Study

Daedalus Composites, a producer of high-end, zero emission yachts partnered with Steelhead Composites to investigate the feasibility of producing a small scale VAWT for installation on their vessels. Since

wind power is not the primary source of energy on ship, there was increased importance on aesthetics, low noise, small form factor, and power generation at low wind speeds. With funding and guidance from the Institute for Advanced Composite Manufacturing Innovation (IACMI), Steelhead Composites, Colorado State University, National Renewable Energy Laboratory (NREL) and Arkema Inc. collaborated to perform the techno-economic evaluation to provide a cost basis to evaluate different technologies and then to develop and fabricate the VAWT rotor assembly [48]. IACMI solicits and selects project proposals that advance the nation's energy and economic security by sharing existing resources and co-investing to accelerate research and development innovation with advanced composites. IACMI projects validate manufacturing technologies to respond to private industry's need for faster and more cost, material, and energy-efficient composite manufacturing, including recycling and the end-of-product life [49]. The major goal of the technical collaboration was to demonstrate the design and manufacture of a VAWT rated between 0.5 and 1 kW using thermoplastic reinforced composites. Colorado State was primarily concerned with developing a manufacturing strategy as well as examine the potential thermoplastic resin systems have in transforming the way VAWT rotor assemblies are constructed by utilizing thermally welded joints. These thermally welded joints enable lower cost manufacturing, allow blades to be joined both in the factory and in the field, and can increase reliability by eliminating mechanical fasteners or adhesively bonded joints. The infused composite blades manufactured during this program are an excellent example of these benefits made possible by the Arkema thermoplastic resin system and demonstrate the potential of recyclable blades to combat issues with end of life uses encountered with thermosetting blades.

1.7.1. *Project Objectives*

To that end, an investigation was undertaken into the application of post-process deformation in the manufacture of 'C'-shaped blades, starting from straight, hollow, resin infused airfoils. In addition, this work investigates the deformation of the airfoil at the transition to the hub plate attachment and the joining of the airfoil to the hub plate bracket. Ultimately, the findings were intended to provide the

groundwork to inform decisions for larger scale manufacturing techniques applicable to a broader VAWT commercialization strategy.

1.7.2. Motivation for Elium® Joining Study in VAWT Application

After the previous work of NREL using Elium® thermoplastics it was evident that using thermal bonding techniques to join thermoplastic composites is far superior than to using adhesives. The benefits to using thermal bonding techniques over adhesives include drastically decreasing the required preparation as well as faster manufacturing times and higher quality bonded joints. This study focuses on identifying the best surface texture for heat welding created by consumables used in the resin infusion process. The ability to bond the airfoil spar to root hub bracket was the primary joint this research focused on. These brackets can be seen in blue in the figure below. An additional benefit to this study was also if the team could not successfully thermoform the 90° bends in the airfoil the contingency plan would be to manufacture composite Wing-To-Strut brackets seen in yellow in Figure 12 below and bond the brackets in place to create the bend in the airfoil.

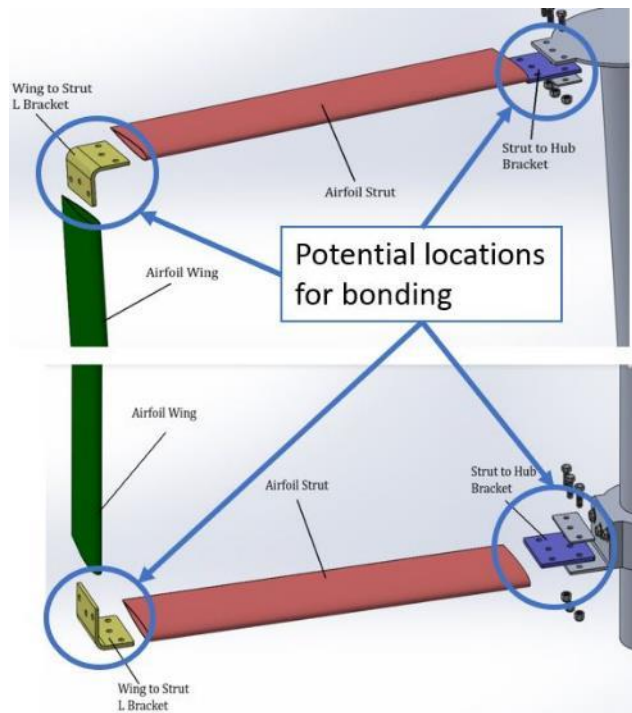


Figure 12: Potential locations for fusion bonding in initial VAWT Design

The method for attaching the blades to the root hub was specified by Steelhead Composites to be a three-bolt pattern that allowed the blade sections to be attached to the rotating hub at the two Strut to Hub brackets seen in Figure 12 and again in the updated CAD model that included the fusion bonded blade to root hub bonded joints seen in Figure 13.

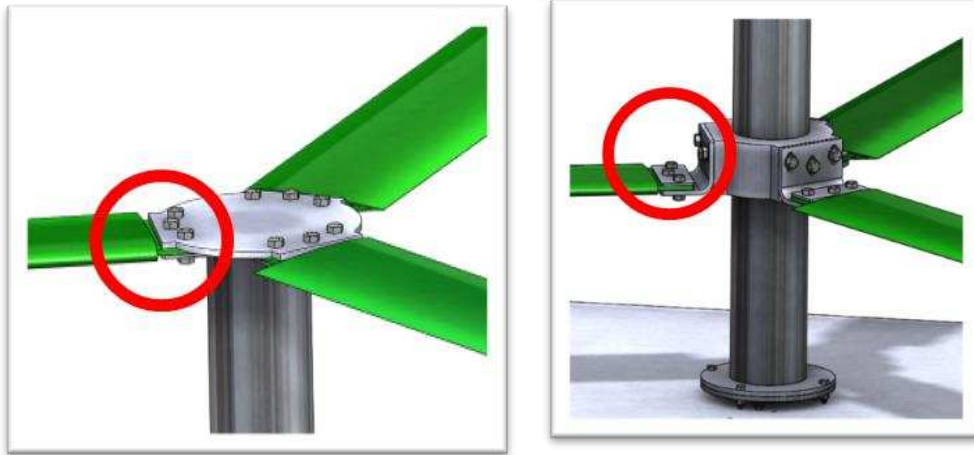


Figure 13: Upper and lower airfoil blade strut to hub attachment points

The original plan for mounting the blades to root hub was a metal mounting bracket that was to be inserted into the airfoil and the airfoil would be attached using traditional mechanical fasteners, the holes for which can be seen in Figure 14.

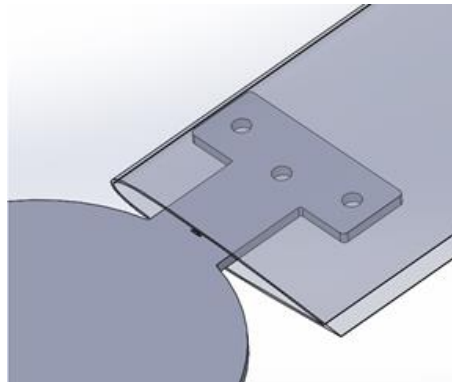


Figure 14: Baseline rotor assembly with metal mounting bracket detail

It was evident that this method greatly increased stress concentrations due to the mechanical fasteners as well as bearing loads where the blade would rest on mounting bracket. Additional reinforcement would likely be necessary to support the loading conditions and decrease the likelihood of failure in the region. This would have caused greater difficulty during manufacture since thickness throughout the blade was

designed to be constant for manufacturability. In order to replace the T-shaped blades in Figure 14 experiments were carried to evaluate the effectiveness of fusion bonding via heat welding Elium® composite plates to the VAWT which then could be bolted to the hub assembly. The feasibility of this was evaluated by first bonding lap shear coupons to validate bonded joint strength and these values were used to estimate the required bond area in the full-size assembly.

1.8. Research Hypothesis

With the objectives specified by Steelhead Composites and the lack of published literature on fusion bonding Elium® thermoplastics, there was a need to further investigate the feasibility of manufacturing a hollow airfoil with a high aspect ratio and increase the knowledge on the process of using bulk heating to fusion bond structural components of thermoplastic Elium® composites. With the information presented in prior literature finding that additional matrix material at the bondline improves bond quality and as Elium® is manufactured using a liquid molding technique such as a resin infusion, the question arose if the consumables used in manufacturing fiber reinforced Elium® thermoplastic composites via resin infusion could contribute to higher bond quality. Specifically, how could the use of different consumables that provided varying degrees of additional matrix at the bondline affect and the effect of surface roughness produced by consumables effect the quality of bonded joints? The research objective of this project was to address the hypothesis that utilizing infusion consumables that increased the amount of neat resin at the bondline would improve the quality of bonded joints and thus would allow the team to manufacture the Steelhead VAWT blades from entirely out of carbon fiber reinforced Elium® laminates providing a higher quality end product than adhesively bonded sections of airfoil or mounting brackets.

1.8.1. Research Approach and Methods

The method for answering the research hypothesis and the completion of the IACMI/Steelhead project were addressed in conjunction. The preliminary task of the VAWT project was to demonstrate the ability to use resin infusion molding to create a hollow, carbon fiber reinforced airfoil section using Elium® thermoplastic material. The assembly potential of fusion joining and post process deformation could be

evaluated only if blade manufacturing was successful, therefore this document will cover briefly the manufacturing process of the airfoil blade since it was a crucial aspect of manufacturing samples to test fusion bonded joints. This will cover the early vacuum assisted resin infusion molding (VARIM) approach taken to manufacture 32” airfoil blades, the evolution of consumables used to successfully manufacture blade sections and the issues encountered when manufacturing early blade sections. It will then cover the successful manufacturing of 64” blades with glass blades and then the transition to manufacturing with carbon fiber. After manufacturing blades successfully, it was then possible to experimentally address the research hypothesis of factors contributing the strength of fusion bonded joints. The ASTM 3528 Standard Test Method for Strength Properties of Double Lap Shear Adhesive Joints by Tension Loading [50] was used to evaluate quantitatively the strength of a fusion bonded joint with a geometry similar to that would be found in the bonded airfoil attachment brackets. This document then describes the testing and nomenclature related to ASTM 3528, the manufacture of double lap shear (DLS) laminates to be bonded and then characterizes the surface roughness produced with varying consumables of the adherends prior to being bonded. After samples were characterized the method of compression molding sample coupons and various processing parameters are detailed. The results of this research were then obtained by tension loading ASTM 3528 samples for strength data, by analyzing failure methods and surfaces, and then with microscopy imaging to investigate and qualitatively correlate the visual quality of the bonds to data obtained in strength data testing. With strength testing data, failure analysis trends and microscopy information results could be discussed and correlations between additional matrix at the bondline and surface roughness could be determined. Having the information obtained from lap shear testing of the laminates the overarching VAWT turbine project was able to proceed with full scale manufacture of 3.4-meter blades, thermoforming the C-shaped blade sections, and fusion bonding the blade to root hub attachment points to complete the manufacture of the prototype. Additional conclusions are addressed in the final section that review the benefits of manufacturing the blade via resin infusion, the success of fusion bonding assembly methods with Elium®, the effect of surface roughness on bond quality and recommendations for further study.

2. EXPERIMENTAL MANUFACTURE OF VAWT BLADE PROTOTYPE

This section reviews the process undertaken to manufacture turbine blade sections that would then be used to investigate the feasibility of fusion bonding experimentation. The following details the blade geometry that was selected by Steelhead Composites and how it was selected, then discusses the process that was undertaken to achieve repeatable quality results in manufacturing blade sections. The manufacturing process is documented as well as the evolution of consumable materials and issues encountered by the team during manufacturing that needed to be overcome to continue to full scale assembly. This section concludes with the transition from 32” molds to 64” molds and the transition from glass fiber reinforcement to that of carbon fiber reinforcement that would be used in the final VAWT prototype.

2.1. Blade Geometry and Selection

The blade geometry was selected by Steelhead Composites with guidance from the National Renewable Energy Laboratory. After comparing the NACA 0012 and 0015 blade profiles the NACA 0015 was selected due to the higher power coefficient produced at various tip speed ratios (TSR) calculated via CFD and FEA analysis by NREL and Steelhead. NACA 0015 with a 6” chord length gave a height of .72” which was a major factor in the method of manufacture and for determining ply layups to meet performance requirements of less than 2” deflection during constant wind speeds of 60 mph.

2.2. Early VARIM Manufacturing Process

It was decided early in the project to manufacture the VAWT blades as hollow, high aspect ratio sections and this directed the team to manufacturing via a resin infusion process using a Vacuum Assisted Resin Infusion Molding (VARIM or RIM) process. This process has been traditionally used with liquid thermosets to create high volume fraction advanced composites, however with the advent of the infusible reactive polymer Elium®, the team was able to attempt to manufacture a thermoplastic blade to meet goal

for recyclability and experiment with fusion bonding and post process bending to create the desired C shape. The infusion and vacuuming bagging process can be seen below in Figure 15 which from left to right illustrates the resin inlet and outlet, initially using a semi-permeable membrane Dahlpac shown in blue and spiral tubing with red resin flow media on both sides of the airfoil. The next image shows the inner vacuum bag setup and mandrel used to position consumables including peel ply and dry fiber within the mold, the third image shows the preform in mold, while the fourth and fifth images show the fully bagged mold, and airfoils after demolding.



Figure 15: Initial manufacturing process to infuse a 32''-long hollow airfoil cross section

The preform has a resin inlet at the top and an outlet on the bottom, where both the inlet and the outlet run the length of the mold. The outlet material (Dahlpac - blue) is a semipermeable membrane that allows air to flow through while preventing resin from leaving the system. The mold is envelope bagged with an inlet on one side and the outlet on the other side of the mold. The resin flows down the length of the inlet, wetting out the top of the preform before flowing radially around the mold to the outlet.

2.3. Evolution of Manufacturing Process and Infusion Consumables

Many trials using different expendable materials and process techniques were attempted by the CSU team before a final process was defined that resulted in good repeatability and successful part infusion. While infusing the blade sections there were five specific variables altered to control the infusion. This included: i) the resin inlet and outlet material type ii) resin inlet and outlet location iii) flow media type iv) lateral

break zones in infusion materials and v) lengthwise break zones of infusion materials. Figure 16 illustrates the concepts described in the evolution of the infusion process. In this approach the inner tubular plastic vacuum bag (c) is placed over a simple flat plastic mandrel (b) and the infusion consumables (d) including flow media, a resin inlet, and a vacuum outlet are positioned on the inner bag. The fiber reinforcement (e) is wrapped around the infusion consumables and then placed in between the upper and lower clamshell style mold halves. Another larger tubular plastic vacuum bag is pulled over the mold and sealed to the inner bag, resulting in an envelope bag that consolidates the fibers to the inside mold surface and holds the mold halves together. Additional variables that were considered were the leading and trailing edge break zones (f) illustrated by the red regions in Figure 13 as well as lengthwise break zones along the length of the mold.

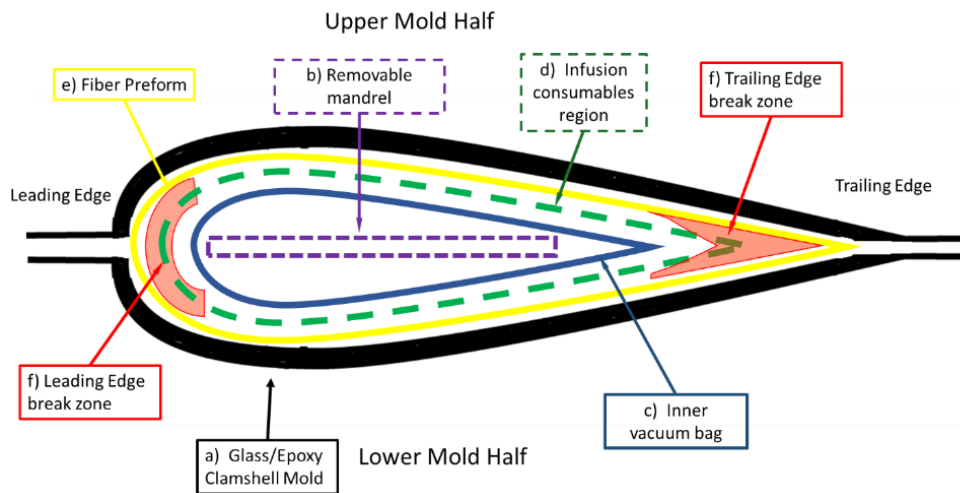


Figure 16: Schematic of material placement and infusion terminology

During initial manufacturing trials the team encountered multiple issues that caused difficulty producing the desired quality airfoil. The first challenge was positioning the mold halves to correctly orient the preform within the mold. This caused the preform to get pinched within the mold halves which created dry spots along the leading or trailing edge or excessive resin flash between the molds. This problem was mitigated by using bolted connections as well as a rubber gasket in between mold halves to prevent flashing.

The next and major challenge was obtaining a quality composite part that was free from defects and dry spots in the laminate. The team went through multiple iterations and varied things such as inlet and outlet material, the location of the inlet and outlet, as well as the leading and trailing edge break zones illustrated in Figure 16. The evolution of material placement and locations can be seen in Figure 17 with the black outline representing the dry fiber placement and the infusion consumables placed inside. To begin the study first infusions used traditional high-density polypropylene grid infusion flow media (shown in red). Flow media is highly permeable compared to the fiber that it is trying to impregnate, and it aids in moving resin throughout the dry fiber. However, it was determined that the flow media needed to be restricted in some areas for without break zones along the leading and trailing edges the resin had free flow to travel along the length of the mold due to the lower permeability in these areas which did not allow significant time for the fiber in other sections of the airfoil to wet out. As the process evolves in Figure 17 it can be seen that break zones along the leading and trailing edges were necessary to prevent resin from racing along the edges.

Another development in early trials was the location of the resin inlet and vacuum outlet had a major effect on the composite quality. Early iterations had the inlet on the lower mold surface as seen in Infusions 1-4. It was eventually realized after experimenting with having the inlet placed at the leading edge seen in infusion 5 that the best results were obtained from placing the inlet on the upper mold surface. As for the vacuum outlet the placement was originally on the upper mold surface and the team used both flow media wrapped in peel ply (Infusion 1) as well as spiral tubing wrapped in peel ply (Infusion 2). However these methods allowed excess resin to escape the composite before the entire part was wet out so the switch to Dahlpac MC79, a semipermeable membrane shown in blue in Figure 17, first used in Infusion 4 that allowed air to flow through the part while preventing resin from leaving the system and gave better fiber wet out throughout the entire part. The location of the Dahlpac was varied, again beginning on the upper mold half, but eventually the best results were obtained with the Dahlpac located on the lower mold surface with the resin infusion inlet on the top seen in Infusion 6.

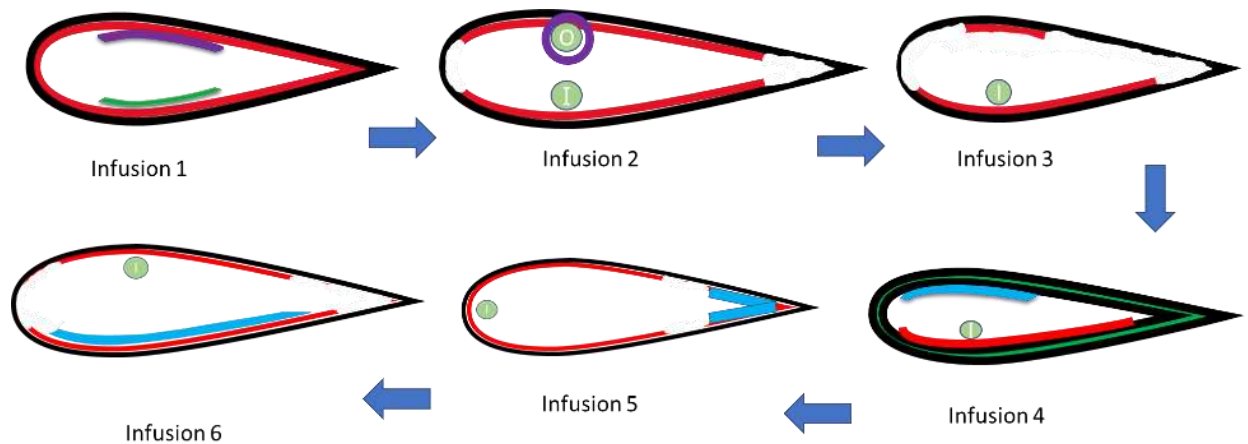


Figure 17: Evolution of infusion material placement and consumables

The initial manufacturing approach, shown in prior images produced a glass fiber reinforced Elium® composite with a hollow airfoil cross section; however, this process was inconsistent and large dry spots along the leading and trailing edges were commonly observed. The limited repeatability of this process was attributed to poor control of the position of consumables and unintended pleating of the inner vacuum bag and peel ply. The team began the study using spiral tubing coupled with peel ply and polypropylene infusion flow media however the resin distribution was uneven, the inlet tube often and other consumables were shifted when vacuum pressure was applied to the inner bag and it was difficult to nearly impossible to remove from consumables from the part after infusion due to the relatively high release force of the peel ply as well as consumables becoming physically trapped along the trailing edge.. The use of Dahlpac semi-permeable membrane drastically improved the manufacturing process and provided enough evidence that the team needed to begin using simpler consumables specifically designed for infusion. Additionally, it was also necessary to scale up to larger 64” molds for the 32” mold did not provide enough information to test to the scalability of the process to ultimately be able to infuse blades up to nearly 12 feet long.

2.4. Transition to 64” Mold

Initial trials of the 64” mold began to focus on reducing the number of consumables as well as the complexity required through the implementation of infusion-specific materials. Removing the inner bag

and the two strips of flow media was one of the most challenging aspects of processing due to the size of the blade and tooling. The greatest breakthrough came with the use of Compoflex® RF3, a combination of distribution media and peel ply that greatly simplified the manufacturing process as it reduced the number of consumables required, replacing both the peel ply and polypropylene flow media used prior. The team additionally switched to EnkaFusion Filter Jacket, a three-dimensional "V" shaped nylon mat core encased in a thermally bonded, nonwoven polyester sock designed specifically for resin infusion that allows for maximum resin infiltration and ensures even resin distribution. Dahlpac MC79, shown as the blue strip in Infusions 4-6 in Figure 17, as well as in Figure 18 was chosen for the vacuum outlet as it has a low profile and prevents resin from flowing out of the system while maintaining vacuum throughout the infusion. Jacketed Enka fusion, shown as the green strip in Figure 18, was determined as the preferred resin inlet material due to its low profile which increased the available space inside the airfoil and reduced the effort required to remove the consumables. Additionally, the Compoflex® had a much lower release force than the previous peel ply, facilitating the removal of the consumables. Figure 18 shows the final infusion consumables selected after successfully infusing 64" molds.

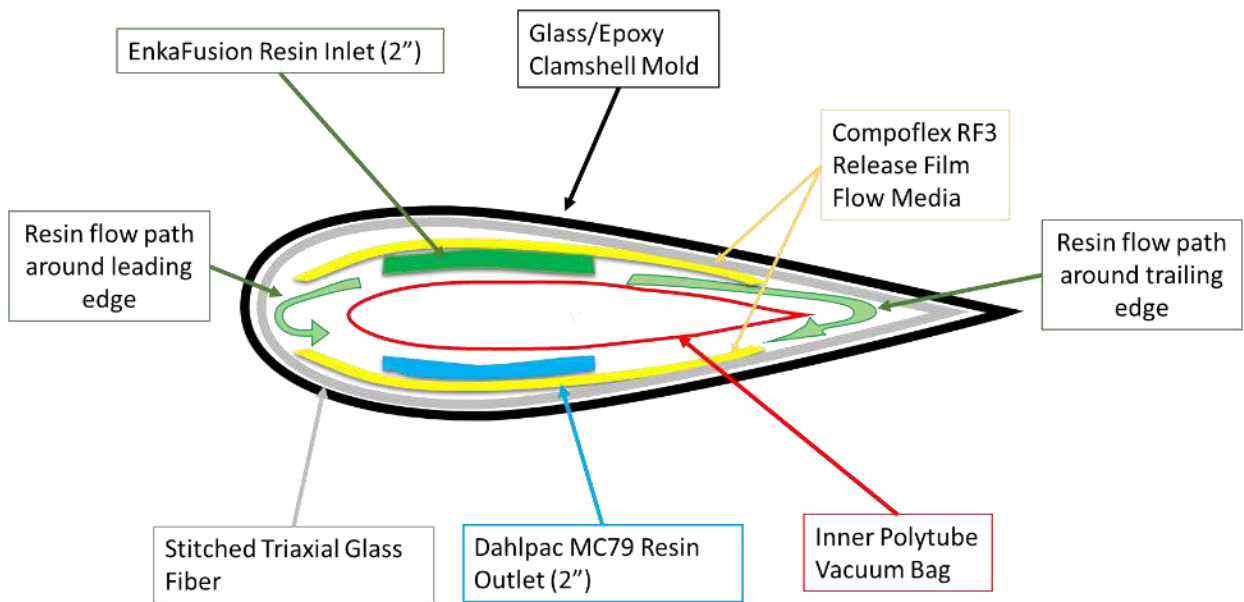


Figure 18: Cross section view of consumable materials for infusion

Additional variables that allowed the team to begin successfully producing quality airfoils was adjusting resin flow during infusion using various size inlet and outlet tubing to limit the volumetric flow rate of resin into the part. In early trials resin rapidly moved along the length of the EnkaFusion inlet media however if this occurred too quickly there would be dry spots along the leading and trailing edge of the airfoil due to short circuiting down the length of inlet media and lack of material in those areas. The team discovered it was necessary for the inlet media to fully fill along the length of the airfoil then resin flow was limited to allow the wetted perimeter of the airfoil to gradually fill. This concept is illustrated with the resin path arrows in Figure 18. An additional issue the team needed to mitigate was caused by the exotherm of the Elixir® resin during the polymerization process. Since the resin inlet located on top of the airfoil contained relatively large volumes of resin these areas resulted in higher temperatures that compromised the inner polyethylene vacuum bag therefore a switch to a higher temperature bag was required. Additionally, when the exotherm occurred the resin would boil resulting in areas of high void content in localized regions. It was then necessary to cool the molds by placing bags of ice on top of the epoxy molds once a temperature of 50°C was reached within the mold. After addressing the issues with the infusion specific consumables, gaining the ability to remove the consumables from the infused airfoil, adjusting resin flow rates, and by controlling the exotherm of the resin the team began to repeatably infuse quality airfoils free from major defects.

2.5. Successful Infusion and Trials with 64” Mold

After addressing the modification discussed above the team began repeating the process and manufacturing quality airfoils of 64” molds. The finalized process is illustrated below in Figure 19. Figure A shows the consumables used which consisted of the Dahlpac MC79 resin outlet, two strips of Compoflex® RF3 for the upper and lower mold surfaces and the higher temperature polytube bagging material. Figure B illustrates the process of wrapping the consumables around the inner mandrel and vacuum bag, then placing the three layers of E-TLX 2400 (0/45/-45 Warp) Stitched Triaxial E-Glass Fabric from Vectorply. Each ply had a thickness of 0.035 in. (0.89 mm), an areal weight: 26.11 oz/ yd²

(885 g/ m²) giving an overall laminate thickness of 0.105 in (2.67 mm). Once the glass fiber preform was placed in the mold the upper half of the mold was placed on top, the entire mold was envelope bagged, the outer envelope bag and inner polytube bag were sealed and then air was evacuated from the system closing the mold halves together and consolidating the fiber preform to the inner mold surfaces. Then the infusion took place and figures C illustrates the completed 64” airfoils and figure D shows a cross section view of the consumables used and once they were removed from the interior of the airfoil.

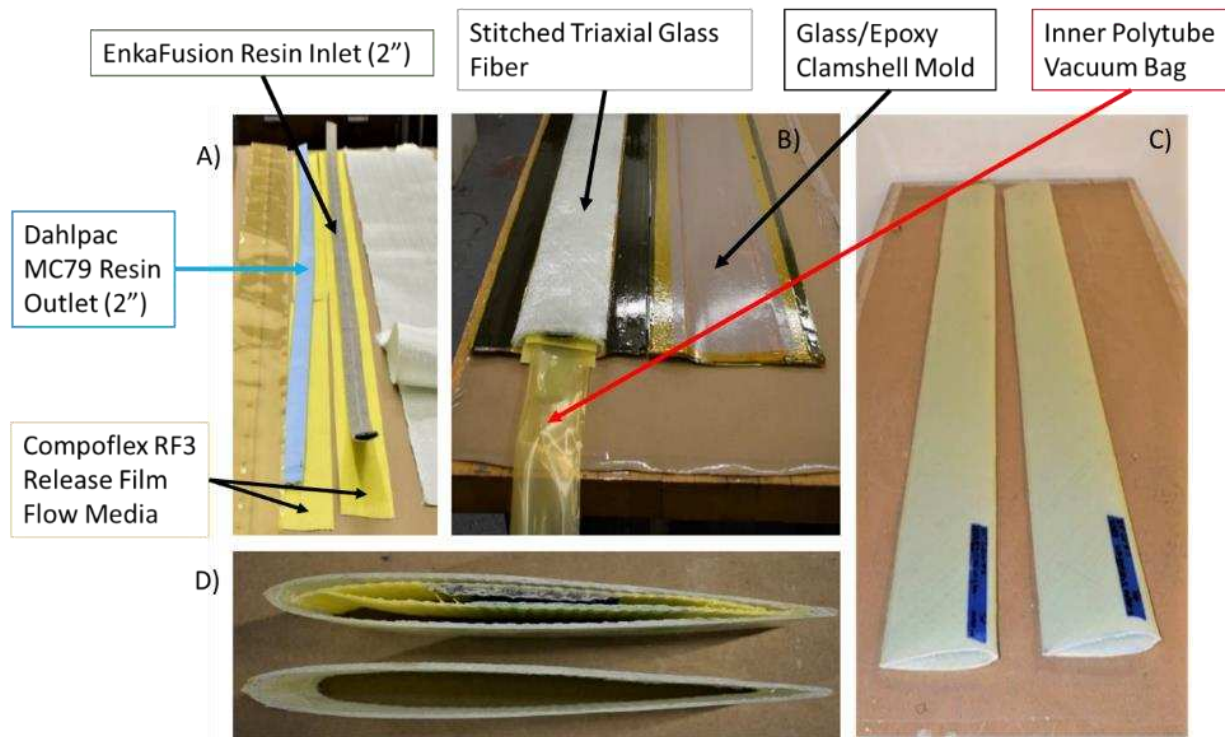


Figure 19: Manufacturing of 64” glass fiber airfoil blades, including consumables, positioning in mold, and after infusion

2.6. Carbon trials with 64” Mold

Minimal changes to the manufacturing process were required to transition from glass fiber airfoils to carbon fiber airfoils manufactured using braided and stitched uni-directional (UD) carbon fiber reinforcement. Figure 20 below illustrates the sequence of steps required to transition to manufacture carbon fiber blades. Image A in the figure illustrates the same consumables used from the glass fiber airfoils explained in the previous section. Image B shows the 18oz braided carbon fiber, supplied by Highlands Composites and A&P, and the three plies of Vectorply C-LA 0912 stitched 9oz UD carbon fabric with integral 1.2oz chopped glass mat which served as an integral flow media. The use of braid

simplified the manufacturing process as it could be placed over the mandrel and rolled back over itself capturing the UD fabric within illustrated in image C. This resulted in the final desired stacking sequence $[\pm 45, 0_3, \pm 45]$ along the top and bottom of the airfoil, and $[\pm 45, \pm 45]$ at the leading edge and trailing edge, which was consistent with the planned reinforcement for the final demonstration blade set. Image D shows the preform being placed in the mold ready to be vacuum bagged and infused and image E illustrates the infused blade with consumables removed.

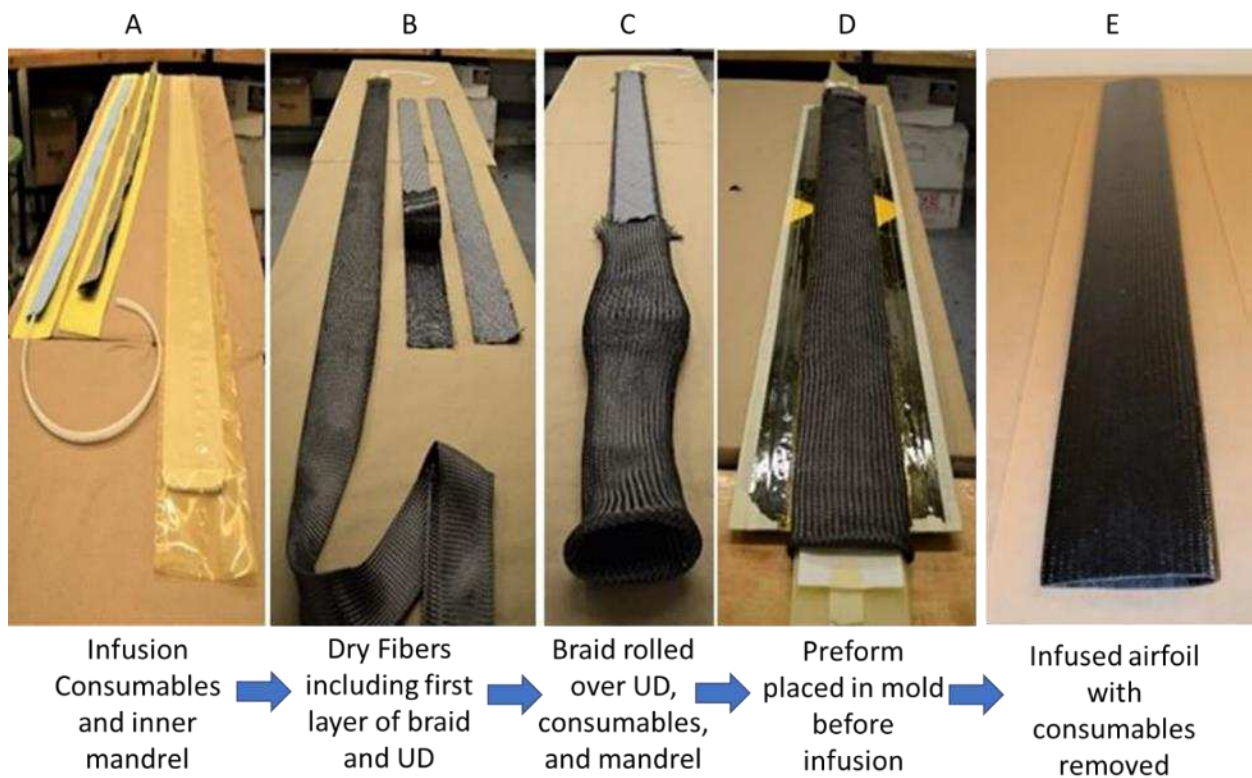


Figure 20: Manufacturing process of 64" carbon fiber airfoils, illustrating UD & braided fabric usage, and completed airfoil

3. FUSION BONDING EXPERIMENTATION AND METHODS

3.1. Demonstrate Fusion Bonding with Elium® Thermoplastic Composites

This study used the most basic of fusion bonding techniques, bulk heating, where composite laminates were heated in a hot press until they were above T_G and pressure was applied to consolidate the laminates together. The process began using glass fiber reinforcement and then into carbon fiber reinforced samples to evaluate the feasibility of bonding end fitting plates into the airfoil blades of the prototype VAWT. These experiments investigated both processing parameters as well as manufacturing consumables used during the resin infusion process that altered the surface texture of the laminates to be bonded. ASTM 3528 was followed to determine the Double Lap Shear Strength (DLSS) of bonded specimens. The following sections describe the process used to test coupons via ASTM 3528, the methods used to manufacture the double lap shear adherends that produced the various surface textures to be tested, characterizes the surfaces via surface topology measurements, and documents the processing parameters evaluated to bond sample coupons together. The variables were first tested using glass fiber/Elium® laminates. When acceptable values for lap shear strength were obtained for the glass fiber test samples, the change to carbon fiber/Elium® sample testing took place using the surface texture and processing parameters that displayed the most consistent and highest values for lap shear strength. The study performed was not a full matrix analysis or attempt at optimizing joint strength since it was found that an optimization of the joint strength would not be required for the loading requirements expected in the VAWT.

3.2. Heat Fusion Bond Testing Overview

Experiments were carried out to evaluate the effectiveness of fusion bonding via heat welding Elium® composite plates to the VAWT blade in order to determine the required bond area for loading conditions as well as to compare heat welded shear strength values to those obtained using induction, resistance, and

ultrasonic welding in prior literature. Surface texture was predicted to influence strength based on both intimate contact development during the fusion bonding process and the resulting effective bondline thickness thus four different surface textures of varying roughness and topology were investigated. This was investigated by manufacturing lap shear adherends with four different surface textures that would then be bonded in between the airfoil cross section. The inside surface finish of the airfoil sections was held constant as that introduced by the Compoflex® RF3 which was necessary to manufacture the airfoil sections. This is illustrated in Figure 21 where the dark blue line illustrates the Compoflex® surface texture of the airfoil section and the dark red line illustrates the area of varying surface texture produced in the lap shear adherends.

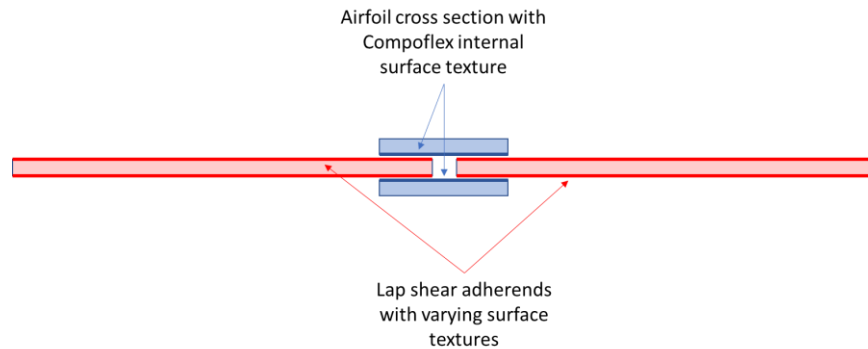


Figure 21: Description of sample coupon terminology

In total four different surface textures were investigated. The first three were produced only using infusion specific consumables requiring no secondary processing before bonding. These included G-FLOW™, Peel Ply, and Compoflex®. The final surface texture was manufactured using Compoflex® to create a resin rich area at the laminate surface after which the adherend was molded to create a uniform flat surface with little variation in roughness or waviness. This was a control to determine the effect of having a resin rich bondline without having a rough textured surface. The bonding parameters investigated the processing variables of (i) applied pressure, (ii) cooling method, and (iii) time at temperature. The temperature evaluated was fixed at 200°C, based on the Elium® 150 properties. The pressures were 185 psi and 370 psi and the times at temperature evaluated were 5 minutes and 10 minutes.

3.3. Experimental Testing via ASTM 3528

3.3.1. Description and Nomenclature

Shear properties of the welded joints were determined using ASTM 3528 or the Double Lap Shear Strength Test. This test essentially loads a bonded joint in tension and eliminates peel stresses often created when testing using only single lap shear tests. This test was selected due to the geometry created when joining the airfoil cross section to the strut to root hub attachment plate having bonded joints on both the upper and lower surfaces of the plate. Additionally, manufacturing sample coupons for DLS testing via compression molding was nearly identical to how the final blade and strut to root hub plates would be bonded.

The geometry of the sample coupons to be tested are shown below in Figure 22. Test specimens are comprised of two 4.25" x 1" laminates separated by 0.1" and bonded on the top and bottom faces with a second adherend providing an overlap of 0.5" for a total shear area of 1". The top and bottom adherents that simulate the airfoil blade are half the thickness of the 4" coupons to create an equal cross section throughout the joint. After being cut to the proper dimensions the test specimen is loaded in tension at a rate of .05 "/min and loaded until failure. After the specimen has failed the maximum load, type of failure, and images of the fracture area were recorded.

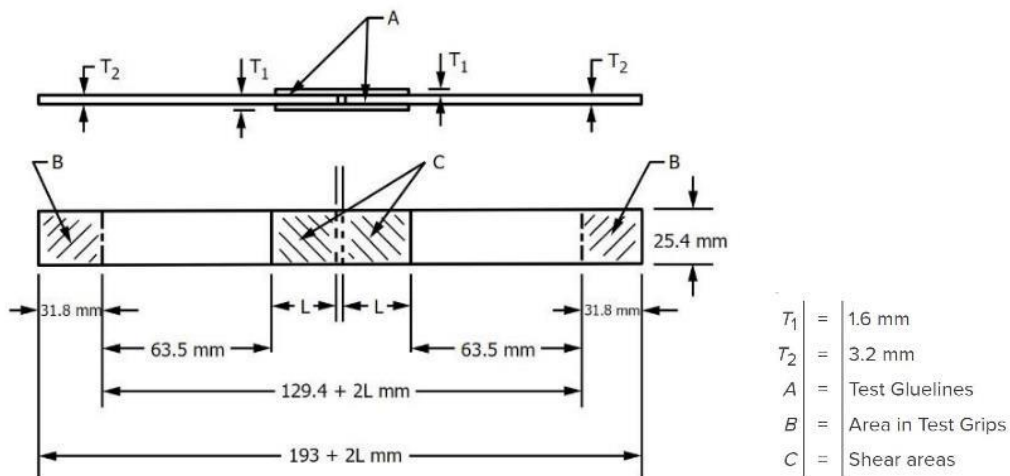


Figure 22. ASTM 3528 Double lap shear sample configuration and definitions according to ASTM International [50]

3.4. Materials and Manufacture of Double Lap Shear Laminates

Initial manufacturing of airfoil sections was completed using an 885 gsm stitched triaxial fabric [E-TLX 2400](#) with a $[0,\pm45]$ orientation. Since the airfoils used for bonding trials had a thickness of three plies of triaxial fabric which was roll wrapped around the internal mandrel this resulted in a $[0, \pm45]_3$ stacking sequence with a total thickness of 0.105 in (2.67 mm). The airfoil laminate positioned $\pm45^\circ$ fibers on the internal side of the airfoil that would be bonded to the DLSS adherends. This was advantageous as it oriented $\pm45^\circ$ fibers to resist the shear forces that would be seen during testing. The airfoil section can be seen below in Figure 23 which illustrates the thickness described and the rough Compoflex® surface on the internal portion of the airfoil.



Figure 23: Glass Fiber Airfoil Cross-Section

The lap shear adherend laminates to be bonded between the airfoil cross section were required to be double the thickness of the airfoil to match ASTM requirements, therefore they were made from six plies of the same fabric. The stacking sequence for the six-ply laminate was $[\pm45,0]_{3S}$ giving a total thickness of .21 in. (5.67 mm) This was to orient the ±45 plies on the top and bottom surfaces to resist the shear stresses in the joint when loaded in tension. The 885 gsm stitched triaxial fabric [E-TLX 2400](#) has a $[0,\pm45]$ orientation and.. The glass fiber airfoil can be seen in Figure 23: Glass Fiber Airfoil Cross-Section.

3.5. Double Lap Shear Coupon Adherend Manufacture

Laminates for DLSS testing were manufactured via a vacuum assisted resin infusion molding process. The three lap shear adherend laminates using the original surface texture (non-molded surfaces) were manufactured simultaneously by having a single dry fiber preform approximately 710mm x 710mm (28"x28") divided into three separate sections each containing a different surface ply or flow media that provided varying degree of roughness as seen in Figure 24 below.

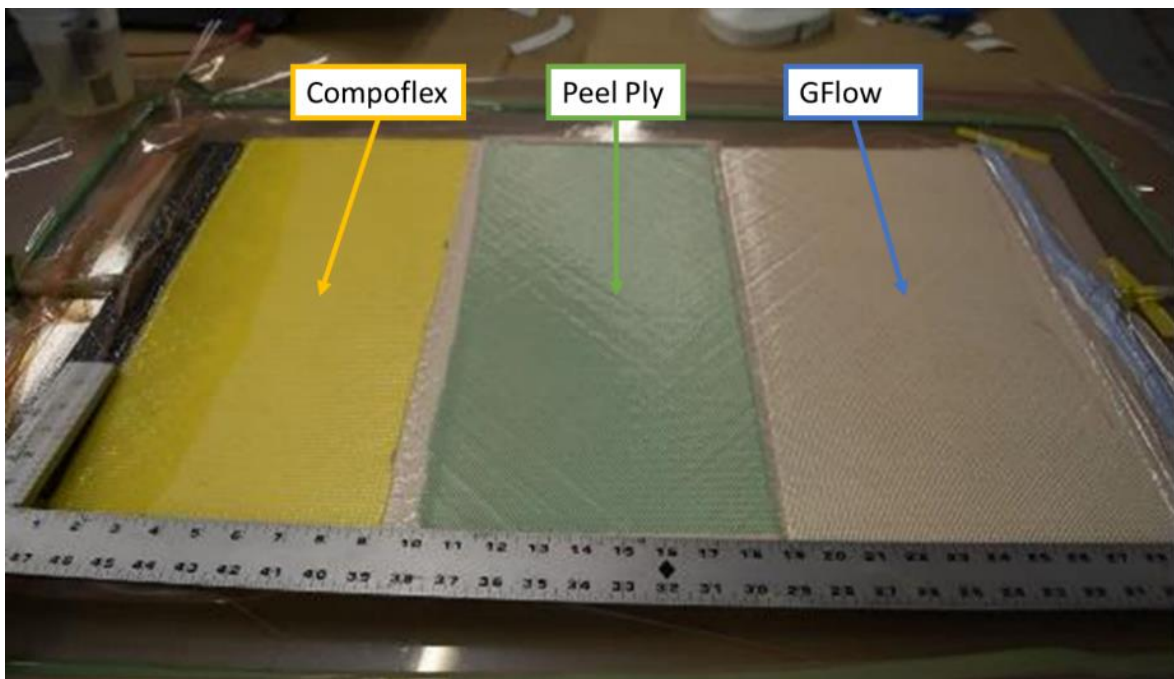


Figure 24: Glass Fiber/Elium® Plate manufactured to give three distinct surface textures

The first material shown in yellow in the figure was Compoflex® RF3, a combination of peel ply, release film and flow mesh (300 gsm), used to control flow rate, distribute resin and release consumables from a composite laminate. The second section illustrated in green utilized a standard green polyethylene flow media on top of Release Ply Super A from Airtech, a heavy weight (139 gsm) nylon peel ply. The nylon peel ply was selected for its heavy weight and large weave to give a larger amount of surface roughness as well as because nylon has been shown in prior research [51] to not leave any contaminants on the bonding surface once removed. The final surface texture on the right of the image was created using G-FLOW™, a structural flow media for infusion processes made with 100% glass fibers. G-FLOW™

contains a heavy weave (500 gsm) of woven glass fibers which open mesh increases resin flow rates during infusion without adding an external or internal flow media. The G-FLOW greatly increases resin distribution and was expected to provide a resin rich area on the surface of the laminate. The three surfaces can be seen in Figure 25 after removing vacuum bag as well as the Compoflex® and Peel Ply in the left and center sections from the outer surfaces of the laminate. The vacuum bag was placed directly over the G-FLOW™ since it is designed to be a structural flow media it was left in the laminate and not removed prior to bonding.

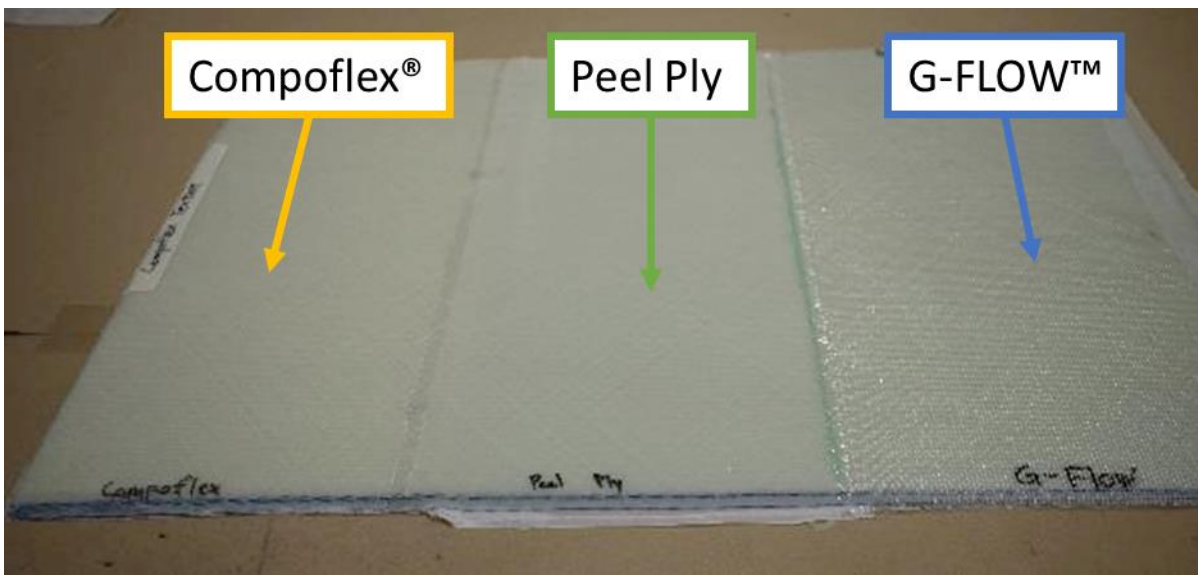


Figure 25: Surface textures created from a) Compoflex® b) Peel Ply c) G-FLOW™

This large flat laminate seen in Figure 25 was subsequently used as the feedstock to produce the flat adherends for the double lap shear specimens. Compoflex® and Peel Ply were left on the laminate and removed just prior to compression molding the double lap shear specimens to provide a fresh surface for bonding and reduce the possibility of the surface becoming contaminated.



Figure 26: Comparison of Compoflex® (Left) Peel Ply (center) and G-FLOW™ (right) surface textures

Figure 26 illustrates how the Compoflex® (left) and nylon peel ply (center) were removed from the surface. The surface created by the G-FLOW™ had the largest vertical profile, however exhibited a smooth texture as the vacuum bagging surface was directly on top of the laminate during infusion. The Compoflex® had the second roughest surface followed by the Peel Ply. The figure illustrates the relative roughness of each texture, the Compoflex® was the most varied and is visibly very different from the peel ply. In the figure on the right the glossy G-FLOW can be seen in comparison to the more translucent color of the peel ply as well as the difference in surface texture. Both the Compoflex® and Peel ply were left on the laminate and removed just prior to compression molding the DLS samples to provide a fresh surface for bonding and reduce the possibility of the surface coming contaminated. Since the G-FLOW™ and molded surfaces did not have a peel ply layer on the outermost surface, the sample coupons were lightly sanded with 220 grit sandpaper and cleaned with acetone prior to bonding.

The final surface texture, that of a molded surface (MS) was manufactured during testing of airfoil consumables and lap shear adherends were manufactured from this feedstock. The upper image in Figure 27 shows a laminate with dimensions of 12” tall by 32” long that was simulating the fabric layup used in the early stages of airfoil manufacture. The sample has a Compoflex® surface in the center and outside edges were the combination flow media was used to wet out the fiber. The vacuum bagged surfaces highlighted are locations where the vacuum bag was placed directly on the laminate. The bottom figures show the longitudinal view of the laminate, sections that were covered in Compoflex®, and the difference between the smooth vacuum bagged surface and the rough textured surface of the Compoflex® section.

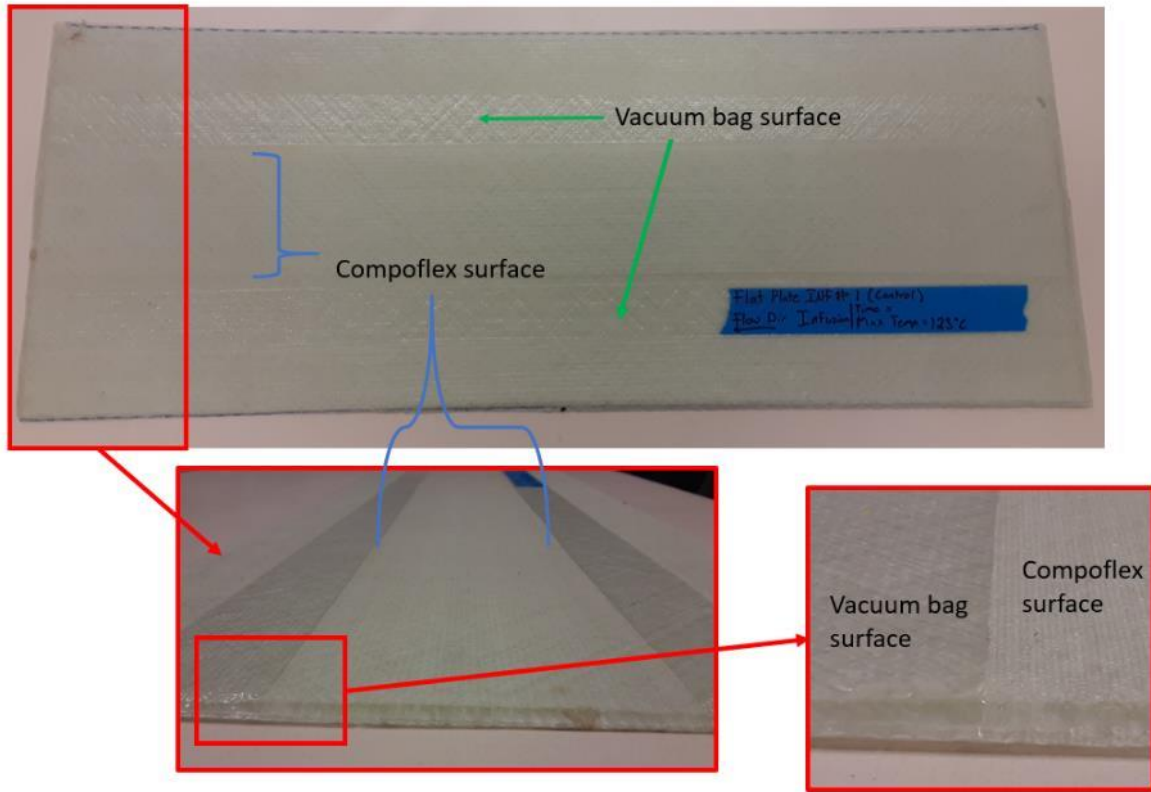


Figure 27: Molded surface laminate showing regions of Compoflex® and vacuum bagged sections

Since the airfoil chord length was only 6” and with the tapered trailing edge, it was determined that sections would be cut from the full-size laminate into 5” wide by 4.25” long (127mm x 108mm) samples that were able to produce four 1” wide quality welded lap shear coupons, the maximum that could be manufactured using a section of airfoil as the 2nd adherend. For each of the three surface textures that were unmodified after infusion four 5” x 4.25” sections were cut shown in the left image below in Figure 28 that would provide a total of 16 individual double lap shear strength test tensile coupons. The image on the right shows the sections that were cut from the molded surface (MS) panel in Figure 27. The set of three pairs of MS lap shear adherends at the top of the figure had a uniform profile across the bonding surface as they were cut transverse to the length of the plate however these were cut in a methods that oriented the fibers in a 90° orientation to the tensile stress that was applied to the joint during testing. The three pairs in at the bottom of the right hand image had approximately half of the surface with the

Compoflex® surface finish and the other half with the vacuum bagged surface similar to the bottom right image in Figure 27.

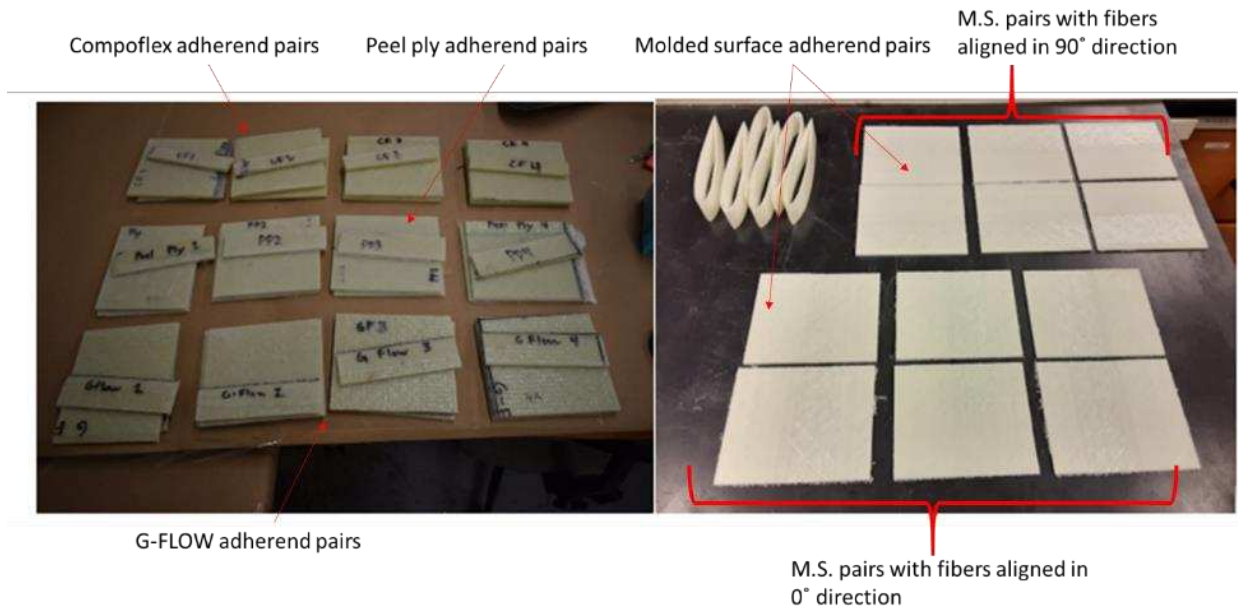


Figure 28: 5''x 4.25'' cut lap shear adherends with various surface finishes

Before bonding the sample coupons, the surface roughness was measured to characterize the surfaces. This include measuring the profiles of the unmodified surface textures as well as measuring the surface roughness of the molded surface adherends before and after they were compression molded to give a smooth texture.

3.6. Double Lap Shear Coupon Surface Roughness

As described in the last section the three different consumables used to manufacture DLSS samples produced four surfaces of varying surface roughness and textures. These surface textures will be further referred to as i) G-FLOW, ii) Compoflex®, iii) Peel-ply, and iv) Molded Surface or MS. To analyze and measure the variation in texture a Taylor Hobson Surtronic S25 surface profilometer was used to take measurements of the sample coupons. Two roughness parameters, mainly the average surface roughness (Ra) and the maximum surface roughness (maximum height of profile, Rz) were used to evaluate the surface quality of the specimens used in this study. Additionally, the waviness profile is documented which is determined by irregularities who's spacing is greater than the roughness sampling length and less

than the waviness sampling length by the selected cut-off (l_c) wavelength. The waviness profiles are compared qualitatively amongst specimens by taking profile measurements with a uniform cut-off wavelength. Each of the four specimens was measured multiple times and average values are outlined in Table 2.

Table 2: Surface roughness measurement averages

Surface Texture	Peel Ply	G-FLOW™ Upper	G-FLOW™ Bottom	Compoflex	MS-Vacuum Bag side	MS-Vacuum Bag Molded	MS-Compoflex Molded	MS-Sanded	Carbon Peel Ply
Ra	16.1 μm	2.57 μm	2.73 μm	23.0 μm	4.83 μm	9.8 μm	0.6 μm	2 μm	15.81 μm
Rz	78.5 μm	11.45 μm	5.78 μm	109.9 μm	25 μm	61 μm	4.25 μm	12.8 μm	14 μm
Rt	105.7 μm	44.75 μm	23.6 μm	140.4 μm	45.6 μm	105 μm	6.6 μm	18.3 μm	64 μm

The values documented above were profiled however the profile curves give a better representation of the surface textures created by the infusion consumables. These were selected as they accurately captured the surface profile and were not subject to numerous cut-off errors or overrange measurements that occurred when taking measurements. The largest issue experienced was that the Surtronic S25 profilometer had a maximum vertical range of 400 μm which often proved too small to measure the larger asperities of the roughest surfaces such as the Compoflex. This was mitigated by taking roughness measurements at multiple points and adjusting to only measure the maximum asperity in regions, then measuring the valley to get an accurate picture of the profile. Additionally, the waviness profile gives a good representation of the form and overall surface of the bonded specimens. In the profile plots below the blue line is the as-measured surface roughness and the waviness profile was created using the Taylor Hobson Talyprofile Lite software using a Gaussian filter cut-off of 0.8 mm to construct the waviness profile. All plots showing the red waviness line have a vertical scale of 400 μm so a comparison between surfaces can be easily made. Figure 29 illustrates the uniform, repetitive surface imprinted by the peel ply on the surface

of the laminates that utilized this consumable. The average roughness Ra was 16.1 μm and average peak to valley distance was 78.5 μm .

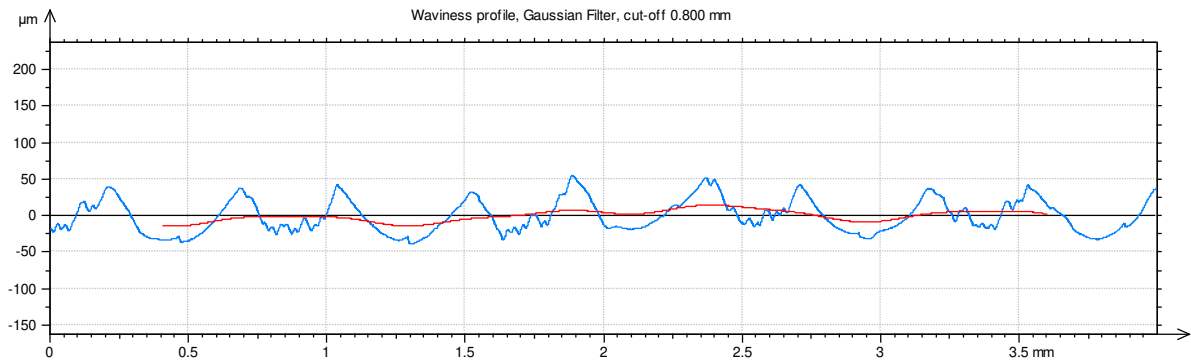


Figure 29: Roughness (Blue Line) and Waviness (Red Line) Measured Profile of Peel Ply Sample Coupon

The second profile illustrated in Figure 30 is that of the G-FLOW™ flow media that is a series of woven glass fibers used to promote resin flow during infusions. Since the polyethylene infusion vacuum bag was placed directly on the surface this created a very smooth surface, illustrated by an average roughness of only 2.57 μm . The fibers created large rolling hills and valleys that can be seen in the figure, with peak to valley heights of over 100 μm .

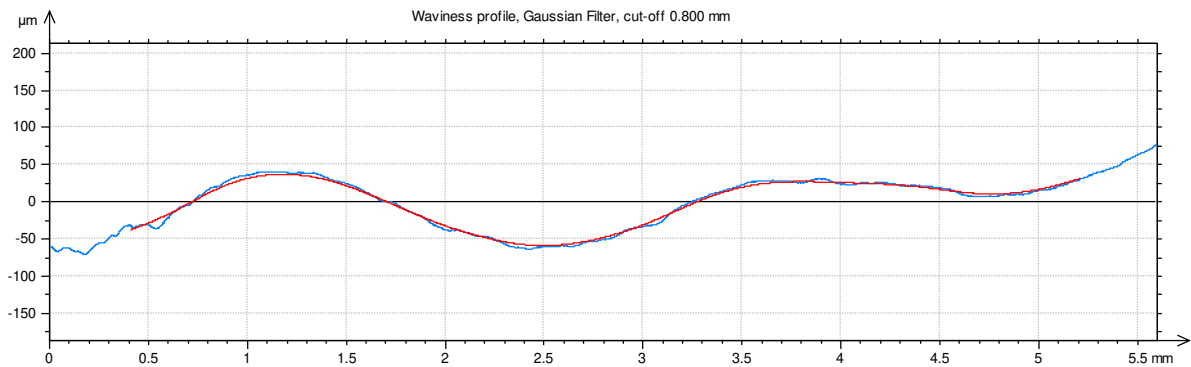


Figure 30: G-FLOW™ upper surface roughness (blue line) and waviness (red line) measured profile

The next image, Figure 31 shows the lower molded surface of the G-FLOW™ sample adherends. Since the G-FLOW™ was placed on the bottom layer of the laminate which was directly placed on the glass plate used for infusion this surface was extremely uniform showed no waviness and had a roughness of 2.7 μm .

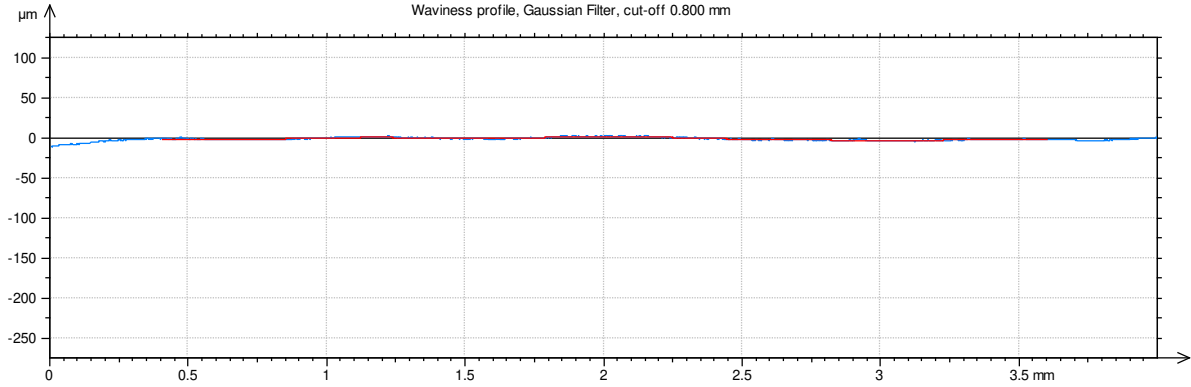


Figure 31: G-FLOW™ bottom molded surface roughness (blue line) and waviness (red line) measured profile

Figure 32 illustrates the wavy profile of the Compoflex surface finish with peaks and valleys with an average peak to valley height R_z of 109.9 μm . This value is under stated as mentioned previously as the maximum range of the profilometer was only 400 μm so there are areas that were truncated which can be seen between the 0.5mm and 1.2 mm distance on the x-axis. This illustrates that the value for R_z and R_t for Compoflex should be much greater than the numerical values measured and produced via the Talyprofile Lite software. This image shows the most uniform display of waviness however other measurements showed peak-to-valley distances in the Compoflex of upwards of 300 μm .

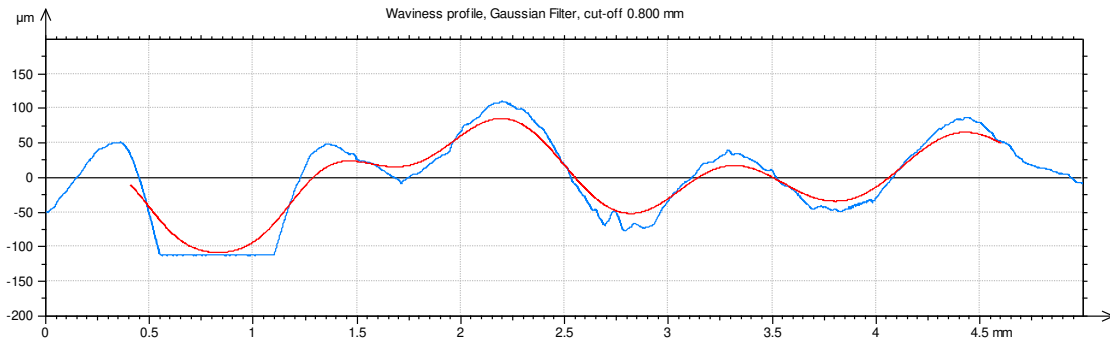


Figure 32: Compoflex® roughness (blue line) and waviness (red line) measured profile

Figure 33 illustrates the as molded side of the vacuum bagged portion of the molded surface specimens described in section 3.5. The figure illustrates the roughness and waviness still apparent after molding sections of the vacuum bagged surface. It also shows the areas where the mold compressed surface asperities, illustrated between the ranges of 0-0.5 mm and again from 1.7 - 2.7 mm. Compare this to Figure 34 which illustrates the surface created by the molded region where the Compoflex flow media

was located. This profile curve is shown with a vertical axis scale of 50 μm so a comparison can be illustrated in greater detail between before and after sanding the specimen. It is evident that the increase in resin in the Compoflex generated a much more uniform bonding surface when compared to Figure 33. The molded surface of the Compoflex section has a roughness (Ra) of only 0.6 μm which was the lowest value recorded.

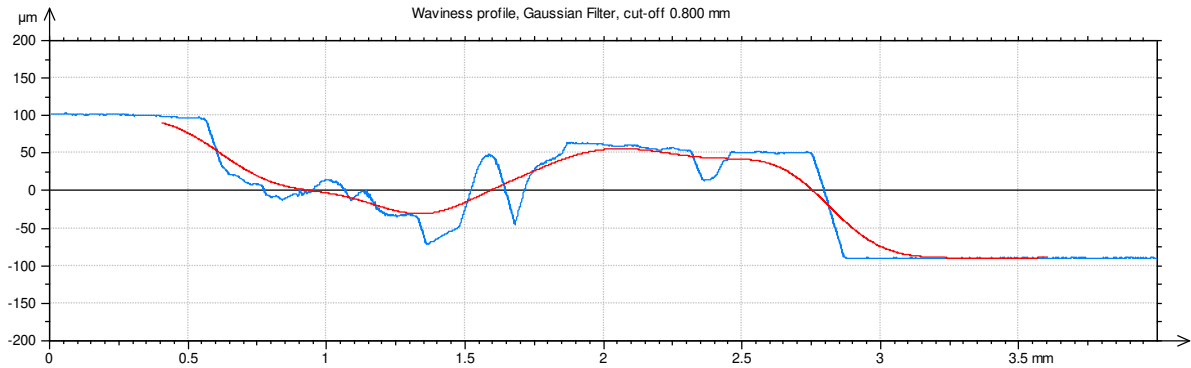


Figure 33: Side of Molded Surface (VB Side) Coupon roughness (blue line) and waviness (red line) measured profile

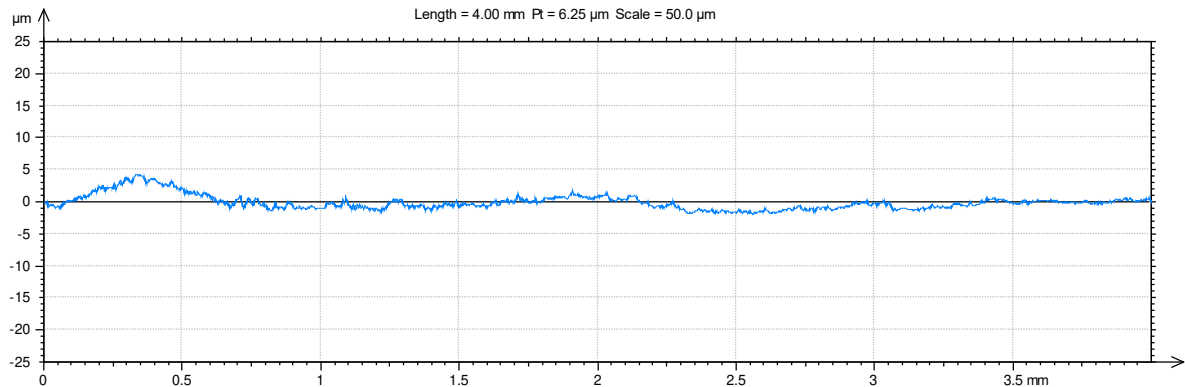


Figure 34: Molded Surface (CF Side) Coupon roughness (blue line) with 50 μm vertical axis scale

The final surface profile measured was that of the molded section after sanding with 220 grit seen in Figure 35 also shown using a scale of 50 μm . It is evident after a comparison to Figure 34 which is the molded section before sanding that sanding does not alter the waviness of the profile however it greatly roughs up the surface. The surface roughness of the sample increased from 0.6 μm to 2.6 μm in this comparison. This can be assumed with other specimens that were sanded and thus the roughness was slightly increased however the overall form of the surface does not change.

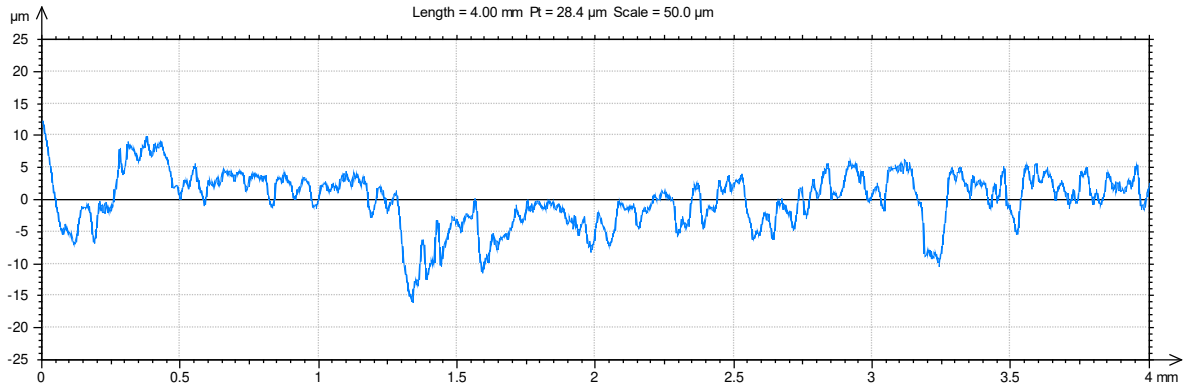


Figure 35: Molded surface after sanding with 220 grit roughness measured profile with 50 µm vertical scale

3.7. Compression Molding ASTM 3528 Sample Coupons

Once the 5" wide sections were cut to ASTM 3528 they were placed into aluminum tooling seen in Figure 36 that was machined to compression mold the DLS sample coupons.



Figure 36: Double Lap Shear Molding Jig

The dies were made from $\frac{3}{4}$ " aluminum and the 1.1"x 0.1" deep cavity in the center positioned the airfoil section while the 5" wide x .07" deep machined area and the four dowel pins correctly oriented the matching upper side of the die as well as positioned the plates being bonded to maintain a 0.1" wide spacing between the 4.25" long coupons in accordance to ASTM 3528. The positioning of the sample coupons can be seen in Figure 37. For each test sample plate, which would ultimately be cut into 4 double lap shear coupons, a short, 28mm (1.1"), length was first cut from an infused hollow airfoil. As indicated in Section 2.1, the triaxial glass reinforced airfoil laminate was made from 3 plies with a

processed thickness of 2.1mm (0.083"). The flat laminates were made up of 6 plies of the same glass fiber reinforcement, resulting in a nominal thickness of 4.2mm (0.167").

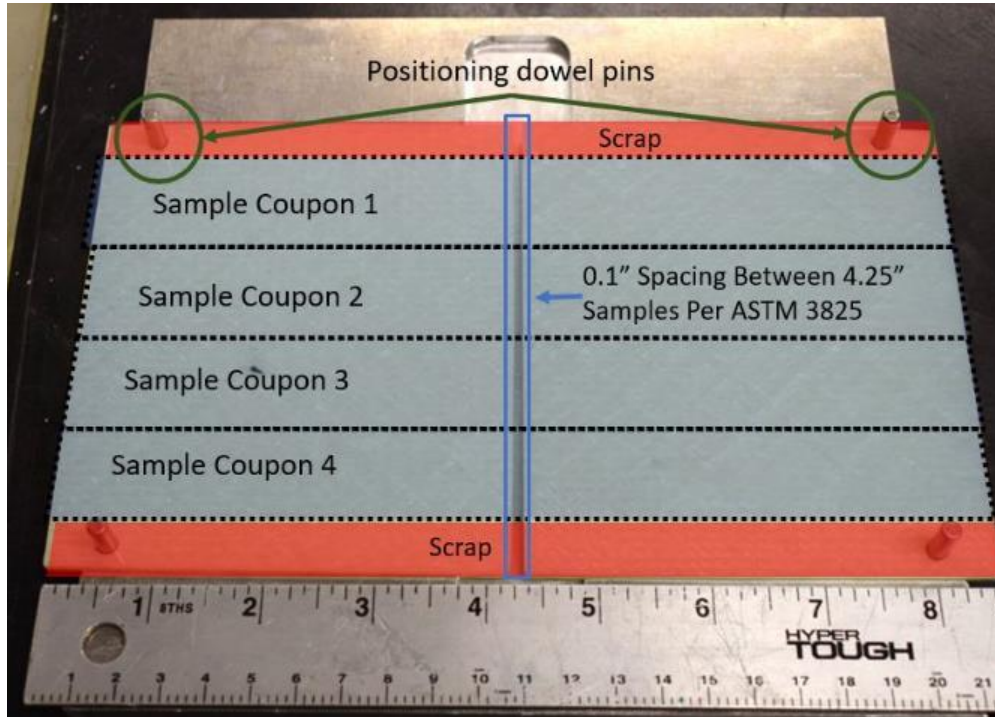


Figure 37: ASTM 3528 Coupon Placement in DLS Molding Jig

To manufacture consistently sized composite double lap shear test plates fixturing was required to hold the two flat laminate panels in alignment, with the correct separation and to accurately position the airfoil section to generate a consistent bond overlap which is illustrated in Figure 37. The fixturing that resulted was a set of identical matched dies. These dies were made from 19mm ($\frac{3}{4}$ ") thick aluminum with areal dimensions of approximately 200mm x 200mm (8"x8") to just fit into the heated press. A 28mm (1.1") wide by 2.5mm (0.1") deep trough, approximately 190mm (7.5") long was milled in the middle of each die half to position the airfoil section while a 127mm (5") wide x 1.8mm (0.07") deep machined area and four dowel pins correctly oriented the matching upper die half and position the flat laminate plates being bonded to maintain a 2.5mm (0.1") wide spacing between the two 108mm (4.25") long adherends, in accordance to ASTM 3528. The die set and the positioning of the composite adherends can be seen in Figure 38. Test sample plates were prepared by aligning the airfoil section and the two adherend flat

laminated panels in one half of the die set and then placing the second die half on top and putting this assembly in the hot press. The platens of the hot press were then closed, applying the specified temperature and pressure for a predetermined period of time, which flattened the airfoil section onto the two plates creating the joint which is illustrated also with the orange box in the diagram on the right of Figure 38. The short airfoil section and these two flat laminate panels then needed to be assembled, by sliding the two flat laminate panels inside the hollow airfoil section and crushing the airfoil, at temperature, resulting in a fusion bonded test sample plate with a cross section consistent with the ASTM requirements illustrated in Figure 22.



Figure 38: Glass samples positioned in DLS bonding jig

The resulting sample plate was then cut into four double lap shear coupons as shown schematically on the right diagram in Figure 38. Thus, the final test specimens are comprised of two 108mm x 25mm (4.25" x 1") laminates separated by 2.5mm (0.1") and bonded on the top and bottom faces with a second adherend (the flattened airfoil section) providing an overlap contact length of 12.7mm (0.5") on each flat laminate for a total shear area of approximately 645mm² (1 in²). The top and bottom adherends that simulate the airfoil blade are half the thickness of the 108mm (4.25") laminates to create an equal cross section throughout the joint.

3.8. Compression Molding and Processing Variables in DLS Bonding Trials

The samples were positioned in a Honacomp CM 8x8, a 20-ton molder with an 8"x8" platen, and the upper and lower platens were heated to temperatures ranging from 180 °C to 200°C. Once the heated platens, aluminum tooling, and composite laminates reached a uniform temperature pressure was applied to the bonded area to consolidate the joint. The consolidation pressure ranged from 187 to 256 psi. Additional variables investigated included the amount of time that consolidation pressure was applied and the method of cooling after that time elapsed. Early trials were not cooled completely below T_G under pressure, meaning that after the specified time consolidating elapsed, pressure was removed, platen heaters were turned off, and the mold and bonded specimen were allowed to cool until at room temperature when the molds could be opened. When it was realized via early testing that cooling under pressure was critical a water cooled chilling machine was connected to the compression molding machine and after the elapsed time at the correct consolidation pressure was reached the platen heaters were powered down, water cooling was turned off, and the mold and samples were cooled under the specified consolidation pressure until the mold was just above room temperature or below T_G of Elium® (110°C). The left image in Figure 39 shows the Honacomp 20-ton compression molder, and the right images shows the first sample bonded, referenced further as Bond Test 1 (BT1). It can be clearly seen that the compression tooling applied pressure and significant melting occurred in the bonded region where the composite laminate turned to a more translucent color. Visual comparison to subsequent welding samples illustrated that this was a good predictor of bond quality.



Figure 39: Honacomp 8x8 inch 20 Ton Compression Molder and preliminary bonding trial Bond Test 1 (BT1)

3.9. Double Lap Shear Strength Testing Procedure

After the adherends were bonded they were subsequently cut on a water-cooled tile saw and then wet sanded to mitigate damage to the outer edges of the coupons. The 1" width tensile coupons for ASTM 3528 testing can be seen below in Figure 40. After cutting samples to the correct size according to ASTM 3528 measurements were taken so the lap shear strength could be calculated and any discrepancy between the four coupons across the bonded joint could be analyzed. The measurements taken included the airfoil width (blue), the bond width (red), and the bond thickness (yellow). The airfoil width and bond width were used to calculate the shear area assuming a 0.1" spacing according to ASTM 3528. Even though the airfoil section was cut to exactly 1.1" prior to being molded there was a small amount of variance after molding the coupon, so these values were taken into account when calculating the shear strength. Once coupons were measured, they were loaded into an ATS Series 900 load frame using wedge-lock grips to transfer load into the double lap shear coupons. The joints were loaded at a rate of 0.05 in/min (1.27 mm/min) according to ASTM standards. When each specimen failed the maximum load was recorded, load and displacement data was recorded, and images of the fracture were recorded.

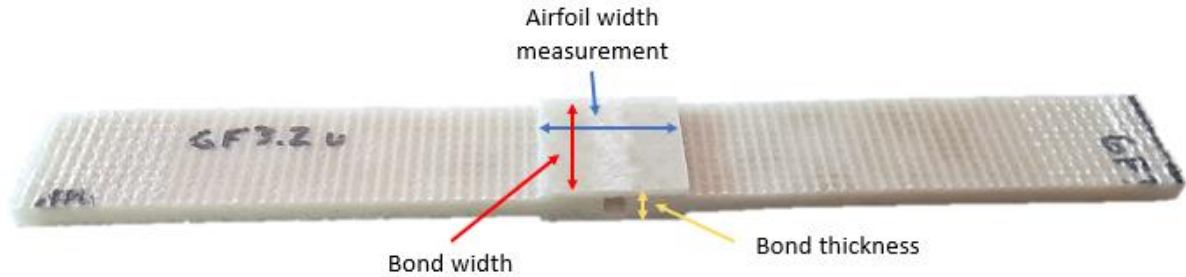


Figure 40: ASTM 3528 tensile coupon and measurement locations

3.10. Glass Fiber Double Lap Shear Bonding Trials and Processing Parameters

Initial testing with glass samples was carried out to validate that the compression tooling could adequately apply pressure to the bond area and that the heated platens and aluminum tooling adequately heated material above T_G to allow the fusion bond to occur. After it was established that the aluminum tooling could bond the laminates together, a comparative evaluation was performed using glass fiber reinforced laminates so it could be determined what infusion consumables should be used when attempting to manufacture the strut to root hub plates in the final manufactured VAWT in addition to the processing variables worked well fusion bonding Elium® thermoplastic so the variables could be used when processing carbon fiber reinforced laminates. Table 3 below lists the 17 trials that were performed to develop a processing technique sufficient to proceed to testing using carbon fiber. Each bonding trial produced four lap shear coupons for a total of 68 individual tests of glass fiber reinforced coupons.

Table 3: Glass fiber fusion bonding processing variables and trials tested via ASTM 3528

#	Surface Texture		Consolidation pressure applied		Cooled under pressure	Hold time at 200°C (minutes)
	Expendable Material used at Surface	Sanded with 220 Grit	(MPa)	(psi)		
1	Compoflex®RF3	No	1.28	185	Yes	5
2	Compoflex®RF3	No	2.56	370	No	10
3	Compoflex®RF3	Yes	2.56	370	Yes	10
4	G-FLOW™	Yes	2.05	296	No	5
5	G-FLOW™	No	1.28	185	No	10
6	G-FLOW™	No	2.56	370	Yes	10
7	G-FLOW™	No	1.28	187	Yes	10
8	Peel Ply	No	1.28	185	No	5
9	Peel Ply	No	2.56	370	Yes	5
10	Peel Ply	Yes	1.28	185	Yes	5
11	Peel Ply	Yes	2.56	370	Yes	5
12	Molded Surface-(VB/CF)	Yes	2.56	370	Yes	10
13	Molded Surface (VB/CF)	Yes	1.28	187	Yes	5
14	Molded Surface (VB/CP)	Yes	1.28	187	Yes	10
15	Molded Surface-Uniform Surface	No	2.56	370	Yes	10
16	Molded Surface-Uniform Surface	No	2.56	370	Yes	5
17	Molded Surface-Uniform Surface	No	1.28	187	Yes	5

3.11. Carbon Fiber Double Lap Shear Bonding Trials and Processing Parameters

Based on these results for the glass fiber reinforced Elium® 150 results, 10 carbon fiber reinforced Elium® 150 specimens were created using the parameters judged best. The carbon fiber reinforced double lap shear specimens were produced at 180°C, 150psi, held for 10 minutes at temperature and pressure and cooled in the hot press. The surface texture on the flat plates was molded in using peel ply and the inside surface of the airfoil was that of the Compoflex®. Once testing was completed with the glass fiber samples testing was performed on Elium® laminates with carbon fiber as the reinforcement.

The samples were manufactured using a ± 45 biaxial and two uni-directional non-crimp fabrics from Vectorply to obtain a plate thickness twice that of the laminate in the airfoil. The airfoil was infused with a stacking sequence of $[\pm 45, 0]_s$ using the [CBX-0900](#) ± 45 Biaxial NCF (300gsm & 0.48 mm thick) and [CLA-0912](#) 0° UD NCF (352 gsm & 0.6mm thick) giving a total thickness of 2.16 mm. The plate was infused with a stacking sequence of $[\pm 45, 0_2]_s$ using the CBX-0900 ± 45 Biaxial NCF (300gsm, 0.48 mm thick) and heavier weight [CL-1800](#) 0° warp unidirectional non-woven (590 gsm, 0.9mm thick) giving a total thickness of 4.56 mm, slightly twice the thickness of the airfoil. The carbon samples were all manufactured using a standard green flow media and the nylon Super Release A peel ply as this gave the best results in the preliminary bonding trials using glass fibers. Processing variables are documented in Table 4 below. All tests were performed without sanding as the results from glass fiber testing showed that sanding had little effect on bond quality. Additionally, the samples were all cooled under pressure since that was a major conclusion from previous trial. The variables that were altered to account for the increase in thermal conductivity was the hold time at 200°C and the consolidation pressure.

Table 4: Carbon fiber fusion bonding processing variables and trials tested via ASTM 3528

#	Surface Texture		Consolidation pressure applied		Cooled under pressure	Hold time at 200°C (minutes)
	Expendable Material used at Surface	Sanded with 220 Grit	(MPa)	(psi)		
1	Peel ply	No	2.56	370	Yes	10
2.	Peel ply	No	1.28	185	Yes	10
3	Peel ply	No	2.56	370	Yes	10
4	Peel ply	No	2.56	370	Yes	20
5	Peel ply	No	1.28	185	Yes	10
6	Peel ply	No	1.28	185	Yes	5

4. EXPERIMENTAL RESULTS AND DISCUSSION

The results outlined below were obtained by loading ASTM 3528 double lap shear coupons in tension to attain values for lap shear strength characterized by the maximum load at failure. The resulting failure methods and surfaces were documented to determine the resulting quality of the bonded joint. Digital microscopy imaging was used to analyze both the surfaces of unbonded adherend samples as well as bonded areas, to qualitatively correlate to data obtained in strength testing data and the resulting failure analysis to trends seen in the microscopy imaging. With strength testing data, failure analysis trends, and microscopy images, results are discussed and correlations between additional matrix at the bondline, surface topology of adherends, and bonding parameters from these results can be used in the final VAWT assembly. The majority of analysis was performed on the glass fiber samples, results from the carbon fiber samples are summarized however further research is needed to draw significant conclusions for fusion bonding carbon fiber reinforced samples.

4.1. Glass Fiber Double Lap Shear Strength Testing Results

4.1.1. *Overview*

The glass samples tested showed a wide range of values for shear strength but overall produced adequate results. The shear strength results were much higher for glass fiber reinforced than carbon fiber reinforced Elium® which is evident in Figure 41 which documents the average shear strength displayed by each surface texture tested. The highest average was from a preliminary experiment labeled Bond Test 1 that was used to verify the tooling created to manufacture the ASTM 3528 double lap shear coupons was effective at creating the bonded joint. This experiment utilized a peel ply surface finish however only four coupons were tested and processing variables (consolidation pressure) were not consistent with later testing variables. It is only highlighted in this figure because it displayed similar results to the other peel ply samples. Of the four surface textures tested the peel ply performed the most consistently. The average value for all peel ply specimens was 14.3 ± 1.9 MPa. The Compoflex® also performed well and produced

the highest performing individual average. The average for all Compoflex® samples tested was 12.35 ± 3.5 MPa illustrating a much wider variability than the Peel Ply samples.

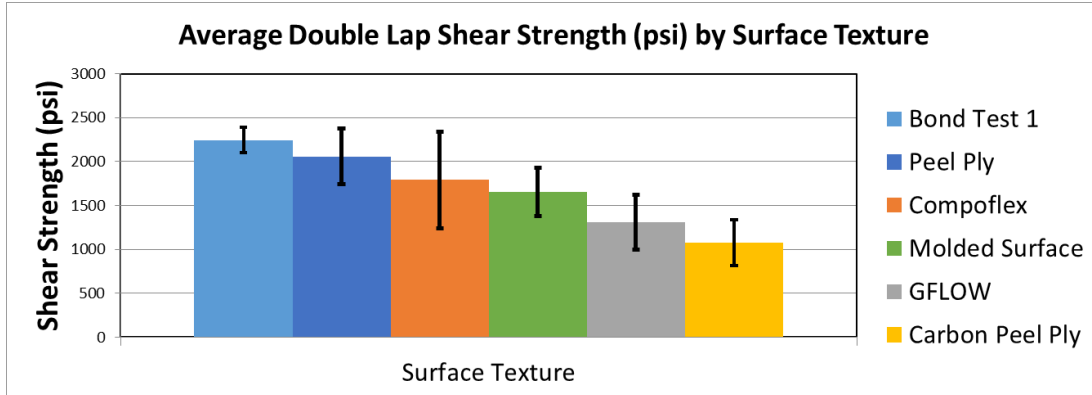


Figure 41: Average values for double lap shear strength by surface texture

The molded surface texture laminates performed poorly, having an average strength of only 11.4 ± 2.0 MPa, (1656 ± 290.4 psi) however this value doesn't represent the full range of variables that were supposed to be examined as half of the mold surface specimens failed within the adherend so values for the bond strength were not obtained. Additionally, half of the molded coupon had a non-uniform vacuum bagged texture on half of the specimens that performed far worse than the area where the resin rich Compoflex surface was located. The average value for lap shear strength of G-FLOW™ samples was 9.02 ± 2.14 MPa (1308 ± 310 psi) which was the worst of all four surface finishes tested using glass fiber reinforcement. The highest performing peel ply and Compoflex trials produced statistically the same values of double lap shear strength value with the Compoflex® RF3 surface finish at 15.8 ± 0.4 MPa versus 15.5 ± 0.4 MPa for the Peel Ply surface finish. Figure 42 illustrates the full range of strength results from all glass fiber specimens tested. The colors of data series match those observed in Figure 41, the blue samples show the trend of peel ply specimens, the Compoflex is shown in orange, G-FLOW™ again is illustrated with grey circles, and mold surface coupons are shown in green. The highest average strength produced from all specimens was 16.1 MPa which was roughly 73% of the shear strength of neat Elixir® resin quoted from the technical data sheet, which for the purposes of this study were conclusive

to move onto further bonding trials and manufacture of the VAWT prototype. Discussion of individual trends for each of the surface textures are described in section 4.2

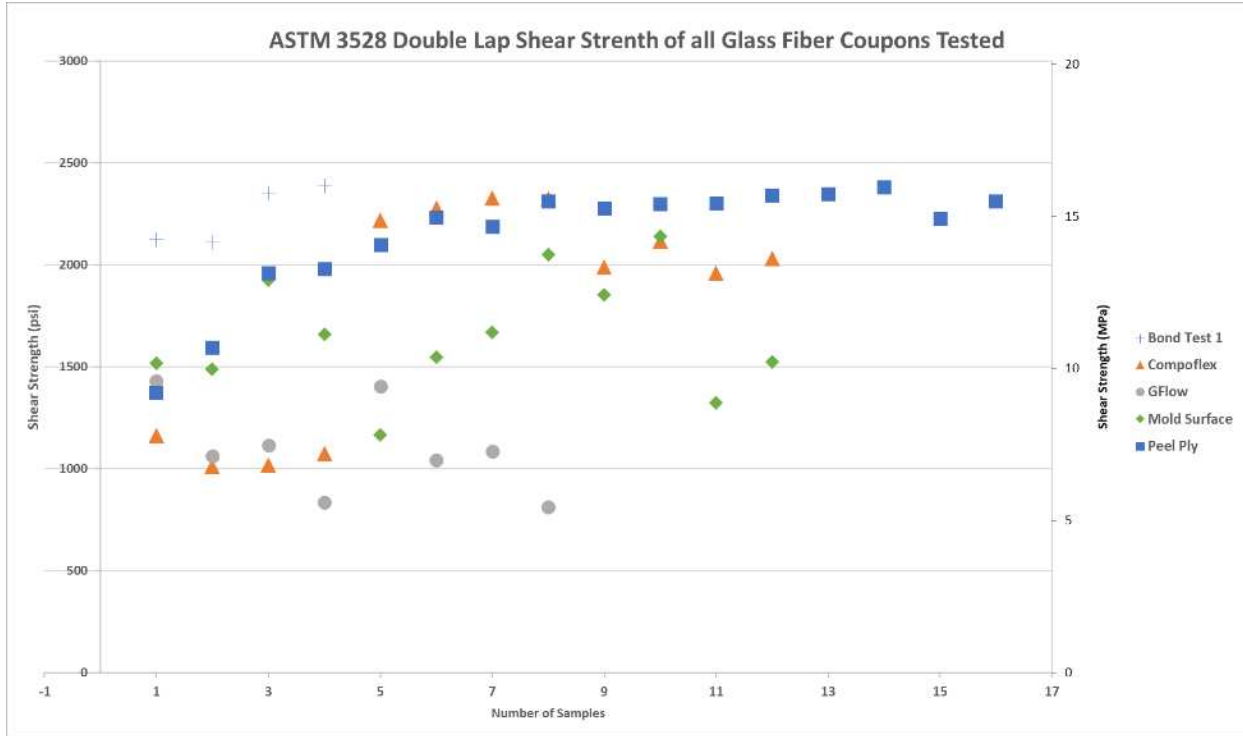


Figure 42: Lap Shear Strength Produced with Varying Surface Textures

4.2. Surface Texture Effect on Bond Strength

Surface texture was predicted to have an effect based on both contact area during the heated compression and the effective bondline thickness. The surface texture was varied through the use of different expendables in contact with the two surfaces of the flat infused laminates. The inside surface finish of all of the airfoil sections was held constant as that introduced by the Compoflex® RF3 which was used in all the airfoil sections of interest. The effect of surface texture had the largest effect on weld quality and there were clear differences in the strength values produced with each surface. Key takeaways are documented in the following sub-sections and then a final discussion of the results including interpretations from fracture testing and microscopy imaging are reviewed in section 4.6.

4.2.1. *G-FLOW™ Bonded Samples*

The samples created using G-FLOW™ as the exterior flow media did not display quality bonds and the strengths exhibited were drastically lower than the other variables. The highest strength value obtained in testing was only 10.8 MPa, half the quoted number for lap shear strength of Elium. The G-FLOW™ adherends had in essence two drastically different surface textures at the bond interface. The upper surface where the laminate was vacuum bagged during infusion was a smooth wavy texture with large amplitudes between peaks and valleys. The difference in these surfaces produced much lower values for strength due to the inhomogeneity between the upper and lower bondline. More evidence of this conclusion is supported by failure analysis in section 4.4 and microscopy images in section 4.5.

Table 5: *G-FLOW™ lap shear strength values and corresponding processing variables*

Trial #	Sanded with 220 Grit (Y/N)	Pressure Applied (psi)	Cooled under pressure (Y/N)	Hold time at 200°C (minutes)	Lap Shear Strength (psi)	Standard Deviation (psi)	Lap Shear Strength (MPa)	Standard Deviation (MPa)
GF1	Yes	296	No	5	1111.3	245.3	7.7	1.7
GF2	No	185	No	10	1086.1	244.0	7.5	1.7
GF3	No	370	Yes	10	1564.3	234.5	10.8	1.6
GF4	No	185	Yes	10	1473.6	258.9	10.2	1.8

4.2.2. *Molded Surface Bonded Samples*

The molded surfaces had the second lowest values for strength and the largest deviation in bond strength observed between sets of molded coupons as seen below in Table 6. The highest performing trial of molded surface tests was from MS3 which obtained an average shear strength of 11.8 ± 2.5 MPa. The highest performing individual sample reached a value of 14.8 MPa however a sample on the same trial with the same processing variable had a value of 9.1 MPa. This large discrepancy between individual coupons manufactured in the same trial was caused by the use of manufacturing samples from a separate sheet of glass fiber reinforced Elium, not specifically designed for double lap shear testing which was manufactured during infusion trials to simulate resin flow between Compoflex sections and vacuum bagged areas that would be experienced in the airfoil. Half of the bonded samples were from areas where

the vacuum bag was located which produced drastically lower results. The difference between the two areas and the resulting quality of molded sections can be seen in Figure 43, the image on the left shows the two varying regions produced by the Compoflex (blue arrows) and the vacuum bag (red arrows). The image in the middle shows how the molded adherends appeared visually distinct with the Compoflex region on the left being significantly more resin rich than the molded area on the right. This discrepancy was seen in all three trials (MS1-MS3) where lap shear adherends were bonded in this orientation. In trials MS4-MS6 the adherend orientation was altered by 90° so that the uniform molded surface was uniform across the entire bondline. However, after altering the orientation by 90° the 0° fibers in the triaxial laminate were thus oriented perpendicular to the applied tensile load during testing and exhibited stock break failure and the bond strength was not able to be determined. The difference between the vacuum bagged region and the Compoflex region was distinct, the vacuum bagged area exhibited an average strength of 9.9 MPa while the samples from the resin rich Compoflex region with a more uniform surface topography exhibited a value of 13.0 MPa.

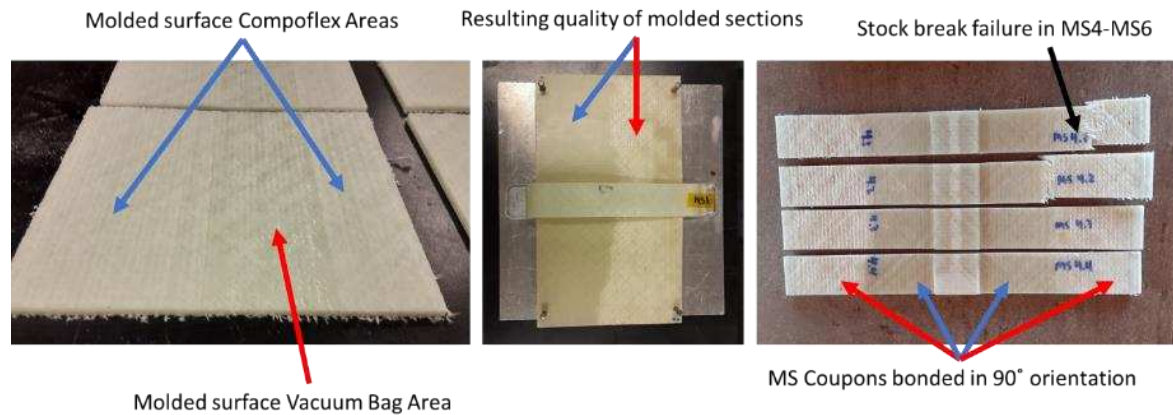


Figure 43: Difference between Compoflex areas and Vacuum Bagged areas in molded surface coupons

Table 6 reviews the cumulative results obtained from molded surface samples. The results are a bit misleading as mentioned due to the variation in the bond interface in half of the samples from MS1-MS3, however even the strength results from the uniform bonding surface created by the Compoflex area were less than those obtained from peel ply and Compoflex surface textures.

Table 6: Mold surface shear strength values and corresponding processing variables

Trial #	Sanded with 220 Grit (Y/N)	Pressure Applied (psi)	Cooled under pressure (Y/N)	Hold time at 200°C (minutes)	Lap Shear Strength (psi)	Standard Deviation (psi)	Lap Shear Strength (MPa)	Standard Deviation (MPa)
MS1	Yes	370	Yes	10	1648.1	200.5	11.4	1.4
MS2	Yes	187	Yes	5	1609.2	364.5	11.1	2.5
MS3	Yes	187	Yes	10	1710.7	359.4	11.8	2.5
MS4	No	370	Yes	10	Failure in coupon due to inadequate fiber in adherend resulting in stock break failure			
MS5	No	370	Yes	5				
MS6	No	187	Yes	5				

4.2.3. Compoflex® Bonded Samples

Across all glass samples, Compoflex had an average lap shear strength of 12.35 ± 3.5 MPa, however it also displayed the highest standard deviation between the four infusion consumables examined. The reduction in average strength was caused by trial CF1 that was not cooled under pressure. The average strength for Compoflex would then be 14.9 MPa if CF1 was excluded. The Compoflex trials produced the highest performing individual lap shear coupon which had a strength of 16.1 MPa. This was encouraging since the internal surface of the airfoil that the blade to root hub bracket would be bonded was manufactured using Compoflex. In agreement with prior literature the increase in available resin from the Compoflex produced quality results. The results of all bonding trials are documented below in Table 7 and show that the best values were obtained from using higher pressure and a longer hold time. This is likely caused by the additional time to melt and then flatten the larger asperities seen in the Compoflex adherends.

Table 7: Compoflex® lap shear strength values and corresponding processing variables

Trial #	Sanded with 220 Grit (Y/N)	Pressure Applied (psi)	Cooled under pressure (Y/N)	Hold time at 200°C (minutes)	Lap Shear Strength (psi)	Standard Deviation (psi)	Lap Shear Strength (MPa)	Standard Deviation (MPa)
CF1	No	370	No	10	1067.1	69.4	7.4	0.5
CF2	Yes	370	Yes	10	2286.8	50.9	15.8	0.4
CF3	No	185	Yes	5	2023.7	69.6	14.0	0.5

In addition to the high values for strength obtained from the Compoflex surface, the failure mode of all Compoflex coupons cooled under pressure shown below in Figure 44 was via fiber-tear indicating that the bond between the airfoil and the adherends was sufficient to transfer loads into the adherend fibers. The fiber-tear failure observed in these specimens illustrates that fusion bonded joints using this surface finish are adequate to cause interfacial failure of the composite adherend which would be the limiting factor in joint design.



Figure 44: Compoflex® trials CF2 and CF3 all exhibiting cohesive fiber tear failure

4.2.4. Peel Ply Bonded Samples

Peel ply was the best performing surface texture. The average value for all peel ply specimens was 14.3 ± 1.9 MPa. The results showed the lowest standard deviation across all samples tested which is further improved when PP1 is excluded from the results because it wasn't cooled under pressure. When

excluding PP1 the average value for lap shear strength increases to 15.25 MPa with a standard deviation of only 0.53 MPa. This uniformity of bonding values and low deviation across samples is why it was chosen as the surface texture for testing with carbon fiber reinforcement. The highest performing sample was un-sanded, molded at the higher pressure of 370 psi and held at that pressure for 5 minutes and produced a maximum value of 16.0 MPa. The results of all trials are compiled in Table 8. The processing results illustrate that there was little difference in sanded vs un-sanded specimens and that bonding at a higher consolidation pressure yielded only slightly improved results.

Table 8: Peel ply lap shear strength values and corresponding processing variables

Trial #	Sanded with 220 Grit (Y/N)	Pressure Applied (psi)	Cooled under pressure (Y/N)	Hold time at 200°C (minutes)	Lap Shear Strength (psi)	Standard Deviation (psi)	Lap Shear Strength (MPa)	Standard Deviation (MPa)
PP1	No	185	No	5	1679.3	286.2	11.6	2.0
PP2	Yes	185	Yes	5	2145.2	87.4	14.8	0.6
PP3	Yes	370	Yes	5	2239.6	26.5	15.4	0.2
PP4	No	370	Yes	5	2251.9	64.5	15.5	0.4

4.3. Results of Processing Variable Effect on Glass Fiber Samples

Due to the complexity of the fusion bonding process there was no clear set of processing variables that provided the best bond strength for all surface textures. It appears that the best bonding parameters varied for each individual surface except for cooling under pressure which was evident in all bonding trials. The highest performing specimens from each surface are illustrated in Table 9 which shows that different variables were able to produce quality bonds.

Table 9: Highest performing trials of all surface textures

Surface Texture	Sanded (Y/N)	Pressure Applied (psi)	Hold time at 200°C (minutes)	Lap Shear Strength (MPa)
Compoflex (CF2.3)	Yes	370	10	16.1
Peel ply (PP4.2)	No	370	5	16.0
Molded Surface (MS3.2)	Yes	187	10	14.8
G-FLOW™ (GF3.3)	No	370	10	12.8

The statistical significance between the processing variables of sanding, pressure applied and hold time are indeterminate for all the samples tested and a conclusion cannot be statistically validated that one variable should be used for all glass fiber surface textures. Interpretations though can be made on the results shown in Table 8 that higher pressure and longer hold time did have an improved effect on surfaces with a greater surface roughness (Ra) and peak amplitude of asperities (Rz) The Compoflex and G-FLOW™ had the largest peak to peak maximum from the surface profile measurements documented in Table 2 so it is reasonable to assume that the longer hold time of 10 minutes and higher pressure of 370 psi allowed sufficient time to achieve intimate contact, flattening asperities, and improving the quality of fusion bonds. The peel ply and the molded surface which had fewer surface asperities required less time and pressure to consolidate the asperities found on the surface of adherends. The molded surface required a lower pressure which can be expected since the adherends already had a sufficiently smooth surface for bonding, but the longer hold time allowed for longer time for intermolecular diffusion thus leading to stronger bonds. With the peel ply the hold time was only tested at 5 minutes which was an oversight when designing the DOE, but likely results would have improved with a longer hold time. The effect of cooling under pressure was found to be statistically significant. This was validated by a Paired Two Sample for Means t-test with a two tailed t-test resulting in a p-value of 0.0004. The difference in strength values obtained from samples cooled under pressure to those without pressure is seen in Figure 45.

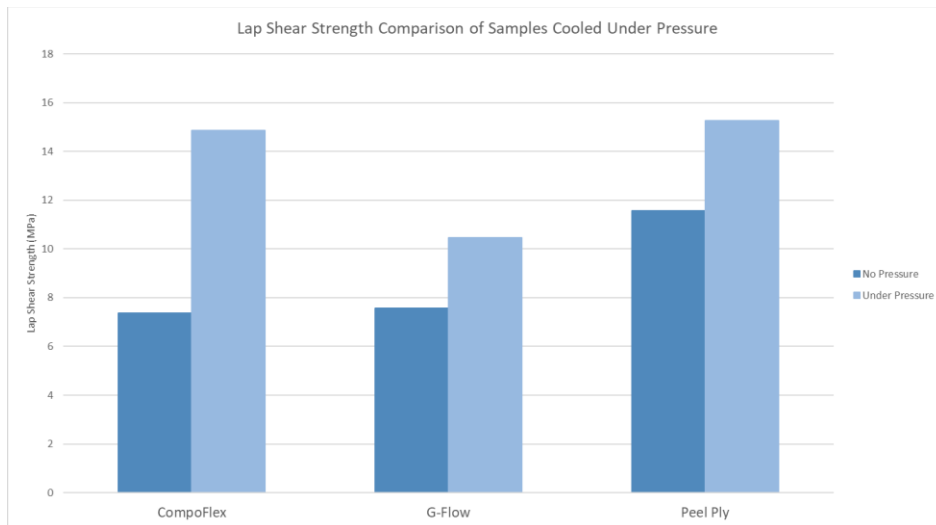


Figure 45: Comparison of strength values obtained when cooling samples under pressure

4.4. Glass Fiber Double Lap Shear Failure Mode Analysis

Resulting failure methods and surfaces were analyzed to determine the resulting quality of the bonded joint. Failure modes were classified according to ASTM D5573 - Standard Practice for Classifying Failure Modes in Fiber-Reinforced-Plastic (FRP) Joints, which gives 6 potential joint failure modes including; adhesive failure, cohesive failure, thin layer cohesive failure, fiber-tear failure, light fiber-tear failure, and stock break failure which can be seen in Figure 11 in the introduction. The major challenge categorizing the failure modes was difficultly to visually observe the difference between adhesive failure, where the failure is at the interface between the adherend and the matrix filled region and a cohesive failure where the failure occurs in the matrix region between the airfoil and the adherend. Since there wasn't the presence of an additional adhesive intermediate material it was difficult to visually observe the difference. Further visual inspection would be required to fully classify specimens as either adhesive or cohesive failure, so cohesive failure was used if there were no signs of fiber tear and interlaminar failure in the adherend.

Figure 46 illustrates the compilation of all glass fiber coupons tested via ASTM 3528. In can be seen in the figure below as well as in Figure 44 and Figure 49 one of the airfoil-sourced adherends of the double lap shear coupon generally was fully debonded from the coupon, while the second airfoil-sourced

adherend remained attached to one of the flat plate adherends. This was extremely evident with G-FLOW™ samples where the airfoil debonded from the vacuum bagged wavy surface rather than the smooth molded surface on the bottom of the adherend.

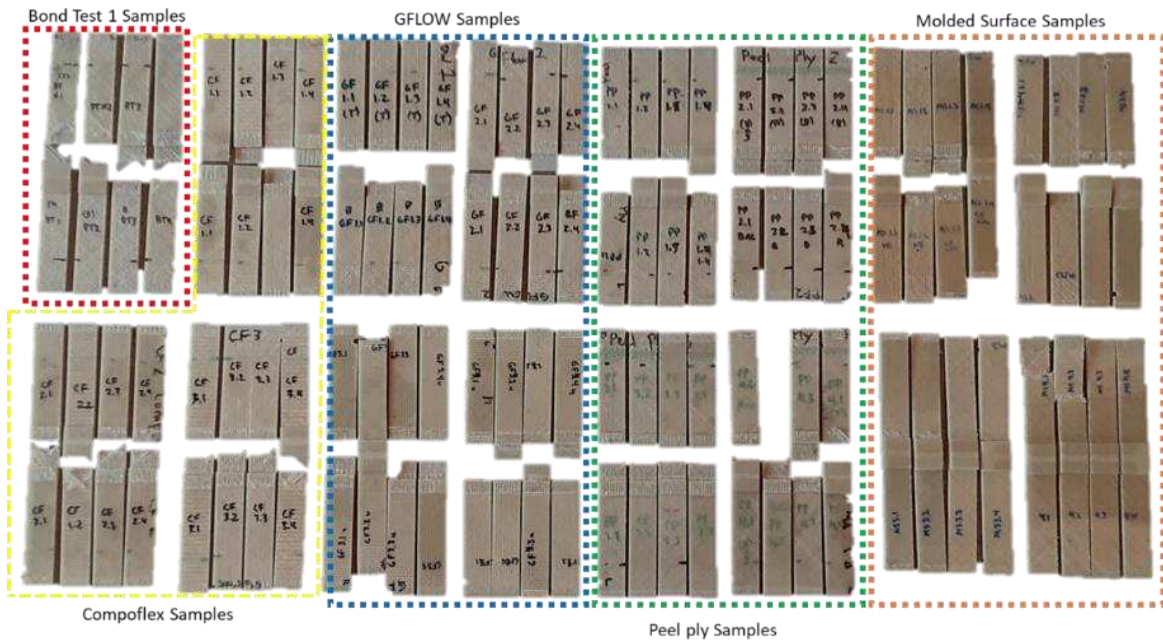


Figure 46: Collection of glass samples for failure analysis

The following subsections describe the failure modes observed by the glass fiber fusion bonded samples. A review of the failure modes across all samples is illustrated in Figure 47 which shows how specimens failed in regard to each surface texture. It can be seen in this figure that most specimens exhibited three forms of failure, fiber tear shown in green, light fiber tear illustrated in blue, and cohesive failure in yellow. The only surface finish that failed completely in cohesive failure was G-FLOW™, all other samples showed signs of fiber tear.

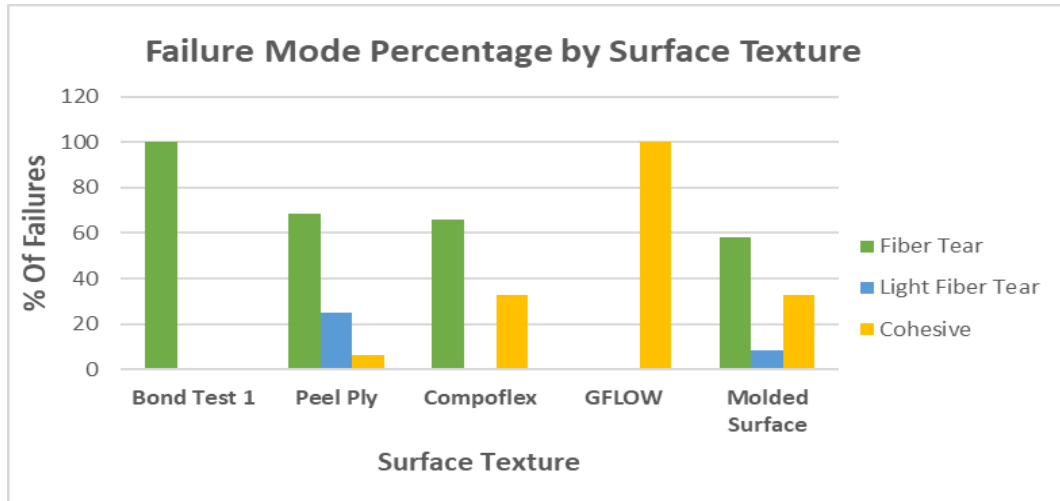


Figure 47: Failure mode percentage by surface texture

4.4.1. Cohesive Failures

Cohesive failure was characterized by the failure within the bonded region without significant damage to either the adherends of the airfoil straps bonding the two. This type of failure suggests that only mild fusion bonding occurred between the adherends and the airfoil. This was likely caused by voids or defects at the interface or the lack of pressure to consolidate asperities leaving air pockets within the bonded region. This was clearly evident in G-FLOW™ samples where all failures were cohesive since there were no signs of the glass fiber flow media debonding from the laminate, however there were signs that regions of bonded materials were either pulled off the glass fiber flow media or left on the flow media from the airfoil adherend. Other surface textures that exhibited cohesive failure showed resin from the Compoflex surface of the airfoil on the fracture surface of the adherend illustrating that there was adherence between the two interfaces but not enough to adequately transfer loads into the fibers. The presence of resin transfer between the airfoil and the adherend (or vice versa) can be seen in the Figure 48.

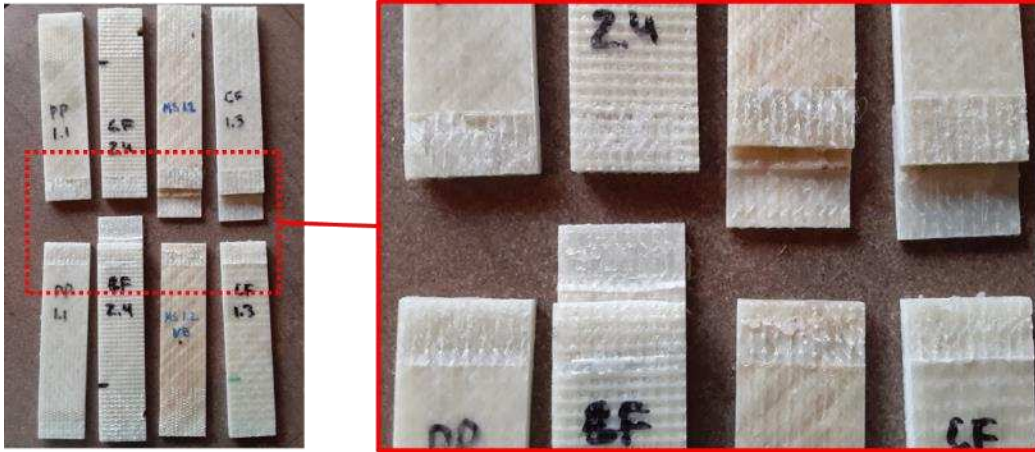


Figure 48: Cohesive failure exhibited in all 4 surface finishes

4.4.2. Fiber-Tear Failures

For specimens with the higher failure strengths there was damage to the underlying composite plate adherend. This was distinguished as either light fiber-tear where there were signs of fibers in adherends being pulled from the laminate but not enough damage for full interlaminar failure where the ± 45 -degree fiber were peeled from the adherend laminates. Samples that exhibited this cohesive fiber tear failure mode displayed much higher values for shear strength than those where there was only damage to the matrix material. In many of the experiments where a large amount of fiber tear occurred was evident that the fusion bond is nearing its interlaminar shear strength of laminate thus debonding or first ply failure is occurring. Figure 49 shows that three of the four surface textures exhibited fiber tear during mechanical testing failure thus were successful in transferring loads from the bonded joint into the fiber in the adherends. The left image in Figure 49 shows the damage to Compoflex® trial CF2.1, which resulted in the highest measured performance. Thus, the indication is that the highest double lap shear values observed are limited by the laminate and not the joint itself, suggesting that there was little to gain by further joining process parameter optimization during the manufacture of the prototype VAWT.

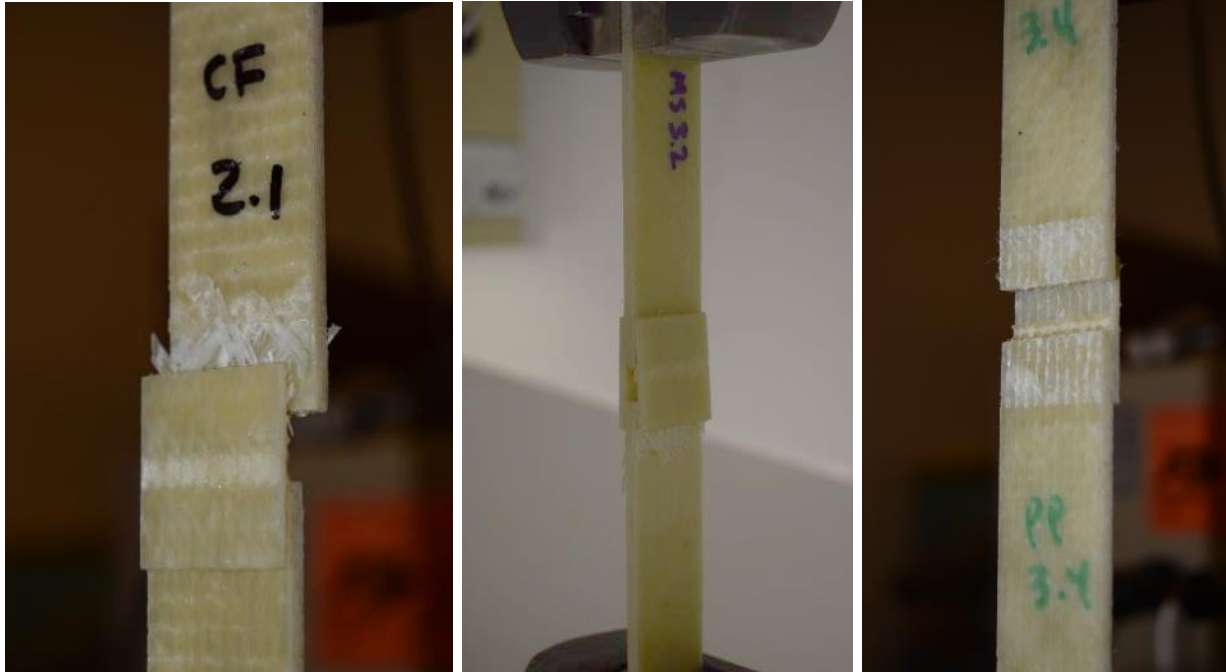


Figure 49: CompoFlex®, Mold Surface, and Peel ply coupons illustrating fiber tear during failure

4.5. Microscopy Analysis of Glass Fiber Bonded Samples

Analysis via microscopy was performed to investigate both the properties of the unbonded lap shear adherends and bonded specimens. Of the unbonded specimens the area of interest was the upper and lower surfaces of the specimens where the bond would be created. Factors effecting the quality of bonds that were viewable in microscopy analysis was the amount of resin available at the surface, the topology which was well illustrated in the cross-sectional view of the sample, and resin rich areas within the laminate caused by different infusion consumables.

Microscopy analysis was utilized on bonded regions to investigate factors such as bondline uniformity, the effect of waviness of adherend surfaces, the presence of voids in the bonded area, and the difference between the bondline produced by the upper and lower surfaces of adherends when the two were not uniform. The results of the microscopy analysis supported the findings of the strength testing and fracture analysis of the bonded joints.

4.5.1. *Manufacture of Microscopy Samples*

Microscopy specimens to investigate the unbonded adherends were taken from unused sections of material from the feedstock used to create the 4.25" x 5" lap shear adherends. Bonded samples were cut from the edges of the molded lap shear samples near the leading and trailing edges of the airfoil adherend. Sections were cut in roughly 0.75" long x .25" wide sections that were the thickness of the adherend laminate or bonded joint, approximately 0.2" thick for the adherends and 0.3" thick for the bonded sections. Once a total of a total of 9 bonded samples and a sample from each adherend type was cut to size it was molded into inspection cups using CASTAMOUNT™ Acrylic resin, a two-part methyl methacrylate that provided a rapid cure and was compatible with the Elium resin used in the samples. The samples were mounted into the cups where they were then prepared for microstructural investigation. Samples were wet sanded from 320 to 600 grit then final polishing utilized silicon carbide abrasive discs up to 1200 grit after which they were ready for viewing. Samples manufactured are shown below in Figure 50.



Figure 50: Five microscopy cups manufactured; top row identifies samples, lower row is of the imaging surface

Samples were inspected via a Leitz ERGOLUX microscope with bright field/dark field illumination at magnifications of 6.4x up to 40x. A Nikon DSLR digital camera was used to record the images and multiple stitching software including Adobe Photoshop and Microsoft Composite Image Editor was used to stitch multiple images together to view the entire sample when magnified.

4.5.2. *Unbonded Samples of Lap Shear Adherends*

Unbonded specimens of lap shear adherends included a single sample of Compoflex, a peel ply specimen, a G-FLOW™ specimen and that of a molded surface specimen that had not yet been compression molded to investigate the adherend features that would have an effect on bonding. It was additionally discovered that there was the presence of voids in the surface asperities produced in both the G-FLOW™ and the Compoflex®. It is evident that the consumables used had a varying effect on the quality of the laminates manufactured, not just the bonded joint. Visible resin rich regions in the laminate were observed, especially evident when using Compoflex. Figure 51 illustrates the difference in the cross section between the vacuum bagged surface and the Compoflex surface prior to molding the sections to manufacture the mold surface adherends. It can be seen that the area on the right (vacuum bagged portion) is free from the large resin rich section outlined underneath the Compoflex. This explains the drastically different appearance of molded adherends visible in Figure 43. The resin rich area likely contributed to the higher bond strengths obtained from the mold surface specimens that were bonded to the regions corresponding to the Compoflex region.

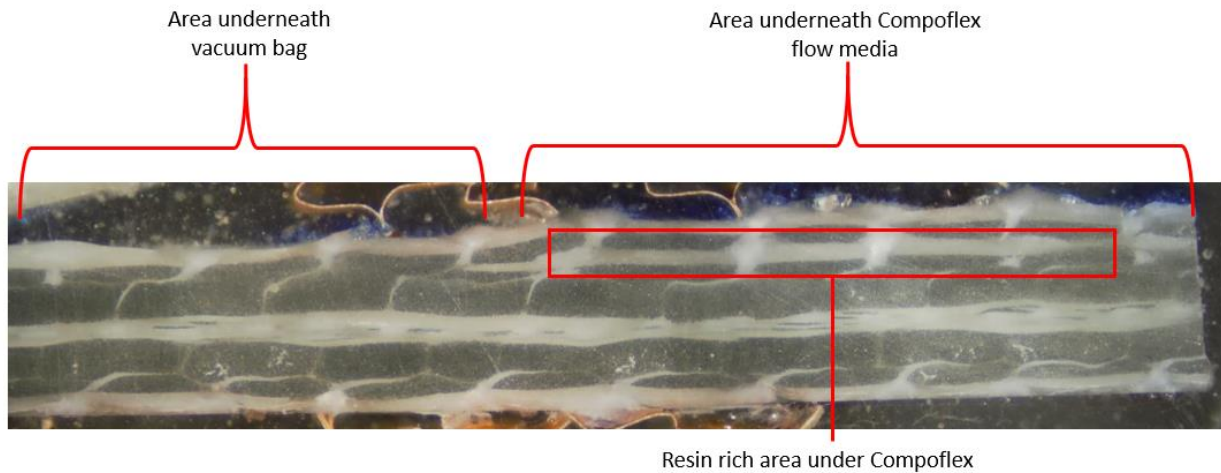


Figure 51: Resin rich area under Compoflex® in molded surface manufacturing sample (6.4x)

Figure 52 illustrates an unbonded Compoflex adherend and the rough variable surface texture that appears on the upper and lower surface of the adherend. Voids in the form of air bubbles and microcracking is seen within the surface asperities at the upper surface. This likely is a result of removing Compoflex

consumable prior to bonding specimens. The cracking of the matrix rich surface asperities is likely not detrimental however the presence of bubbles within the asperities likely cause local stress concentrations as they cannot be removed by consolidation pressure alone.

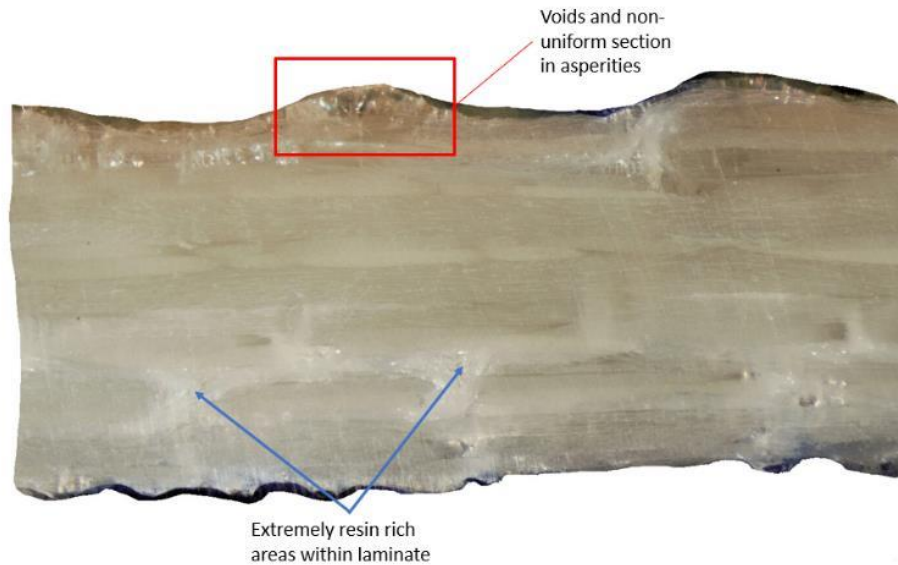


Figure 52: Unbonded Compoflex adherend (10x) illustrating resin rich areas and voids within the surface asperities

Comparing the previous image to that of Figure 53 (which illustrates the peel ply bonding surface) it is easy to see the difference between the two adherends that produced the best bonding results. The peel ply surface is free of major asperities and there is little excess resin at the surface. Additionally, the peel ply laminate is of better uniform quality. This illustrates that the Compoflex causes a decrease in consolidation pressure when manufacturing laminates which is likely a reason that all samples that were cooled after bonding under pressure exhibited fiber tear in the outer ply of the laminate.



Figure 53: Peel ply adherend (6.4x) and enlargement of surface texture and topology (25x)

Figure 54 illustrates the G-FLOW™ adherends cross section. The glass flow media is clearly visible as the dark spots in the upper and lower surfaces, highlighted in images B) and C) which clearly illustrate how the flow media was placed on top of the laminate and since the media was left in place after infusion there were large wavy sections produced on the sample. It can be seen how resin rich the areas between the glass bundles are, however there is little resin on top of the glass flow media to sufficiently bond to the laminate which was likely due to the vacuum bag creating a barrier between the bag and the glass fibers of the G-FLOW™. An additional thing to take notice of is the difference in waviness between the top and bottom G-FLOW™ surfaces. Image B) shows the upper surface of the G-FLOW™ adherend and C) shows the lower surface which was placed on the mold surface when the adherends were infused and does not feature the hill and valleys that the upper surface did. The wavy surface is a likely source of voids leading to entrapped air in the bonded joint, causing lower strengths.

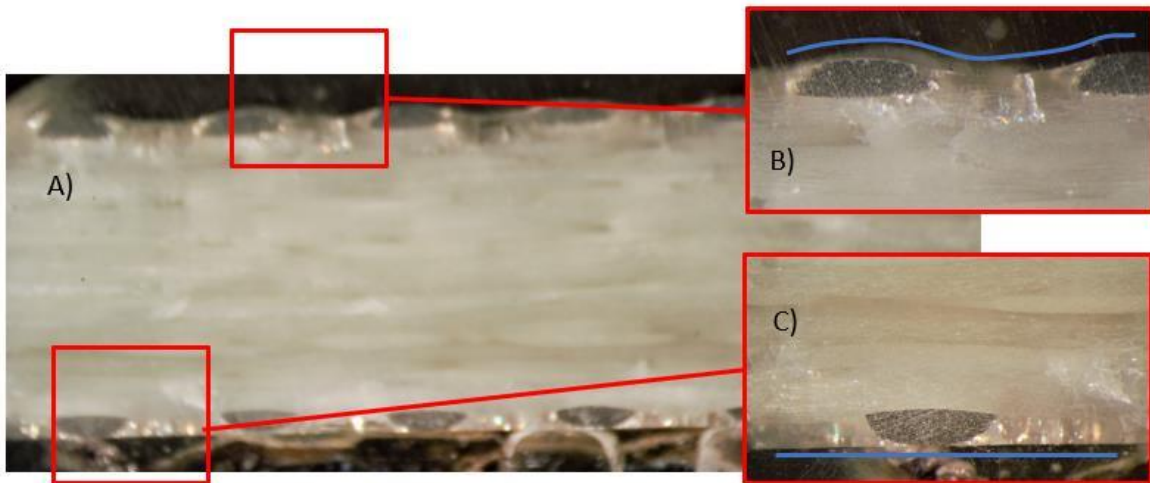


Figure 54: Difference in waviness of G-FLOW™ (A) upper (B) and lower (C) molded surfaces

4.5.3. Bonded Sample Microscopy

Bonded samples were analyzed to correlate results of strength testing values, inspect the consequence of surface topology in adherends, and visually examine the differences between processing variables.

Bonded samples from all four glass fiber surface textures were viewed. These included trials from CF1, PP3, PP4, GF2, GF4, MS1, and MS3. The bonded sample microscopy focused on four main areas of

analysis including bondline uniformity, the presence of voids, variations in bondline caused by surface waviness and asperities, and the difference between samples tested using different bonding parameters. Figure 55 shows the bondline created from the Compoflex surface texture when it wasn't cooled under pressure (CF1). The bondline is filled with voids and defects, likely air pockets that formed when consolidation pressure was removed when bonding while the thermoplastic matrix was still in a viscous state above T_G . The thick defect filled bondline illustrates that cooling below T_G under pressure is essential for maintaining void free bonded regions. If images of Compoflex samples had been taken of Compoflex specimens the bondline thickness would be decreased however it would have been more uniform, have little defects, and have a thick matrix interlayer between the airfoil strap and the adherends. An oversight occurred by only mounting one Compoflex bonded trial so a comparison of bonding parameters between Compoflex samples couldn't be made.



Figure 55: CF1 bonded sample showing large voids and defects in the bondline (6.4x)

Figure 56 is the microscopy images taken from peel ply trial 3 (PP3) which produced an average lap shear value of 15.4 MPa. This figure illustrates the uniform bondline created by the peel ply surface texture. Image A) shows the consistency of the bondline across the entire laminate, especially when compared to samples that utilized other surface textures. Image B) shows the slightly larger thickness bondline than that shown in image C) but neither bondline shows voids, bubbles or much variation in waviness.

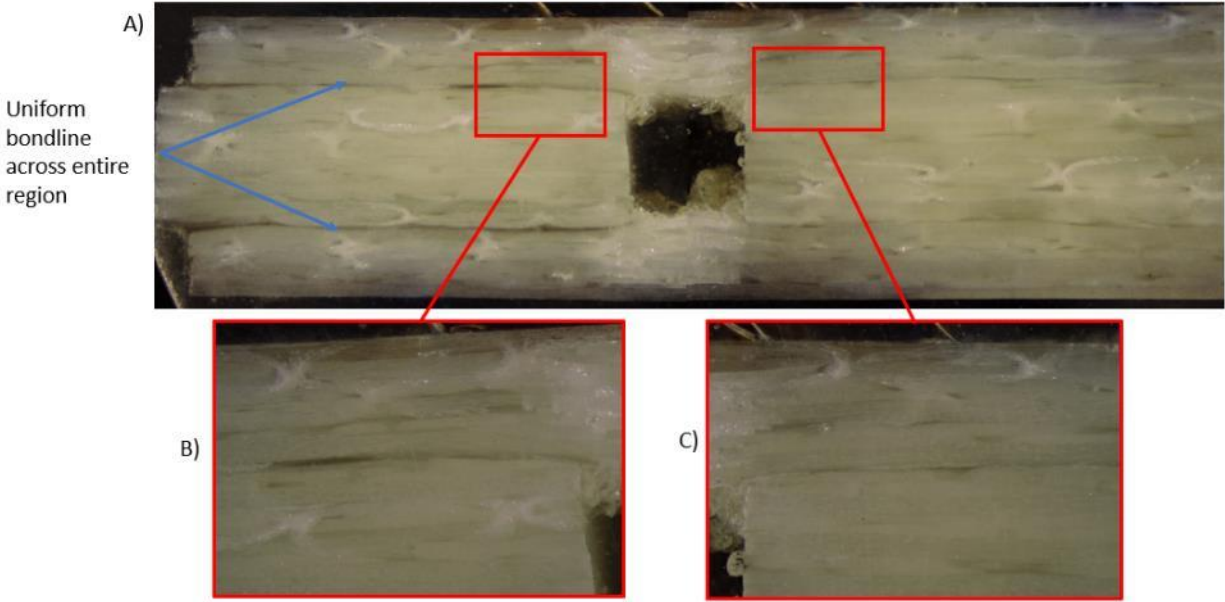


Figure 56: Peel ply 3 bonded sample microscopy images (6.4x) illustrating various thickness bondline in B) & C) (10x)

Figure 57 and Figure 58 illustrates the poor bonding displayed by the G-FLOW™. G-FLOW™ specimen 2 was not cooled under pressure so there are visible signs of air that was entrapped on the upper surface during the bonding process as well as smaller air pockets that resulted from not cooling under pressure.

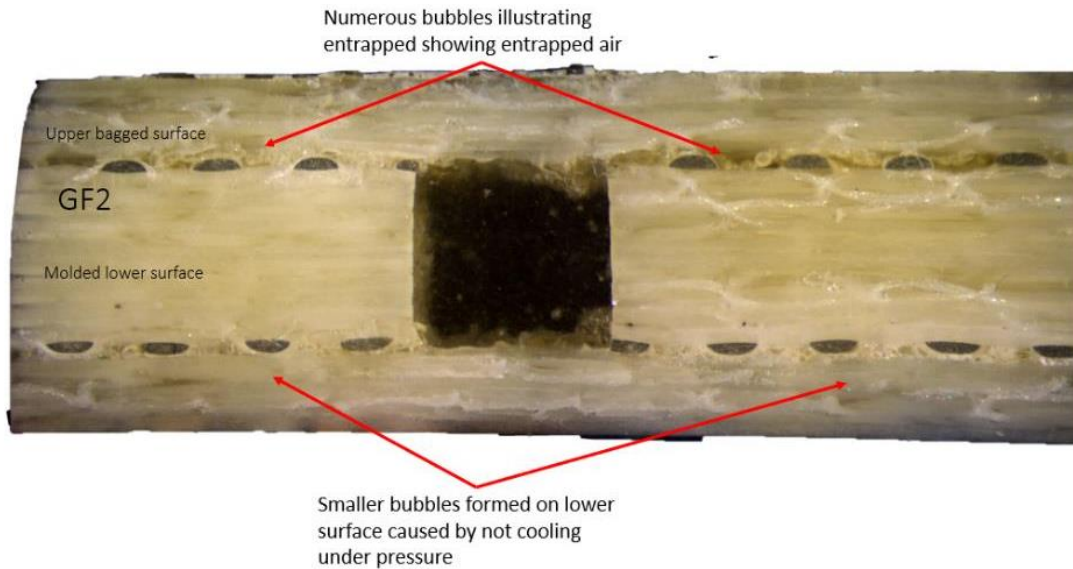


Figure 57: GF2 bonded sample showing large voids and defects in the bondline (6.4x)

Comparing GF2 and GF3 it can be seen that the bondline in GF3 is much more uniform and contains far fewer defects as a result of cooling under pressure. However the closer inspection of GF3 in Figure 58

shows the air bubbles that were entrapped during manufacturing of adherends which was also observed in Figure 54 in the lower surface image C). The presence of voids and air bubbles observed both before and after bonding illustrates that it is critical to create void free adherends prior to bonding because consolidation pressure and the squeezing of matrix material during fusion bonding does not remove entrapped air.



Figure 58: (Main) G-FLOW™ 3 bonded sample highlighting voids entrapped during manufacturing of G-FLOW™ adherends (25x)

The molded surface samples also showed very uniform bondline due to the lack of surface asperities, mitigating the potential for entrapped air during fusion bonding. Figure 59 shows the difference in bondline thicknesses between the upper side of the adherend which had a resin rich Compoflex surface finish before being compression molded and the lower surface which was on the tool side during infusion so little alteration was made when the samples were compression molded. The upper surface has an overall thicker resin rich area around the bondline which was likely due to the presence of excess resin from the Compoflex during molding. The lower surface has a more distinct bondline which is likely from the distribution of resin from the airfoil adherend surface not penetrating into the molded coupon.

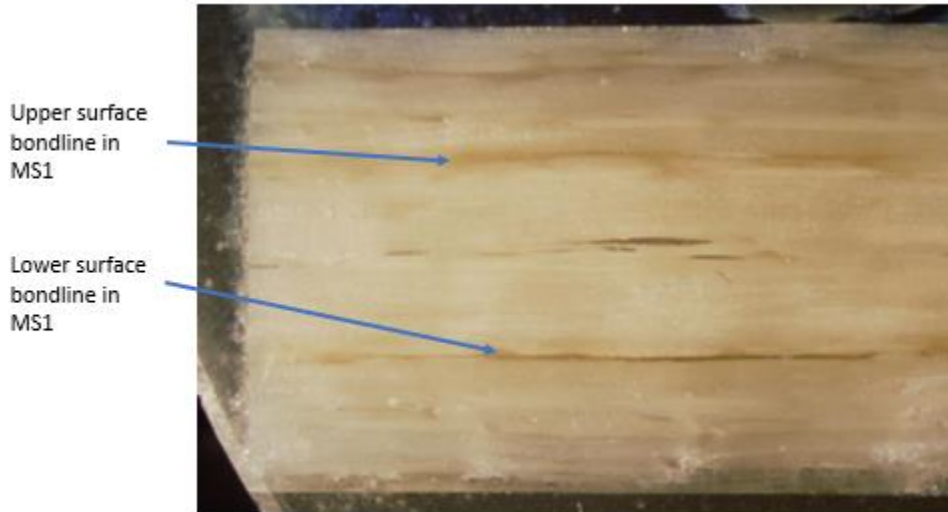


Figure 59: Molded surface bondline comparison between upper surface (molded) vs tool side of adherend

Overall the microscopy images correlate with values obtained from strength testing data and validate assumptions mentioned in previous sections such as the requirement for cooling under pressure, the lack of adherence to G-FLOW™ samples, the improvement of bond quality with un-wavy surface adherends and that the Compoflex surface texture on the airfoil adherends provides enough resin to sufficiently bond specimens, without the need for complex topography consumables.

4.6. Discussion of Glass Fiber Sample Bonding Results

The results of glass fiber Elium thermoplastic fusion bonding trials were sufficient to draw conclusions about how to proceed with later trials of carbon fiber reinforced Elium coupons. Overall the nylon Super Release A peel ply texture provided the most consistent quality bonds out of all surface finishes tested. The average value for all peel ply specimens was 14.3 ± 1.9 MPa and the results displayed the lowest standard deviation across all samples tested. When excluding results from the single trial that wasn't cooled under pressure (PP1) the average value for lap shear strength increases to 15.25 MPa with a standard deviation of only 0.53 MPa. Failure analysis showed better laminate quality was achieved using the peel ply surface texture by samples that exhibit fiber tear compared with samples from the Compoflex that showed much larger amount of delamination of the first ply of the adherend. Microscopy results showed the peel ply surface produced quality uniform bondline across the entire bonded area. There was

clearly enough resin to sufficiently bond the adherend and the airfoil from the matrix at the surface of the airfoil.

Across all glass samples Compoflex had an average lap shear strength of 12.35 ± 3.5 MPa however it also displayed the highest standard deviation across all three trials, though a major source of that deviation was caused by trial CF1 that was not cooled under pressure. If CF1 was excluded from the Compoflex averages strength increases to 14.9 ± 1.0 MPa. This is twice the standard deviation of the peel ply, likely caused by the variability in the surface topography. The presence of surface asperities in the Compoflex texture was likely a source of voids which would initiate failure in a more randomly distributed manner indicative of the higher standard deviation. The Compoflex trials did however produce the highest performing individual lap shear coupon which had a strength of 16.1 MPa. The resin rich surface texture of the Compoflex adherends clearly aided in higher performing joints. Resin rich asperities increased bondline thickness to increase leading to high values for strength yet lower consolidation pressure evident by resin rich areas within the adherend laminate observed in micrography analysis was a likely origin of larger amounts of fiber tear in quality bonded samples.

The molded surface texture laminates performed poorly as well, having an average strength of only 11.4 ± 2.0 MPa, even though all samples were cooled under pressure. Additionally, this value doesn't represent the full range of variables that were supposed to be examined as half of the mold surface specimens failed within the adherend so roughly half of the values for the bond strength were not obtained thus limiting the comparisons that could be made among processing variables. The highest performing individual sample reached a value of 14.8 MPa which was lower than values obtained using peel ply and Compoflex.

Additionally the difference between the vacuum bagged region and the Compoflex region in molded samples and the lap shear coupons tested from these specimens was distinct, the vacuum bagged area exhibited an average strength of 9.9 MPa while the samples from the resin rich Compoflex region with a more uniform surface topography exhibited a value of 13.0 MPa. This does illustrate that the use of infusion consumables can greatly aid in fusion bonding thermoplastic composites and that a purely vacuum bagged laminate is likely not ideal for fusion bonding. However, the molded surface microscopy

images did show a uniform bondline which is a major influence of bond strength. G-FLOW™ was the worst performing specimen, evident in strength testing, failure analysis, and microscopy. The average value for lap shear strength of G-FLOW™ samples was 9.02 ± 2.14 MPa drastically lower than the rest of the consumables. This was caused by a combination of voids created during the infusion process and the lack of resin on top of the glass fiber bundles used to distribute resin through adherends. Voids were created when trying to compress the asperities and hills created from the glass fiber bundles but when the glass fibers could not be flattened, air pockets were created leaving voids between bundles seen in microscopy images. The lack of resin on the surfaces of the G-FLOW™ fibers caused by the vacuum bag being placed directly on the surface resulted in cohesive failure across all specimens. This failure could have been adhesive failure since the Elium resin may have had difficulty bonding to the sizing on the GF fibers however this is only another potential cause of low strengths and the sizing on the G-FLOW™ fibers is unpublished.

It was evident that optimal processing variables were not uniformly applicable to all specimens, instead the optimum process is specific to each surface texture. Larger surface asperities require higher pressure and longer hold time at temperature to flatten the surfaces to achieve intimate contact which is the preliminary step in the intermolecular diffusion aided fusion bonding process. A uniform surface (flat) surface required far less time to initiate intimate contact and these results showed similar values of strength even at lower consolidation pressures during fusion bonding. It is likely that the relationship between consolidation pressure and lap shear strength likely reaches a plateau or peak at a certain value, after which higher pressures only cause fiber distortion and resin flash out of the bonded region causing lower values for strength.

Results from the failure analysis showed at least a portion of samples exhibiting fiber-tear failure occurred in all surface texture specimens tested. Fiber tear was evident even at failure values of 10 MPa which indicates that the value for interlaminar shear or debonding of the composite adherend are the limiting factor in the joint design. Further testing would be needed to determine a fiber reinforcement

product such as a woven fabric that has a higher inter-ply strength than the non-crimp triaxial fabrics used in this study to achieve higher bond strengths than 16 MPa that were seen in this study.

The results of the testing double lap shear coupons with glass reinforcement provided enough evidence to continue with the planned goal of heat welding the carbon fiber reinforced composite strut to root hub attachment plates to the airfoil blades in the final product. Thus, for the planned VAWT blade set it was determined that, based on the conditions evaluated, the fusion joining process was insensitive to surface condition and hold time at 200°C, but that cooling the press under pressure was important as was the higher 2.56 MPa (370 psi) pressure. Even when using the worst shear strength values obtained from sample testing, with an increased bond area of 16 in² values a bonded joint would be adequate to withstand all loading conditions and failure would not occur in the bonded region.

4.7. Carbon Fiber Double Lap Shear Bonding Results

Six trials of carbon fiber reinforced Elium ® 150 specimens were created using the parameters that resulted in the most consistent performance from earlier glass trials. Carbon fiber adherends were manufactured for testing via ASTM 3528 to investigate how bonding parameters effects were different than those obtained in glass fiber reinforced Elium® trials and to see if the results were sufficient to continue with the planned manufacturing method of fusion bonding the root hub to airfoil strut brackets. Due to the accelerated timeline of the project this testing was performed in conjunction with the manufacture of initial carbon fiber airfoil sections, so the final laminate stacking sequence or infusion process was not finalized. This resulted in two different airfoil laminate stack ups used across carbon lap shear bonding trials but a single run manufacture of the feedstock to create adherends.

The preliminary infusion of carbon airfoils which were bonded to adherends in trials CPP 1 and 2 used a stacking sequence of [± 45 , 0]_s using CBX-0900 ± 45 Biaxial NCF (300gsm & 0.48 mm thick) and CLA-0912 0° UD NCF (352 gsm & 0.6mm thick) giving a total thickness of 2.16 mm. Figure 60 illustrates the fabrics used, notice the carbon biaxial fabric has a layer of +45° placed on top of a -45° ply. These biaxial

fabrics were non-woven so there was nothing preventing inter-ply failure between the biaxial layers. Later carbon airfoil infusion used three plies of 4" diameter, +45° braided biaxial sleeve from A&P Technologies with a weight of 18 oz/yd² with an infusion thickness of 0.69 mm giving a total airfoil thickness of 2.1 mm. Compared to the 2.69 mm thick glass airfoil specimens the carbon airfoil sections were much thinner which caused issues when bonding lap shear samples with the same tooling used for glass. The individual carbon reinforcement plies used to manufacture DLS coupons are visually shown below in Figure 60.



Figure 60: Carbon fiber reinforcement used in lap shear adherend and airfoil manufacture

The surface texture on the carbon fiber laminates used to create feedstock for additional 4.25" x 5" flat adherends for ASTM 3528 lap shear samples was created using the nylon Super Release A peel ply as this gave the best results in the preliminary bonding trials using glass fibers. The inside surface of the airfoil was that of the Compoflex® which was also consistent with the glass trials. The feedstock samples were manufactured using a ±45 biaxial fabric and two uni-directional non-crimp fabrics, both from Vectorply to obtain a plate thickness twice that of the laminate in the airfoil. The plate was infused with a stacking sequence of $[\pm 45, 0]_s$ using the CBX-0900 ±45 Biaxial NCF (300gsm, 0.48 mm thick) and heavier weight CL-1800 0° warp unidirectional non-woven (590 gsm, 0.9mm thick) giving a total thickness of 4.56 mm, slightly twice the thickness of the airfoil in accordance with ASTM 3528. The carbon samples

were all infused using a standard green flow media similar to the glass samples seen in Figure 25 and the peel ply was left directly on the laminate until being bonded in the DLS jig, illustrated in

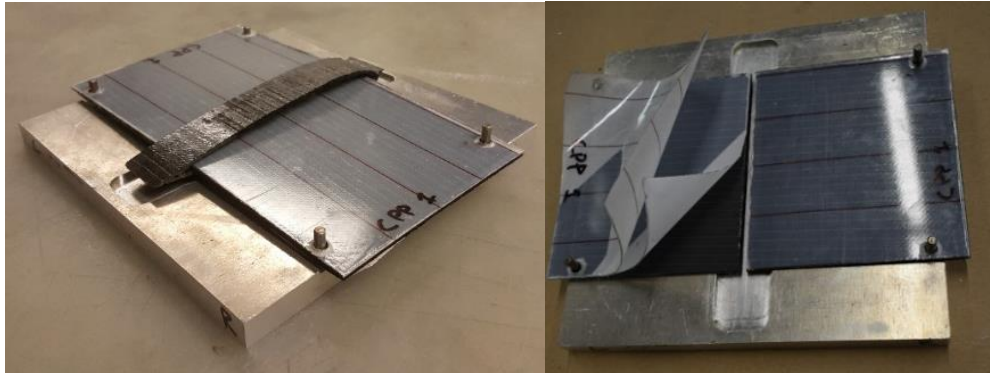


Figure 61: Peel ply left on laminate until molding (left) and removal of peel ply from adherends (right)

The carbon fiber reinforced double lap shear specimens were produced at 200°C, bonded at applied pressures of 185 psi and 370 psi, held for between 5 and 20 minutes at temperature and cooled under using water cooling in the platens of the hot press. The average strength obtained via double lap shear strength testing of these carbon fiber reinforced panels was 7.48 ± 1.2 MPa (1086 ± 298.1 psi), which was comparable to the lowest performing group of the glass fiber reinforced specimens. The highest average value obtained for shear strength amongst trials was 9.5 MPa was in trial #6 that was manufactured at a lower applied pressure and held at temperature for only 5 minutes. Only 17% of all the samples tested displayed values over 10 MPa.

Table 10 documents the results from the processing variables across all carbon samples.

Table 10: Strength results from carbon fiber peel ply trials

Trial #	Sanded with 220 Grit (Y/N)	Pressure Applied (psi)	Cooled under pressure (Y/N)	Hold time at 200°C (minutes)	Lap Shear Strength (psi)	Standard Deviation (psi)	Lap Shear Strength (MPa)	Standard Deviation (MPa)
CPP1	No	370	Yes	10	1055.8	175.7	7.3	1.2
CPP2	No	185	Yes	10	736.0	295.9	5.1	2.0
CPP3	No	370	Yes	10	1067.2	79.5	7.4	0.5
CPP4	No	370	Yes	20	1140.3	272.8	7.9	1.9
CPP5	No	185	Yes	10	1136.9	308.9	7.8	2.1
CPP6	No	185	Yes	5	1379.3	110.4	9.5	0.8

It was predicted that values obtained would be similar to glass reinforcement, however the carbon samples obtained values similar to the lowest performing glass samples. Additional efforts to optimize parameters for these carbon fiber reinforced panels and airfoils was not undertaken, as even this value of shear performance was considered satisfactory for the current application of the demonstration prototype VAWT. Thus, this remainder of this section documents the results obtained and discusses likely sources of the lower bond strength so future work can address these issues.

The major reasons for lower value of shear strength obtained from carbon samples was due to the materials used to manufacture the samples to be bonded and the quality of the airfoil adherends used for bonding. The biaxial fiber reinforcement used for the flat adherends was not as sufficient at transferring loads into the samples and the majority of carbon samples failed by debonding a single 45-degree ply from the adherend surface which is illustrated in the left sample highlighted in Figure 62 (CPP3.2). Using non-crimp biaxial reinforcement in the airfoil for the first two sets of samples was a poor choice but until the infusion process was repeatable the CSU team used fiber that was available for a limited quantity of 4" braid was procured specifically for 132" infusion trials. In addition, it was evident that some of the airfoil infusions appeared to be fully wet out however after bonding showed dry sections of fabric or voids in the airfoil which is shown in the middle sample coupon in the figure below (CPP3.3). The highest quality bonds were observed in the final carbon trial (CPP5) and the right most fractured adherend sample (CPP5.4) shows the fiber debonding from the adherend since there was full wetout in the airfoil.



Figure 62: Carbon double lap shear failed adherends

In addition to the issue with the biaxial reinforcement, the airfoil adherends were only 2.1 mm thick compared to 2.69 mm airfoils used in testing glass specimens. Since bonding trails used the same tooling there was likely less consolidation pressure or an uneven pressure applied to carbon samples to adequately bond the surfaces. This was exhibited by bulging of the airfoil adherend, fiber migrating to the gap between the adherends, or a visible gap between adherends which are seen in Figure 63. The higher thermal conductivity of the carbon fiber compared to glass likely compounded the mold alignment issues which led to fiber wash and distortion in bonded area.



Figure 63: Bonded Carbon Fiber Peel Ply Double lap shear samples and cross section of bonded joint

Based on the issues documented for carbon reinforcement the final strut to root hub bonded connection utilized a 2x2, low profile twill weave woven fabric that has a higher inter-ply strength than the non-crimp biaxial fabrics used with early trials. The fusion bonding process was carried out using processing variables that provided the most consistent results from lap shear coupon testing; a lower mold temperature of 180°C to mitigate thermal effects of the increased thermal conductivity, a hold time of 10 minutes, a consolidation pressure of 370 psi, and cooled under constant pressure. A set of ASTM 3528 coupons were manufactured using the finalized materials documented in Section 5 covering the full-scale manufacturing of the VAWT. The double lap shear coupon was bonded with sections of airfoil that was trimmed directly from the airfoil adherend plates were bonded into in the final manufacture of the prototype VAWT. Unfortunately, these samples were not mechanically testing during the spring semester 2020 due to the COVID-19 outbreak and closure of the CMMS lab at CSU however the appearance of both bondline uniformity, and airfoil adherend shape indicate a drastically improved performance.

5. FULL SCALE VAWT MANUFACTURING

During the continued material processing investigation processing characteristics of the Arkema Elium® thermoplastic resin were better understood. That post-processing advantage led to improvements and part count reduction in the blade assembly fabrication through two main areas: (1) integrated blade mounting tabs for central hub connections via fusion bonding and (2) 90° bend from vertical blade to horizontal spreader utilizing post process reforming. During the investigation of the fusion bonding study, additional bending trials were conducted on 64” glass fiber reinforced airfoil sections to manufacture the airfoils from a single airfoil rather than having to bond in 90° brackets between the horizontal and vertical blades.

5.1. Evaluation of Post Process Reforming of Thermoplastic Airfoil Blade Sections

The possibility of reforming of thermoplastics gives them a great advantage of thermoset counterparts and allows shaping of complex geometries from simpler shapes. In this application a simple, uniform cross section can be curved into the geometry of a D shaped or helical style Darrieus style blade or bent into the H-type geometry used in this study which can be seen in image A in Figure 64. However, there are challenges to this process and two major issues experienced by the CSU team were maintaining structural integrity of the bended section by eliminating buckling fibers that were experienced in early trials and preserving the aesthetics of the finished blade. The team improved the free form bending process with a set of matched dies seen in image B. Sections of airfoil were heated to 200°C then placed in the die and reshaped. This reduced the inner surface buckling exhibited in the free form bend. However, due to little in-plane shear in the bonded region and the difference in length between the outside surface fiber and the inner surface fiber, the bent region displayed bulging at the inner surface and the outside edges of the die.

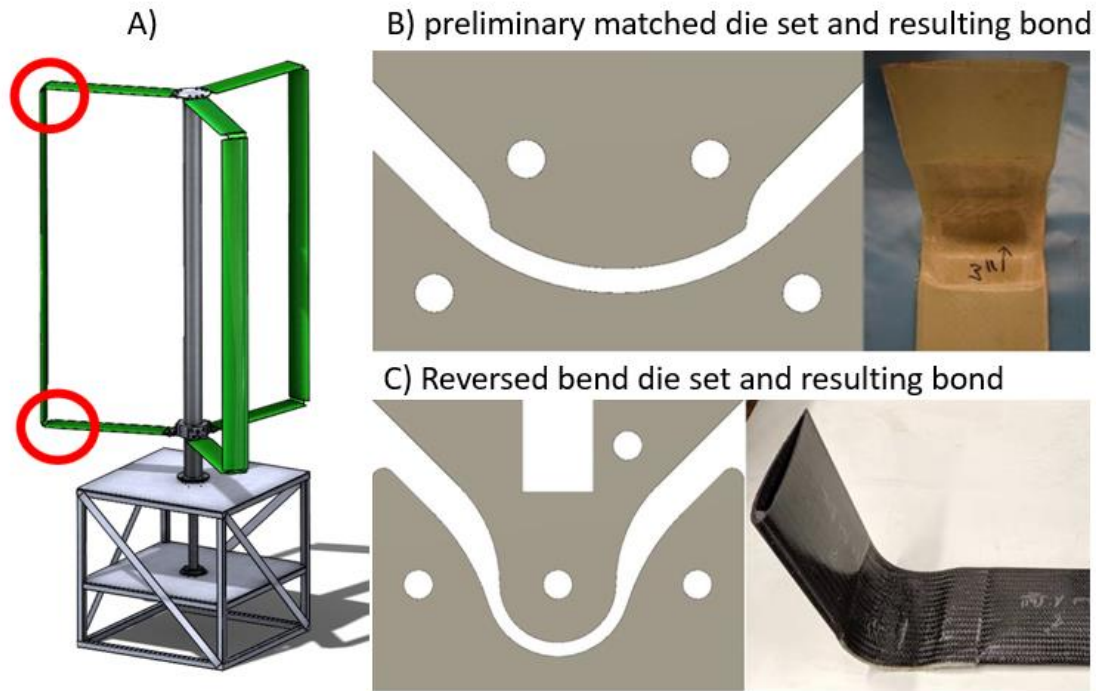


Figure 64: A) 90 Degree bend locations in VAWT, B) preliminary matched die set, C) reversed bend die set

The team designed a second die set that included a reverse bend seen in image C) of Figure 64 that attempted to maintain equal inside and outside fiber lengths. This improved the quality of the bent region and there was little distortion along the bent section yet there was still bulging at the end of the die area which was neither aesthetically pleasing in addition to being a local source of stress in the region. This coupled with the fact that this process required the airfoil to be correctly positioned at the planned bed location in two areas of the midspan of the full airfoil length there was little confidence that the process could be repeated with consistent dimensions and accurate spacing in the required three blade pair for the VAWT prototype.

The final design that was selected and produced quality bent regions with a uniform bent section was that based on a wiping die. In this approach the smaller outside roller rotates while it is swung around the inner static roller as seen in the left image in Figure 65. With this process a consistent controlled radial gap of 0.25" (6.3mm) is established, which was determined by the thickness of the flattened airfoil section in prior testing. This ironing or wiping motion keeps the inner surface stationary which allows for

a repeatable and consistent bended section. The wiping die setup also allowed for the positioning of the airfoil so subsequent and consistent bends could be made using the relative fixturing and the predrilled mounting holes in the hub to strut plate that were fusion bonded into the airfoil sections.

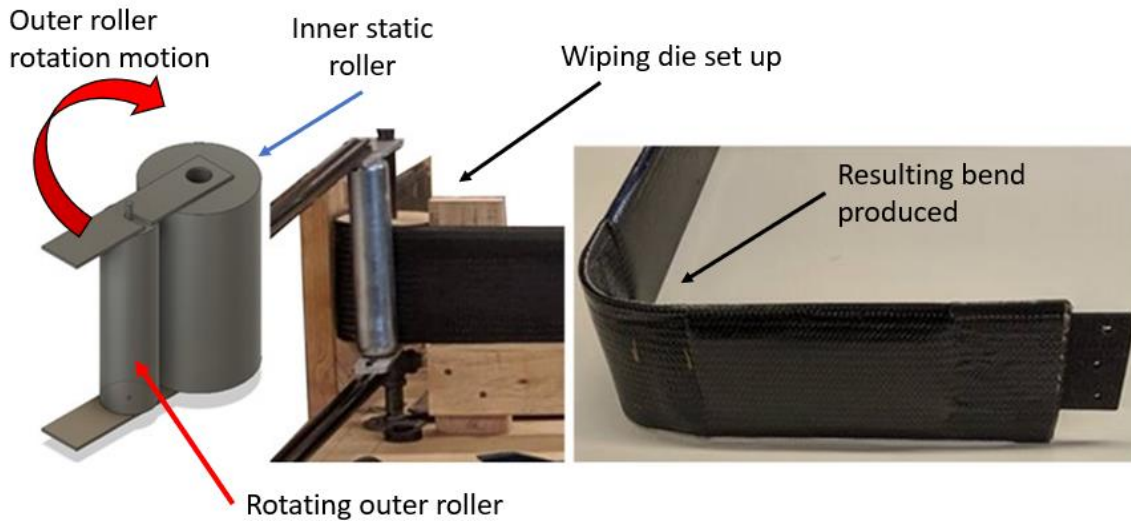


Figure 65: Wiping die set for full scale VAWT bending

5.2. 3.4m Tooling for Full Scale Blade Infusion

Given the success of the fusion joining trial for incorporating the tower to blade attachment plates and the demonstration of post-mold reforming into 90° bends, a hollow airfoil section approximately 129” long was required to fabricate a single VAWT blade that would construct the vertical airfoil and the horizontal spreaders at both top and bottom of the rotor assembly. This required the manufacture of a new high-quality high temperature to manufacture these long hollow airfoils, a high quality, high stiffness mold set was required. A 40 lb./ft³ urethane tooling board with a thin epoxy surface coating was procured, nominally 92” long. The tooling was designed with ‘O’-ring grooves along the length, one near the leading edge and the other near the trailing edge of the airfoil geometry to better contain the low viscosity Elium® 150. 0.5” hemispherical cavities were machined into the flange area of the master to allow ball bearings of the same diameter to be used as alignment features in the resulting molds. Aluminum side and end plates were added to the master as seen in image a) of Figure 66. These were to create a cavity within

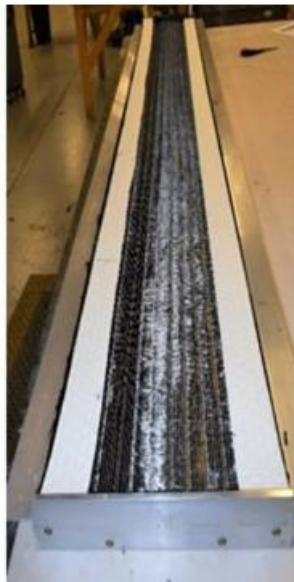
the tooling mold to construct vertical stiffeners in the final mold, increasing stiffness without excessive weight. The end flanges were included were also used in the assembly of the molds, since the tooling master was only 2/3 the length of the required 138” airfoil molds.

Carbon fiber was selected as the reinforcement for the molds to take advantage of the higher thermal conductivity which eased the removal of excess heat generated in the exothermic polymerization of the Elixir® in addition, the increased stiffness provided by the carbon fiber reinforcement was desirable given the dimensions of the mold set. Vectorply supplied non-woven C-4QX 9400, 94.52oz stitched Quadriaxial fabric and C-WV-0600, a 6oz/yd² twill fabric for the molds. A finer twill weave was used at the tool surface to ensure a finer finish on the airfoil surface, and the Quadrax was used to build thickness and structure. One layer of the Quadrax was used on top of the twill weave. Additionally, along the length of the mold flanges, Lantor Soric LRC 3, an infusion specific core material was placed between 2 layers of Quadrax to increase mold stiffness of the flanges. Placement of the dry fiber on the tool surface and the core material on the flanges can be seen in image b) in Figure 66.

a) Tool and vertical stiffeners



b) Infusion consumables



c) Mold infusion process



d) Completed 92” length mold



Figure 66: Mold manufacturing sequence

All the reinforcement material was placed dry and the composite mold was created through a resin infusion approach seen in image c) above. The molds sections were infused using Rhino 1411/4111 epoxy resin at nominally room temperature followed by a freestanding post-cure of 2 hours at 100°C. The walk-in oven at Colorado State University could only accommodate a 92” mold section so it was necessary to manufacture three of the 92” mold halves, one of which was cut in half then the vertical wall at the end was used to join the partial section to the full section creating the top and bottom halves of the 132” finalized mold which provided just sufficient extra length needed for each blade. A completed 92” mold section is seen in image d) of Figure 66.

5.3. Full Scale 3.4m Blade Infusion

The process used to successfully manufacture the full length 129” prototype VAWT blades required only minor variation in preform set-up and infusion procedure from that used in the 64” trial blade manufacture. The preform again utilized 3 layers of the Vectorply C-LA 0912 stitched 9oz UD carbon fabric with integral 1.2oz chopped glass mat trapped between 2 layers of the 4”, 18oz braided carbon fiber, supplied by Highlands Composites (C400-15) and A&P (Z56L400R). This resulted in the final desired stacking sequence $[\pm 45, 0, \pm 45]$ along the top and bottom of the airfoil, and $[\pm 45, \pm 45]$ at the leading edge and trailing edge, where the UD was not positioned. Preform assembly, insertion into the mold and infusion are shown in Figure 67. The liquid Elium® 150 resin travelled, in the flow media, down the length of the 138” mold set within 12 minutes and the infusion was complete in less than 20 minutes. Mold surface temperature was monitored with a thermal imaging camera and when the surface temperature reached 50 C, then bags of ice were applied to the outer mold surface. The mold set was left closed for several hours to ensure process completion.

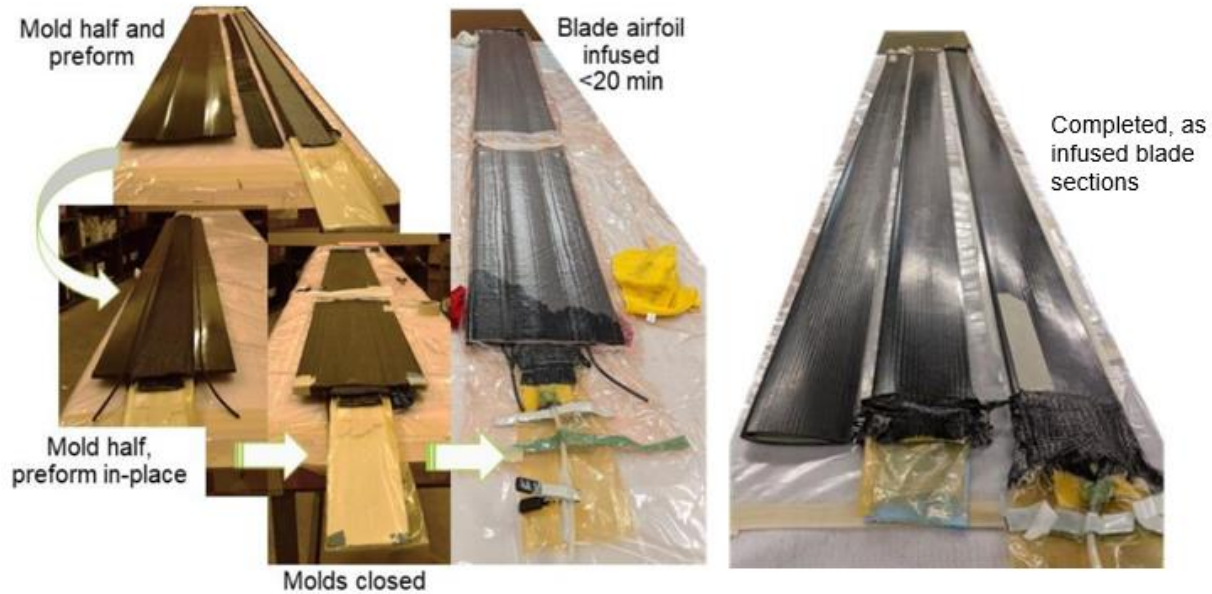


Figure 67: Manufacturing process of 138" airfoil blades

5.4. Blade to Root Hub Attachment Via Fusion Bonding

The fusion bonding of two separate thermoplastic composite plates allowed the mounting tab between rotor airfoil and central hub to be integrated directly into the rotor assembly. By integrating the mounting tab into the airfoil section, local composite considerations are minimized since the reinforcement that would have been required to support the bearing load on the airfoil cross section is no longer necessary at that location. Instead that load is handled by shear forces through the fusion bond which was shown to have adequate strength to withstand the expected loads. The 6" x 4" strut to hub bracket which is illustrated in red in the left image of Figure 68 was manufactured using a single ply of Vectorply's C-4QX 9400, a quadriaxial heavy weight quasi-isotropic reinforcement fabric in conjunction with four plies of a 2x2 Twill weave 3K 6 oz woven Hexcel AS4 carbon fiber fabric procured from Composite Envisions. The extremely heavy weight quadriaxial fabric weighing 94 oz/yd² is constructed utilizing a balanced and symmetric construction $[90^{\circ}/0^{\circ}/45^{\circ}/-45^{\circ}]_s$ and was used to construct the bulk thickness of the roughly 0.25" thick bracket. Two plies of the twill weave fabric were placed on the exterior surfaces in a $\pm 45^{\circ}$ orientation to absorb the shear stresses at the bonded joint. The final stacking sequence for the bonded hub to strut brackets was $[\pm 45^{\circ}_2/90^{\circ}/0^{\circ}/45^{\circ}/-45^{\circ}]_s$. Combined with the 4"x4" bonded region in the

airfoil and a conservative estimate of 1000 psi lap shear strength of the carbon fiber reinforced double lap shear coupons reviewed in section 4.6 the team deemed the 16,000 lb. pullout force required for failure would be beyond the loads that would be experienced by the airfoil. After bonding strut to hub brackets in the airfoil, the ends were trimmed in an atheistic manner that removed the portion of the trailing edge that was compressed during the bonding of the end brackets. The right image in Figure 68 illustrates the completed set of bonded inserts on all three airfoils and the two airfoils on the left having been trimmed to the final shape.

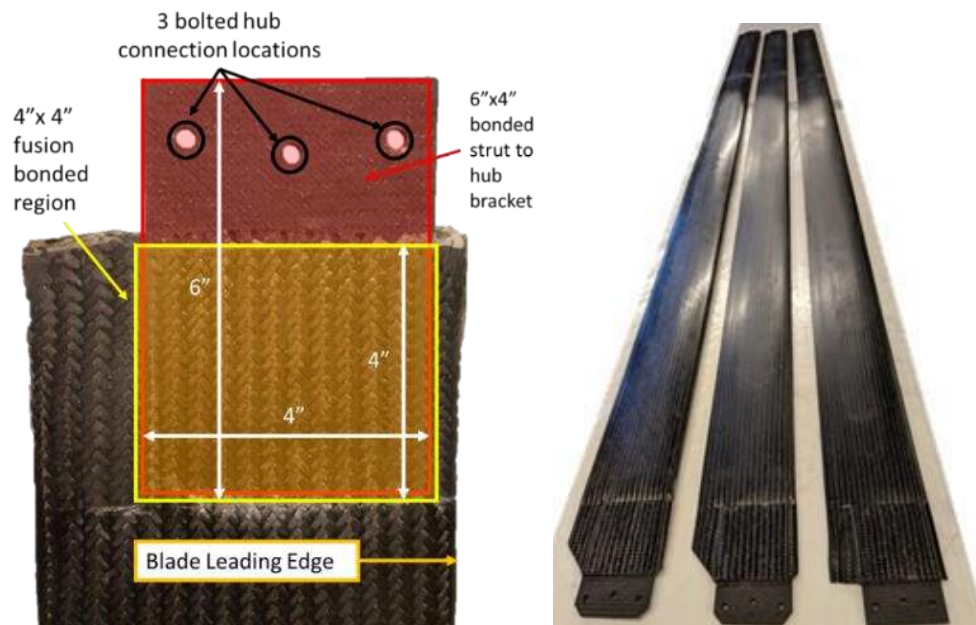


Figure 68: Blade to Tower Mounting Tabs illustrating 16 in² bonded region and completed set of 3 blades with bonded inserts

5.4.1. Method of Bonding End Plates to Airfoil Sections

The end plates were bonded to the 3.4 m infused airfoil blades after the consumable materials were removed from the hollow internal section of the airfoil. The internal surface finish of the airfoil blade was the coarse finish left behind after removing the Compoflex® flow media used to infuse the blade section. No other modifications besides cutting the blade section to the proper length was necessary before fusion bonding in the end fittings. To facilitate the final joining operations two 6" x 8" by 0.5" thick aluminum plates were machined to compression mold the 4" long by 4" wide and ¼" thick carbon fiber/ Elium® plates that would allow the blades to be bolted to the turbine hub. The molding tooling can be seen in

Figure 69. The mold set allowed the airfoil to be inserted into the tooling and the composite strut to root hub attachment plates to be positioned correctly inside the airfoil. The bolt hole locations kept the plate centered within the airfoil during the compression molding process and a positive stop positioned the airfoil.

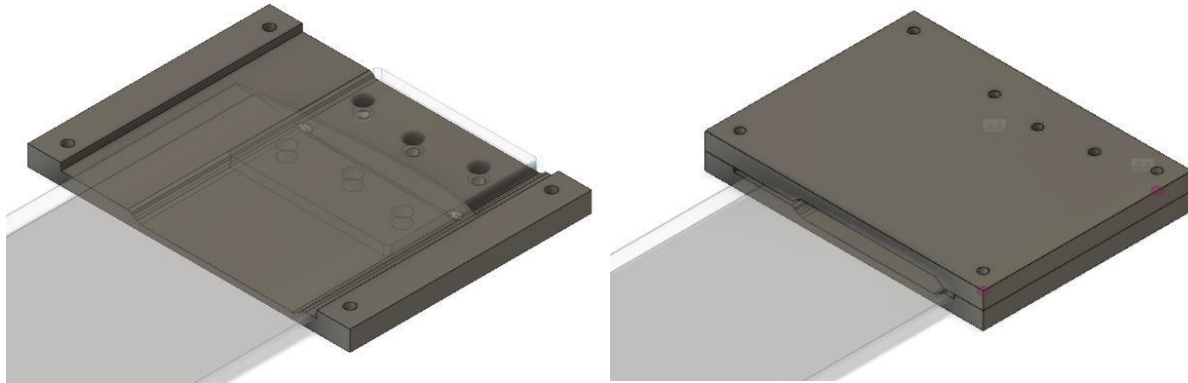


Figure 69: End Fitting Compression Mold Dies

Figure 70 illustrates the process underwent to fusion bond the mounting plates. The mounting plates were positioned inside the molds using the bolted hole locations and dowel pins to correctly orient the mounting plate. After removing consumables from the completed airfoils, they were trimmed to a length of 129” to account for the vertical section of the blade and the horizontal spreader sections. Once trimmed to length the airfoil was slid over the composite strut to root hub attachment plates within the compression molding tooling up to the positive stop that prevented the airfoil from sliding too far into the mold. Once adherends were positioned correctly the fusion bonding process was carried out using processing variables that provided the most consistent results from lap shear coupon testing; a mold temperature of 180°C, a hold time of 10 minutes, a consolidation pressure of 370 psi, and were then cooled under constant pressure.

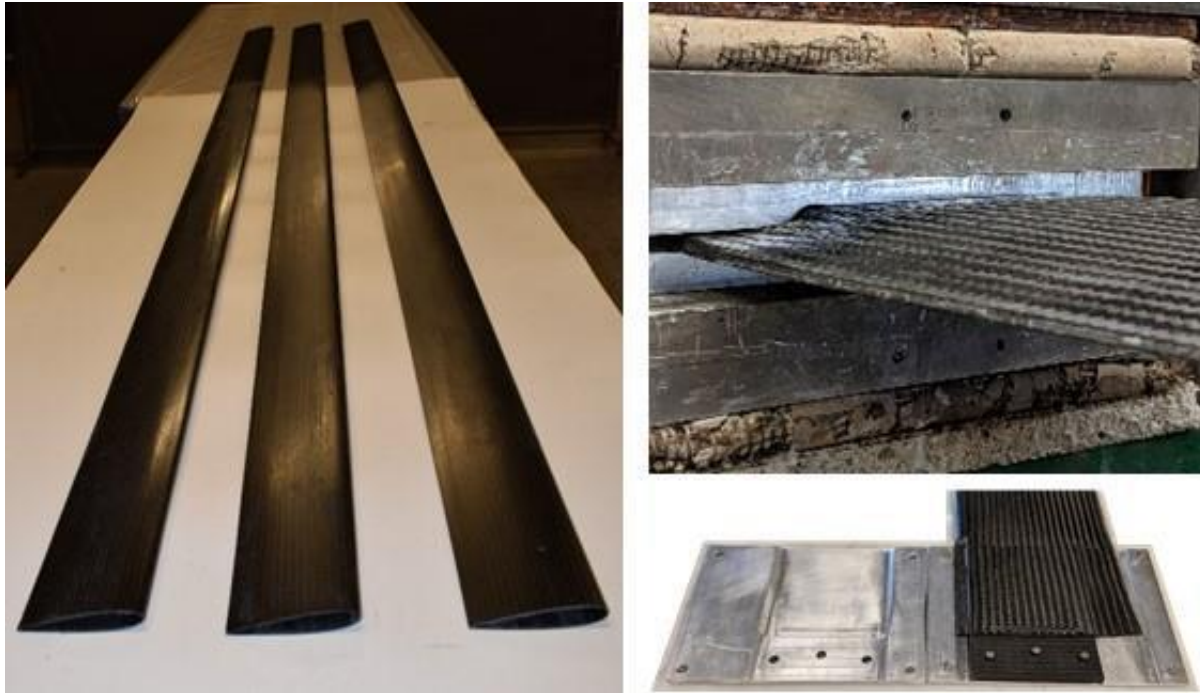


Figure 70: Fusion bonding process showing a) 129" infused airfoils b) compression molding mounting tabs c) completed fusion bond within tooling

5.5. Final Thermoforming of and Post Processing of Thermoplastic Composite Blades

After the strut to hub brackets were fusion bonded into the 129" airfoil sections the predrilled mounting holes in the bonded insert were used as a reference point to complete the final thermoforming of the regions to be bent into the 90-degree junction between vertical blades and the horizontal spreaders. The airfoil regions to be bent were placed in a heated platen press with flat plates and heated until the thermoplastic matrix reached a temperature of 200°C then were carefully transferred to the wiping die bending jig. At this heated state well above T_G the composite is very flexible and must be well supported and held in the correct orientation to reduce the likelihood of sagging or twisting and a subsequent misalignment. The wiping die setup and fixturing allowed for the positioning of the airfoil as well as supporting the airfoil so subsequent and consistent bends could be made using the relative fixturing and that were fusion bonded into the airfoil sections. Once positioned in the jig the smaller outer wiping roller was rolled around the inner static roller to create the bended joint. Figure 71 illustrates the process of putting the second bend in the airfoil section to complete the geometry of the thermoplastic VAWT blade.

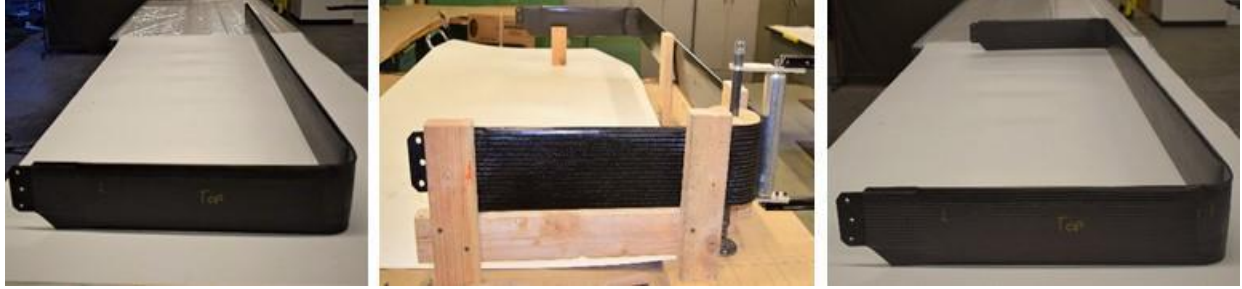


Figure 71: Completion of post process bending in completed airfoil blade

Once the two bending operations were performed the blades were coated with a thin layer of enamel clear coat before being lightly sanded with 1500 and 2000 grit sandpaper to generate a glossy finish for aesthetic purposes. The as molded versus glossy coated surfaces are compared in Figure 72 and following this process the VAWT was ready to be assembled.

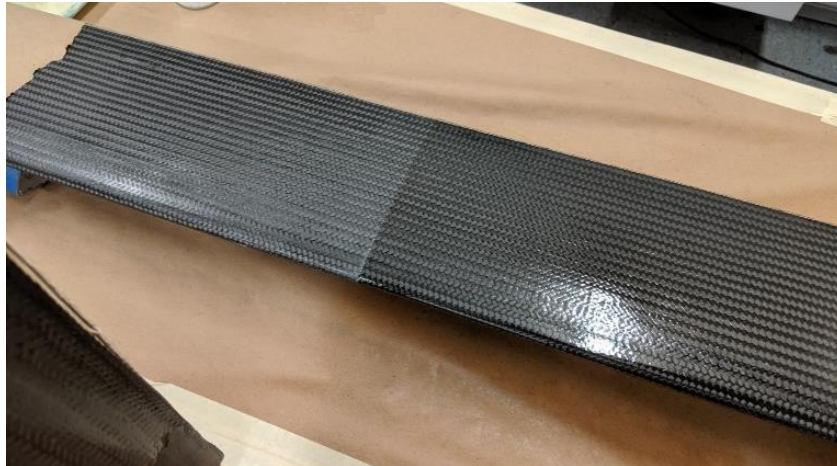


Figure 72: Comparison between molded surface and final post process clear coat finish

5.6. Final Assembly of VAWT Prototype

A full-scale VAWT rotor assembly was fabricated and assembled for display at the July 2019 IACMI Member's Meeting in Denver, CO. The initial CAD model shown below in Figure 73 that utilized the original proposed 90° degree brackets and metal mounting tabs shown in figures Figure 12 and Figure 14 described in Section 1.7.2 included a rotor assembly that incorporated machined components for the mast, central hubs, and bearing housing as well as the composite airfoil sections. The initial rotor assembly was estimated in the CAD model to weigh 47.7 lb. based off material properties of the materials selected by Steelhead Composites. By successfully deforming the airfoil into the bent geometry shown below and

integrated airfoil blade to root hub mounting tabs into the final manufactured VAWT, the updated CAD experienced a 12% reduction in mass from the baseline design down to 41.2 lbs. This theoretical estimate differed slightly from the as fabricated mass, where each airfoil section weighed approx. 7.5lbs as opposed to the theoretical CAD estimate of each airfoil section at 5.1lbs, which did not account for resin rich areas within the airfoil blades. The final manufactured weight of 50 lbs. was thus within 10% of the estimated mass of the original design.



Figure 73: As designed versus as manufactured VAWT prototype

6. CONCLUSIONS

The Colorado State University team successfully met the research objectives of the technical collaboration for the IACMI study by demonstrating the design and manufacture of a prototype VAWT rated between 0.5 and 1 kW using thermoplastic reinforced composites. The research team at CSU developed the manufacturing strategy which included the infusion methods, the consumables used, tooling, and thermoplastic specific approaches of post-mold bending and fusion bonding examined to potentially transform the way VAWT rotor assemblies are constructed. The combination of post-process deformation and fusion joining, available only through the use of the thermoplastic matrix composite, helped demonstrate post-process bending to remove the need for discrete connections between the horizontal and vertical sections of a 'C'-shaped Vertical Axis Wind Turbine blade and integrating composite mounting tabs that increased structural integrity, demonstrated methods of mass manufacture possibilities, and the benefits of novel liquid form thermoplastics over traditional thermosets. If a thermoset matrix composite were used the complex, molded geometry of this VAWT would have necessitated either complicated molds or multiple blade segments that would have been required to be adhesively bonded or mechanically fastened together. It is evident there are many advantages of this type of thermoplastic composite material including its unique post-processing potential, durability, recyclability, and overall strength to weight. The manufacturing techniques utilized for this prototype fabrication show a lot of promise for the manufacturability of similar part geometries, where a uniform cross section shape could be pultruded in a mass manufacturing environment at low cost then reformed or fusion bonded to create complex geometries.

6.1. Fusion Bonding Assembly Methods

The results of this study demonstrate the benefits of using thermoplastic matrix materials in the construction of wind turbine blades as the blade components can be thermally welded to ease manufacture, eliminate adhesive bonding issues, and open the possibility for joining components on site,

a huge challenge when blades are manufactured with increasing blade length. Fusion bonding of two separate thermoplastic composite features allowed the mounting tab between rotor airfoil and central hub to be integrated directly into the rotor assembly. By integrating the mounting tab, local stress concentrations are minimized compared with the baseline design of adhesively bonded tabs since the reinforcement that would have been required to support the bearing load on the airfoil cross section is no longer necessary at that location which also greatly eased the manufacturing of the airfoil sections. In the fusion bonded joints load is handled by shear forces through the adhered region which was shown to have sufficient strength to withstand the expected loads through the experimentation of ASTM 3528 Double Lap Shear Strength testing. From lap shear testing it was determined that, for the glass fiber reinforced Elium® 150 composites, fusion bonded double lap shear coupons created using bulk heating obtained average lap shear strengths values in excess of 15MPa (2,200 psi) with maximum samples having values over 16 MPa (2328 psi). Further, it was realized through failure analysis that the highest failure strengths were related to failures within the composite adherend, indicating that the fusion bond was no longer the limiting factor in the design and manufacture of the VAWT.

6.2. Surface Topology Effect on Strength of Fusion Bonding Joints

Due to the fact Elium® is manufactured using liquid molding techniques the research question arose to determine if consumables used in manufacturing fiber reinforced Elium® thermoplastic composites via resin infusion could contribute to higher bond quality. It was predicted that utilizing infusion consumables that provided additional matrix at the bondline would improve the quality of bonded joints. Since the consumables that produced the most amount of neat resin at the surface left behind a rough texture, a second inquiry was investigated on the impact of surface texture produced by consumables on the resulting effectiveness of fusion bonded joints. The bulk of this research found that there is a tradeoff between additional matrix material at the bond interface and the rough surface topography left behind by the consumables. The results indicated that resin rich bondlines created by using consumables such as Compoflex do increase the joint strength, however the presence of tall surface asperities and deep valleys

lead to large deviations in joint strength from the inclusion of entrapped air during the fusion bonding process. Similar values for strength were obtained from traditional peel ply surface texture that are not as rough or variable across the surface nor introduce extra resin into the bondline. In addition, varying surface textures require different bonding parameters for increasing joint strength. It was observed that the high peaks of surface asperities required higher consolidation pressures and longer hold times above the materials T_G during bonding and consolidating the fusion bonded joint. This allowed asperities to flatten and resin to become viscous enough at the bond interface to achieve intimate contact and allow for molecular diffusion to occur between polymer chains, the fundamental process of fusion bonding thermoplastic polymers. By utilizing a peel ply especially those of nylon material that reduce the contamination at the bond interface minimal secondary processing is required to achieve quality fusion bonded joints in liquid molded thermoplastic composites. This has the potential to eliminate the costly and time-consuming process of surface preparation and adhesive bonding seen in thermosetting polymer matrix composites and wind turbine manufacture.

6.3. Recommendations for Future Work

The results of this study open the potential for further investigation of fusion bonded joints using Elium thermoplastic in fiber reinforced composites. The first recommendation for future work would be the optimization of carbon fiber reinforced Elium thermoplastics. This includes an optimization design of experiments that could keep bonded sample geometry simple, rather than using the inside of difficult to manufacture airfoil sections as part of the adherends in bonded joints and experimenting with the processing variables in this research. Additional investigation is needed to further quantify the effect of the high thermal conductivity of carbon fiber in fusion bonded joints, to investigate if it improves or decreases the ability to fusion welded samples. Once optimization of fusion bonded joints occurs it would be recommended to perform fatigue experiments on joints manufactured with bulk heating to quantify degradation in laminate quality after repeatedly heating and cooling in addition to high cycle experimentation as this could be used in later lifecycle purposes of fusion bonded joints.

REFERENCES

- [1] C. S. Goh, "Energy: Current Approach," , pp. 145-159, 2019.
- [2] E. Möllerström, P. Gipe, J. Beurskens and F. Ottermo, "A historical review of vertical axis wind turbines rated 100 kW and above," *Renewable & Sustainable Energy Reviews*, vol. 105, pp. 1-13, 2019.
- [3] A. Das and P. K. Talapatra, "Modelling and Analysis of a Mini Vertical Axis Wind Turbine," *International Journal of Emerging Technology and Advanced Engineering*, vol. 6, no. 6, 2016.
- [4] L. Mishnaevsky, K. Branner, H. N. Petersen, J. Beauson, M. McGugan and B. F. Sørensen, "Materials for Wind Turbine Blades: An Overview," *Materials*, vol. 10, no. 11, p. 1285, 2017.
- [5] Q. Govignon, S. Bickerton and P. Kelly, "Experimental investigation into the post-filling stage of the resin infusion process," *Journal of Composite Materials*, vol. 47, no. 12, pp. 1479-1492, 2013.
- [6] P. Brøndsted, H. Lilholt and A. Lystrup, "COMPOSITE MATERIALS FOR WIND POWER TURBINE BLADES," *Annual Review of Materials Research*, vol. 35, no. 1, pp. 505-538, 2005.
- [7] K. K. Chawla, *Composite Materials: Science and Engineering*, 1987.
- [8] K. v. Rijswijk and H. Bersee, "Reactive processing of textile fiber-reinforced thermoplastic composites : An overview," *Composites Part A-applied Science and Manufacturing*, vol. 38, no. 3, pp. 666-681, 2007.
- [9] O. d. A. Raponi, L. C. M. Barbosa, B. R. d. Souza and A. C. A. Junior, "Study of the influence of initiator content in the polymerization reaction of a thermoplastic liquid resin for advanced composite manufacturing," *Advances in Polymer Technology*, vol. 37, no. 8, pp. 3579-3587, 2018.
- [10] R. E. Murray, D. Swan, D. Snowberg, D. Berry, R. Beach and S. Rooney, "Manufacturing a 9-Meter Thermoplastic Composite Wind Turbine Blade," in *Proceedings of the American Society for Composites — Thirty-second Technical Conference*, 2017.
- [11] L. Keuthage, D. Heider, J. W. Gillespie, B. Z. G. Haque, J. J. Tierney, S. Yarlagadda, A. Campbell and D. Rinehardt, "Thermoplastic carbon fiber reinforced body-in-white structures for vehicle crash application," *Proceedings of the 25th International Technical Conference on the Enhanced Safety of Vehicles (ESV)*, 2017.
- [12] D. S. Cousins, Y. Suzuki, R. E. Murray, J. R. Samaniuk and A. P. Stebner, "Recycling glass fiber thermoplastic composites from wind turbine blades," *Journal of Cleaner Production*, vol. 209, pp. 1252-1263, 2019.
- [13] W. Obande, D. Mamalis, D. Ray, L. Yang and C. M. Ó. Brádaigh, "Mechanical and thermomechanical characterisation of vacuum-infused thermoplastic- and thermoset-based composites," *Materials & Design*, vol. 175, p. 107828, 2019.
- [14] S. K. Bhudolia, P. Perrotey and S. C. Joshi, "Mode I fracture toughness and fractographic investigation of carbon fibre composites with liquid Methylmethacrylate thermoplastic matrix," *Composites Part B-engineering*, vol. 134, pp. 246-253, 2018.

- [15] M. Haggui, A. E. Mahi, Z. Jendli, A. Akrouf and M. Haddar, "Damage Analysis of Flax Fibre/Elium Composite Under Static and Fatigue Testing," *International Conference Design and Modeling of Mechanical Systems*, pp. 681-691, 2017.
- [16] P. Davies, P.-Y. L. Gac, M. L. Gall and M. Arhant, "Marine Ageing Behaviour of New Environmentally Friendly Composites," , pp. 225-237, 2018.
- [17] J. Beguinel, "Interfacial adhesion in continuous fiber reinforced thermoplastic composites: from micro-scale to macro-scale," , 2016.
- [18] S. K. Bhudolia and S. C. Joshi, "Low-velocity impact response of carbon fibre composites with novel liquid Methylmethacrylate thermoplastic matrix," *Composite Structures*, vol. 203, pp. 696-708, 2018.
- [19] T. Pini, F. Briatico-Vangosa, R. Frassine and M. Rink, "Matrix toughness transfer and fibre bridging laws in acrylic resin based CF composites," *Engineering Fracture Mechanics*, vol. 203, pp. 115-125, 2018.
- [20] S. K. Bhudolia, P. Perrotey and S. C. Joshi, "Optimizing Polymer Infusion Process for Thin Ply Textile Composites with Novel Matrix System," *Materials*, vol. 10, no. 3, p. 293, 2017.
- [21] D. Mamalis, W. Obande, V. Koutsos, J. R. Blackford, C. M. Ó. Brádaigh and D. Ray, "Novel Thermoplastic Fibre-Metal Laminates Manufactured by Vacuum Resin Infusion: The Effect of Surface Treatments on Interfacial Bonding," *Materials & Design*, vol. 162, pp. 331-344, 2019.
- [22] T. Pini, F. Briatico-Vangosa, R. Frassine and M. Rink, "Fracture toughness of acrylic resins: Viscoelastic effects and deformation mechanisms," *Polymer Engineering and Science*, vol. 58, no. 3, pp. 369-376, 2018.
- [23] S. K. Bhudolia, P. Perrotey and S. C. Joshi, "Enhanced vibration damping and dynamic mechanical characteristics of composites with novel pseudo-thermoset matrix system," *Composite Structures*, vol. 179, pp. 502-513, 2017.
- [24] R. E. Murray, J. Roadman and R. Beach, "Fusion joining of thermoplastic composite wind turbine blades: Lap-shear bond characterization," *Renewable Energy*, vol. 140, pp. 501-512, 2019.
- [25] S. K. Bhudolia, G. Gohel, L. K. Fai and R. J. Barsotti, "Fatigue response of ultrasonically welded carbon/Elium® thermoplastic composites," *Materials Letters*, vol. 264, p. 127362, 2020.
- [26] C. Ageorges and L. Ye, "State of the Art in Fusion Bonding of Polymer Composites," , pp. 7-64, 2002.
- [27] C. Ageorges, L. Ye and M. Hou, "Advances in fusion bonding techniques for joining thermoplastic matrix composites: a review," *Composites Part A-applied Science and Manufacturing*, vol. 32, no. 6, pp. 839-857, 2001.
- [28] M. M. Schwartz, *Joining Of Composite-Matrix Materials*, 1994.
- [29] F. Awaja, "Autohesion of polymers," *Polymer*, vol. 97, pp. 387-407, 2016.
- [30] C. A. Butler, R. L. Mccullough, R. Pitchumani and J. W. Gillespie, "An Analysis of Mechanisms Governing Fusion Bonding of Thermoplastic Composites," *Journal of Thermoplastic Composite Materials*, vol. 11, no. 4, pp. 338-363, 1998.

- [31] R. P. Wool and K. M. O'Connor, "A theory crack healing in polymers," *Journal of Applied Physics*, vol. 52, no. 10, pp. 5953-5963, 1981.
- [32] W. I. Lee and G. S. Springer, "A Model of the Manufacturing Process of Thermoplastic Matrix Composites," *Journal of Composite Materials*, vol. 21, no. 11, pp. 1017-1055, 1987.
- [33] F. Yang and R. Pitchumani, "Interlaminar contact development during thermoplastic fusion bonding," *Polymer Engineering and Science*, vol. 42, no. 2, pp. 424-438, 2002.
- [34] Y. H. Kim and R. P. Wool, "A theory of healing at a polymer-polymer interface," *Macromolecules*, vol. 16, no. 7, pp. 1115-1120, 1983.
- [35] F. Sacchetti, W. J. B. Grouve, L. L. Warnet and I. F. Villegas, "Effect of resin-rich bond line thickness and fibre migration on the toughness of unidirectional Carbon/PEEK joints," *Composites Part A-applied Science and Manufacturing*, vol. 109, pp. 197-206, 2018.
- [36] A. Yousefpour, M. Hojjati and J.-P. Immarigeon, "Fusion Bonding/Welding of Thermoplastic Composites," *Journal of Thermoplastic Composite Materials*, vol. 17, no. 4, pp. 303-341, 2004.
- [37] J. C. Fish, M. L. Vitlip, S. P. Chen and K. S. Shin, "Interlaminar fracture characteristics of bonding concepts for thermoplastic primary structures," *AIAA Journal*, vol. 30, no. 6, pp. 1602-1608, 1992.
- [38] A. Smiley, M. Chao and J. Gillespie, "Influence and control of bondline thickness in fusion bonded joints of thermoplastic composites," *Composites Manufacturing*, vol. 2, pp. 223-232, 1991.
- [39] K. N. Shivakumar, R. Panduranga and M. Sharpe, "Interleaved Polymer Matrix Composites - A Review," in *54th AIAA/ASME/ASCE/AHS/ASC Structures, Structural Dynamics, and Materials Conference*, 2013.
- [40] W. Cantwell, P. Davies, P. Bourban, P.-Y. Jar, H. Richard and H. Kausch, "Thermal joining of carbon fibre reinforced PEEK laminates," *Composite Structures*, vol. 16, no. 4, pp. 305-321, 1990.
- [41] B. Bhushan, *Modern Tribology Handbook*, Two Volume Set, 2000.
- [42] "Maximum Height Of Profile (Rz, Pz, Wz) | What Is Line Roughness? | Solving The Questions About Profile And Surface Roughness Measurements! Introduction To "Roughness"," KEYENCE International Belgium, [Online]. Available: https://www.keyence.eu/ss/products/microscope/roughness/line/tab01_b.jsp.. [Accessed 1 March 2020].
- [43] Taylor Hobson, "Surtronic 25 User's Guide," Ametek Ultra Precision Technologies, [Online]. Available: <https://www.taylor-hobson.com/-/media/ametektaylorhobson/files/learning%20zone/user%20guides/surtronic%2025%20user%20guide/surtronic%2025%20issue%204%20gb.pdf?la=en>. [Accessed 1 March 2020].
- [44] A. Ghumatkar, S. Budhe, R. Sekhar, M. Banea and S. D. Barros, "INFLUENCE OF ADHEREND SURFACE ROUGHNESS ON THE ADHESIVE BOND STRENGTH," *Latin American Journal of Solids and Structures*, vol. 13, no. 13, pp. 2356-2370, 2016.
- [45] B. Parker and R. Waghorne, "Surface pretreatment of carbon fibre-reinforced composites for adhesive bonding," *Composites*, vol. 13, no. 3, pp. 280-288, 1982.

- [46] F. Sacchetti, W. J. Grouve, L. L. Warnet and I. F. Villegas, "Effects of release media on the fusion bonding of carbon/PEEK laminates," *Composites Part A-applied Science and Manufacturing*, vol. 94, pp. 70-76, 2017.
- [47] P. Yarrington, J. Zhang, C. Collier and B. A. Bednarczyk, "Failure Analysis of Adhesively Bonded Composite Joints," in *46th AIAA/ASME/ASCE/AHS/ASC Structures, Structural Dynamics and Materials Conference*, 2005.
- [48] K. Mallick, "Vertical Axis Wind Turbine (VAWT) with Thermoplastic Composite Blades," U.S. DEPARTMENT OF ENERGY, Knoxville, TN, 2019.
- [49] H. Jay, ""About"," Institute for Advanced Composites Manufacturing Innovation-IACMI, [Online]. Available: <https://iacmi.org/about-us/>. [Accessed 10 Feb. 2020].
- [50] ASTM International, D3528-96(2016) Standard Test Method for Strength Properties of Double Lap Shear Adhesive Joints by Tension Loading, West Conshohocken, PA: ASTM International, 2016.
- [51] M. K. Moench, "The Effect of Nylon and Polyester Peel Ply Surface Preparation on the Bond Quality of Composite Laminates," *PhDT*, 2014.
- [52] S. H. McKnight, S. T. Holmes, J. W. Gillespie, C. L. T. Lambing and J. M. Marinelli, "Scaling issues in resistance-welded thermoplastic composite joints," *Advances in Polymer Technology*, vol. 16, no. 4, pp. 279-295, 1997.